THE MEASUREMENT OF TRANSITION

PROBABILITIES OF ATOMIC NEON

by

Alexander Maguire Robinson

B.A. Sc., University of British Columbia, 1961

M. Sc., University of British Columbia, 1963

A THESIS SUBMITTED IN PARTIAL FULFILMENT OF

THE REQUIREMENTS FOR THE DEGREE OF

Ph. D.

in the Department

of

Physics

We accept this thesis as conforming to the

required standard

THE UNIVERSITY OF BRITISH COLUMBIA

September, 1966

In presenting this thesis in partial fulfilment of the requirements

for an advanced degree at the University of British Columbia, I agree

that the Library shall make it freely available for reference and

study. I further agree that permission for extensive copying of this

thesis for scholarly purposes may be granted by the Head of my

Department or by his representatives. It is understood that copying

or publication of this thesis for financial gain shall not be allowed

without my written permission.

Department of _Physics_

The University of British Columbia
Vancouver 8, Canada

Date _Sept 13 1966_

THE UNIVERSITY OF BRITISH COLUMBIA

FACULTY OF GRADUATE STUDIES

PROGRAMME OF THE

FINAL ORAL EXAMINATION

FOR THE DEGREE OF

DOCTOR OF PHILOSOPHY

of

ALEXANDER MAGUIRE ROBINSON

B.A.Sc., The University of British Columbia, 1961

M.Sc., The University of British Columbia, 1963

WEDNESDAY, SEPTEMBER 14, 1966 at 3:30 P.M.

IN ROOM 301, HENNINGS BUILDING

COMMITTEE IN CHARGE

Chairman: B. A. Dunell

A. M. Crooker   T. J. Ulrych
F. L. Curzon   W. F. Slawson
A. J. Barnard   R. A. Nodwell

External Examiner: R. W. Nicholls

Professor of Physics

York University

Research Supervisor: R. A. Nodwell

THE MEASUREMENT OF TRANSITION
PROBABILITIES OF ATOMIC NEON

ABSTRACT

The transmission of neon line radiation through
the positive column of a neon dc glow discharge has
been measured. Six lengths of the column were used
and a graphical comparison of the theoretical and
experimental transmissions were made. This permitted
a determination of the absorption coefficient of the
gas, for the case of Doppler-broadened spectral lines.
The relative transition probabilities for transitions
with the same lower level were obtained from the values
of the absorption coefficients. Radial variation of the
density of absorbing atoms and the presence of isotopes
in the column were taken into account.

The relative intensities of several pairs of spectral
lines emitted by neon gas excited by a pulsed electron
beam have been measured. The neon was at a low pressure
(.1 mm Hg) and excited for a short time (200 nsec) to
supress self-absorption of the emitted radiation. The
relative transition probabilities for lines with the
same upper level were determined from the intensity
measurements.

A weighted averaging technique was used to connect
the relative transition probabilities of the absorption
and emission measurements and a complete set of relative
transition probabilities was obtained. The probabilities
were placed on an absolute scale using the results of a
lifetime measurement recently made by van Andel.

GRADUATE STUDIES

Field of Study: Physics

Molecular Spectroscopy   F. W. Dalby

Magnetohydrodynamics   F. L.   Curzon
                                                P. R.   Smy

Special Relativity   P. Rastall

Plasma Physics   L. G. de Sobrino

Related Studies:

Electron Dynamics   G. B. Walker

PUBLICATION

The Measurement of Line Absorption of Excited
Gases, R.A. Nodwell and A. M. Robinson, Proceedings
of the Seventh International Conference on Phenomena
in Ionized Gases, Beograd, 1965 (in press).

ABSTRACT

The transmission of neon line radiation through the positive column of a neon dc glow discharge has been measured. Six lengths of the column were used and a graphical comparison of the theoretical and experimental transmissions were made. This permitted a determination of the absorption coefficient of the gas, for the case of Doppler-broadened spectral lines. The relative transition probabilities for transitions with the same lower level were obtained from the values of the absorption coefficients. Radial variation of the density of absorbing atoms and the presence of isotopes in the column were taken into account.

The relative intensities of several pairs of spectral lines emitted by neon gas excited by a pulsed electron beam have been measured. The neon was at a low pressure (.1 mm Hg) and excited for a short time (200 nsec) to supress self-absorption of the emitted radiation. The relative transition probabilities for lines with the same upper level were determined from the intensity measurements.

A weighted averaging technique was used to connect the relative transition probabilities of the absorption and emission measurements and a complete set of relative transition probabilities was obtained. The probabilities were placed on an absolute scale using the results of a lifetime measurement recently made by van Andel /17/.

TABLE OF CONTENTS

iv

TABLE OF CONTENTS (cont'd)

INDEX OF TABLES

TABLES (cont'd)

INDEX OF FIGURES

FIGURES (cont'd)

x

ACKNOWLEDGEMENTS

I would like to sincerely thank Dr. R. A. Nodwell
for his helpful guidance and assistance to me in this work,
and to other members of the plasma physics group for their
helpful discussions and suggestions. Thanks is also given
to the members of the physics workshop for assistance in con-
struction of equipment.

I am indebted to my committee members Drs. F. L.
Curzon, A. J. Barnard, and A. M. Crooker for suggestions regarding
my research and the writing of this thesis.

Special acknowledgement is given to Mr. H. W. H.
van Andel for making available the apparatus used for measuring
intensities and his assistance given in performing them.

CHAPTER 1 INTRODUCTION

It was in 1916 and 1917 that Einstein /1/ published
his classic papers in which he introduced transition probabilities.
Since that time much effort has been expended in the theoretical
and experimental determination of these probabilities or the
associated oscillator strengths because of their importance in
many fields of basic scientific research.

For example, transition probabilities are essential
in astrophysics. Here, research is restricted to analysis of
radiation emitted and absorbed by stellar bodies. Measurement
of spectral intensities can in principle determine such variables
as electron density and temperature, number density of atoms
and degree of ionization, and the abundance of the elements in
the universe but these determinations depend explicitly on the
transition probabilities. In the field of plasma physics a
similar situation exists. Of course the scientist is not con-
fined to mere observation of electromagnetic radiation and can
to some degree control his experimental environment. Neverthe-
less transition probabilities are needed for virtually all
spectroscopic diagnoses of plasmas. The recent interest in
lasers has produced a spate of research in excitation and de-
excitation processes in connection with excitation decay rates
and population inversions in solid and gaseous materials. A
knowledge of probabilities is imperative for both experimental
and theoretical studies of these processes.

Although quantitative values of transition probabili-

ties are essential in these fields of research, the actual
number of values known accurately is extremely small. The need
for additional and more accurate values is apparent and has led
to marked increase in work in this direction (for a recent bib-
liography of transition probabilities, see Glennon and Wiese /2/).

Theoretically, the transition probability can be cal-
culated from the eigenfunctions of the atom, and the eigenfunc-
tions may be obtained from the potential acting on the electron(s)
involved in the radiative transition. The simplest atomic system
is the hydrogen-like atom whose eigenfunctions may be found
exactly because the electron moves in a simple Coulomb field.
Thus for these atoms, transition probabilities may be computed,
as has recently been done by Karzas and Latter /3/ and Herdon
and Hughes /4/. However, for more complicated atoms, exact
analytic solution of Schroedinger's equation is not possible
and thus theoretical calculations involve some degree of approxi-
mation. The most widely used approximation method is due to
Bates and Damgaard /5/ which uses asymptotic solutions of a
Coulomb potential. Because these approximations are somewhat
doubtful there is some uncertainty in the computed values, and
hence it is desireable to determine the values experimentally.

The experimental techniques fall into two general
classes. The first class measures the rate of decay of atom
populations directly. This method can provide accurate deter-
minations under appropriate experimental conditions but it is
usually difficult to know the rate at which the upper level
is being populated. In addition, if the upper state decays to

more than one lower level individual probabilities cannot be determined by lifetime measurements alone. For most elements, this means absolute transition probabilities can be obtained from lifetime measurements for a few transitions only. The second general technique is less direct and measures parameters related to the transitions probabilities. For example, measurements of emission and absorption of radiation can lead to estimates of transition probabilities. To obtain absolute values the absolute population densities of the two levels must be known. Values of population densities of sufficient accuracy are not usually available. However measurements involving relative emission and absorption can be made accurately, so that relative transition probabilities can be acquired. The lifetime methods usually yield at least one absolute transition probability so when combined with the more numerous relative values, accurate absolute probabilities can be obtained.

In the experiment reported in this thesis the relative transition probabilities have been measured for most of the transitions between the $2p^53s$ and $2p^53p$ configurations of Ne I. This gas was chosen for several reasons. Neon appears in the hotter stars and in some cases is as abundant as oxygen /6/, making it an interesting subject for astrophysical research and it is often used for high-temperature shock tube work in plasma research so that a knowledge of neon transition probabilities is important. From an experimental point of view, neon is rich in spectral lines in the visible region. Finally, there are some significant discrepancies in previous evaluations

of neon transition probabilities and a new determination is highly desireable.

Transitions between the above mentioned configurations of neon have been the subject of several experimental investigations in the past four decades. One of the first was performed by Ladenburg, et al. /7/ who measured the relative transition probabilities from the anomalous dispersion of the gas by the Roschdestwensky "hook method" /8/. This technique was recently repeated by Pery-Thorne and Chamberlain /9/. Doherty /10/ determined the absolute transition probabilities from absolute intensity measurements using a shock tube. Friedrichs /11/ also measured absolute intensities, but with a stabilized arc as a source. More recently, relative values for these lines have been determined by Irwin /12/ using line-reversal and relative intensity methods.

The method of determining the time dependence of populations of the excited states was first attempted on some of these neon levels by Griffiths /13/ who estimated the lifetimes by measuring the phase lag between periodic excitation and emission. Other direct measurements of lifetimes has been performed by Bennett /14/, et al. and Klose /15/, in which the decay of the radiative intensity is measured by sampling.

There is considerable disagreement amongst the values of the transition probabilities obtained by these workers. The presence of self-absorption in some of the experiments and other limitations on the accuracy of the measurements prompted the undertaking of the experiment described in this thesis.

The experiment reported here consists of two separate parts, an absorption experiment which relates probabilities of transitions having a common lower level, and an emission or intensity experiment which relates probabilities of transitions with a common upper level. Combining the results of these two experiments allows one complete set of relative values to be obtained.

The absorption experiment employs a modification and extension of a method due to Hamberger /16/, who measured the transmission of a plasma to intensity-modulated hydrogen radiation to determine the density of excited atoms as a function of time. In the experiment described in this thesis, the transmission of the positive column of a neon dc glow discharge is measured. Use of six absorption lengths enables a graphical comparison of the theoretical and experimental transmissions to be made to determine the absorption coefficient of the gas, assuming Doppler-broadened spectral lines. The values of the absorption coefficients of appropriate spectral transitions allows calculation of relative transition probabilities. Radial variations of the density of excited atoms is observed and compensated for by varying the diameter of the incident beam or by using an annular cross-sectional beam. The presence of isotopes is also taken into account.

The emission experiment measures relative intensities of several pairs of neon spectral lines by a method not believed to have been used previously. The radiation is emitted by a neon source excited by a pulsed electron beam and the intensity

is determined by counting the photons with a photo-electric counting device. The pressure of the gas is low (.1 mm Hg) to eliminate self-absorption. The apparatus was developed by van Andel /17/ for lifetime measurements but was readily adapted for this experiment.

The values of the transition probabilities obtained by this method are estimated to be the most accurate to date and should prove to be valuable for future spectroscopic diagnosis of neon.

The theory of the experiment is developed in Chapter 2. Starting with the general laws of total absorption of a spectral line in a uniform gas, the specific case of Doppler broadened lines is considered. Non-uniformity in a radial direction of a cylindrically symmetric system is next considered, and two methods overcoming this difficulty are discussed. The equations necessary to account for the presence of isotopes in the source and absorber are given. Finally emission theory is developed and discussed. Chapter 3 describes the experimental apparatus and procedure of the absorption experiment while Chapter 4 does the same for the emission experiment. The results of the work are given in Chapter 5 and discussed; attempts are made to account for broadening other than pure Doppler in the absorption experiment and errors in absorption and emission are investigated. The chapter is concluded with a presentation of the absolute transition probabilities based on a lifetime measurement by van Andel /17/. The conclusions are contained in Chapter 6.

CHAPTER 2   THEORY

The theory developed in this chapter indicates how relative transition probabilities may be determined from a measurement of the absorption and emission of radiation by a gas.

2.1   Absorption

The absorption coefficient integrated over a spectral line is proportional to the transition probability (see for example, Garbuny /18/). The theory given in this section calculates the transmission of Doppler-broadened spectral radiation through a gas and relates the absorption coefficient and hence the transition probability to the transmission measurements.

2.1.1   Uniform Gas

When a plane-parallel beam of monochromatic radiation at frequency ν passes through a uniform gas of length ℓ, the intensity of the beam is decreased because of absorption. The fraction of the energy transmitted per second, or the transmission T, is given by $e^{-k(\nu)\ell}$ where $k(\nu)$ is called the absorption coefficient of the gas.

If the incident beam consists of a single spectral line of small but finite width, integration over the line yields the transmission, thus:

$$T = \frac{\int_{line} I(\nu) e^{-k(\nu)\ell} d\nu}{\int_{line} I(\nu) d\nu} \qquad \ldots(2.1)$$

where $I(\nu)$ is the intensity of the incident beam at frequency ν.

The absorption coefficient is a parameter of the absorbing gas and depends on the transition probability. In principle the absorption coefficient may be determined from a measurement of the transmission of a beam of light of known spectral distribution. The transition probability may then be determined from the absorption coefficient.

In this experiment conditions are chosen such that both the source and the absorber have predominantly Doppler-broadened lines. For a source and an absorber having temperatures T_s and T_a respectively, and a spectral line of centre-frequency ν_o, the emission intensity and the absorption coefficient are given by (see for example, Mitchell and Zemansky /19/)

$$I(\nu) = I_o e^{-\omega^2}$$

$$k(\nu) = k_o e^{-\omega^2 \alpha^2}$$

where $\quad \omega = \dfrac{\nu - \nu_o}{\Delta\nu_{DS}} 2\sqrt{\ln 2} \quad = \dfrac{\nu - \nu_o}{.6\Delta\nu_{DS}}$

$$\Delta\nu_{DS} = \frac{2\nu_o}{c}\sqrt{\frac{2\ln 2\, RT_s}{M}} \qquad = \text{Doppler width of the}$$

spectral line of the source, and $\alpha = \sqrt{Ts/Ta}$ = ratio of the Doppler widths of the source and the absorber. When stimulated emission is negligible, as it is in this experiment, the value of the absorption coefficient at the centre of the spectral line, k_o, is given by

$$k_o = \frac{\sqrt{\pi}\, e^2\, N_i\, f_{ij}}{m\, c\, .6\Delta\nu_{Da}} = \frac{\lambda_o^2}{8\pi^{3/2}}\, \frac{g_j}{g_i}\, \frac{N_i\, A_{ji}}{.6\Delta\nu_{Da}} \qquad ...(2.2)$$

where N_1 = the number density of atoms in the lower state of the transition, and f_{ij} and A_{ji} are the oscillator strength and the transition probability respectively, for the absorption transition $i \longrightarrow j$ ($i \equiv$ lower level, $j \equiv$ upper level).

Equation (2.1) then becomes

$$T = \frac{\int_{-\infty}^{\infty} e^{-\omega^2} e^{-k_o l\, e^{-\omega^2 \alpha^2}}\, d\omega}{\int_{-\infty}^{\infty} e^{-\omega^2}\, d\omega} = \sum_{n=0}^{\infty} \frac{(-1)^n (k_o l)^n}{n!\sqrt{1+n\alpha^2}} = F_o(k_o l, \alpha) \qquad ...(2.3)$$

Fig. 1 is a plot of F_o as a function of $k_o l$ for several values of α.

2.1.2   Non-Uniform Gas

A modification of equation (2.1) is necessary when
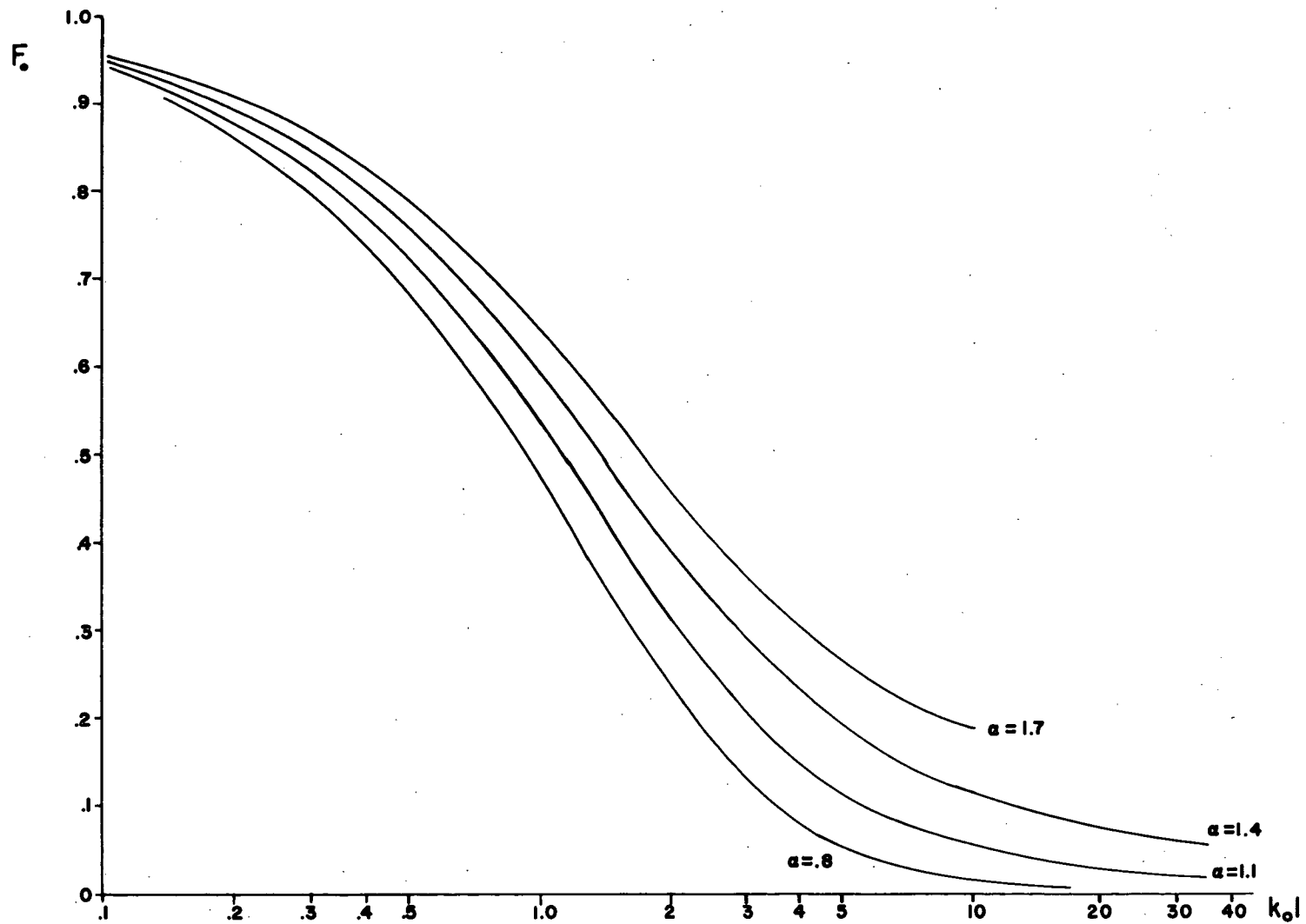
FIG. I. Plot of F_0 as a function of $k_0 l$ and α

the density or the temperature of the absorbing gas is not
constant perpendicular to the axis of the beam (but uniform
along the axis) because the absorption coefficient will vary
with radial position and an integration over the transverse
area is necessary. Equation (2.1) then becomes

$$T = \frac{\int_A \int_\nu I(\nu) e^{-k(\nu,A)\ell} \, d\nu \, dA}{\int_A \int_\nu I(\nu) \, d\nu \, dA} \qquad \ldots (2.4)$$

For an absorbing column with axial symmetry and an
annular cross-sectional beam (with inner and outer radii R_i and
R_0 respectively) centred on the axis of the column,

$$T = \frac{\int_{R_i}^{R_0} \int_\nu I(\nu) e^{-k(\nu,r)\ell} \, d\nu \, 2\pi r \, dr}{\pi(R_0^2 - R_i^2) \int_\nu I(\nu) \, d\nu} \qquad \ldots (2.5)$$

where r is the radial distance from the axis. Fig. 2 shows the

geometry of the system.
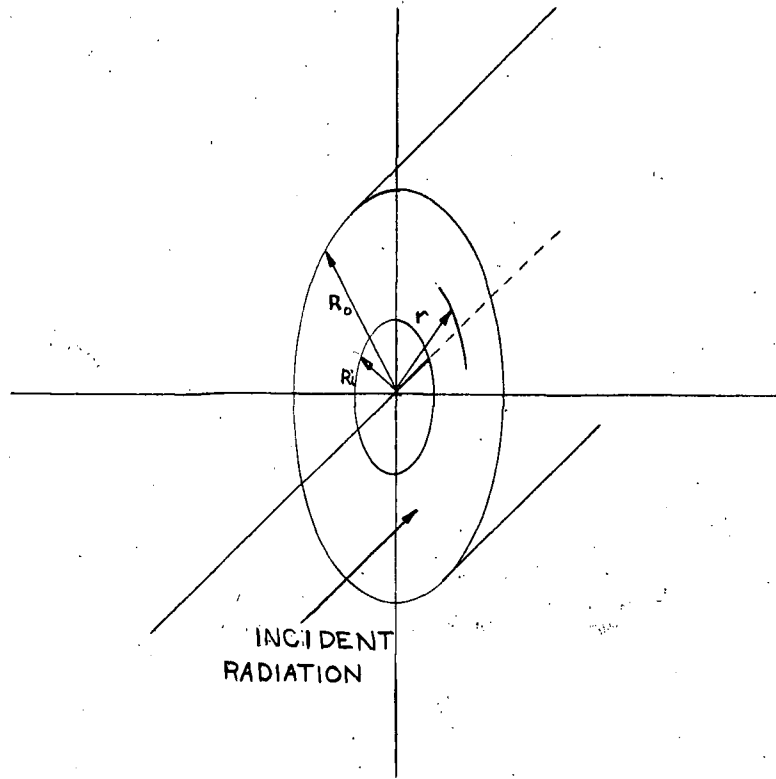
Fig. 2 Geometry of Absorbing Column

If $R_o - R_1$ is small enough so that $k(\nu, r)$ is nearly constant over the annulus, then the form of T becomes identical with equation (2.1).

If R_o is treated as a variable so that T becomes a function of R_o, an expression depending only on the parameters at $r = R_o$ may be obtained by differentiating $(R_o^2 - R_1^2)T$ with respect to R_o^2;

$$\frac{d}{d(R_o^2)}\left\{(R_o^2 - R_i^2)T\right\} = \frac{\int_\nu I(\nu)e^{-k(\nu, R_o)\ell}\,d\nu}{\int_\nu I(\nu)\,d\nu}$$

For Doppler broadened lines this beomes

$$\frac{d}{d(R_o^2)}\left\{(R_o^2 - R_i^2)T\right\} = F_o(k_o(R_o)\ell, \alpha) \qquad \ldots(2.6)$$

For a circular beam ($R_1 = 0$) equation (2.6) becomes finally

$$\frac{d(R^2 T)}{d(R^2)} = F_o(k_o(R)\ell, \alpha) \qquad \ldots(2.7)$$

where R has been written instead of R_o for simplicity. This enables the absorption coefficient to be related to the transmission as the beam diameter is varied.

2.1.3 Hyperfine Structure

So far only spectral lines having a simple Doppler profile have been considered. Many lines possess a structure, which can lead to error if ignored. The fine structure of neon is large enough to separate easily with a spectrograph but the hyperfine structure of the spectral lines is not and must be accounted for in the analysis. In neon, the hyperfine structure of the lines is due solely to the mass difference of the isotopes, since the nuclear angular momentum of the predominant

isotopes is zero /20/.

Naturally occuring neon is composed approximately of 91% atomic mass 20, 9% mass 22, and .3% mass 21. The quantity of Ne^{21} is so small that the effect of its presence will be negligible in this experiment, making neon essentially a two-isotope gas. For a two-isotope gas, the total profile of a spectral line is the sum of the profiles of two components. Each individual profile is centred on a slightly different frequency and if the splitting is large enough the total line will have two peaks or even two separate components. In neon the isotope of mass 22 only contributes about 10% of the emiss-ion energy but in absorption the effect of this isotope can be predominant.

To see qualitatively the effect of this isotope in absorption consider a neon source and absorber whose spectral lines have two isotope components with profiles completely or almost completely non-overlapping. Because of the non-overlapp-ing condition, the Ne^{20} component in the absorber will absorb only the Ne^{20} component emitted by the source, with a similar situation existing for the Ne^{22} portion of the spectral line. The energy entering the absorber will be predominantly from the Ne^{20} isotope. However this isotope has a correspondingly large absorption coefficient and the transmission varies exponentially with absorption coefficient, not linearly. That is, the gas is more transparent to the weaker component of the radiation. With strong absorption the energy transmitted by the absorber can be almost completely due to the less

abundant isotope Ne^{22}. Of course if the line-width of the components are larger than the isotope separation, the two components blend into one line and the isotope effect is not so significant.

A quantitative analysis has been made relevant to the conditions in this experiment. Only the results are given here and the detailed calculations and discussion reserved for Appendix 1. The main postulate of the analysis is that the spectral profile may be represented by two separated Doppler curves. Experimental conditions are such that this is a good approximation, as shown in the appendix.

For a uniform gas the transmission is shown to be

$$T = \frac{1}{1+a}\left[F_0(k_0 l, \alpha) + a F_0(b k_0 l, \alpha)\right] \quad \ldots (2.8)$$

where F_0 is defined in equation (2.3) and

$a = K\sqrt{M/M'} \approx .094$

$b = K\sqrt{M'/M} = aM'/M \approx .104$

K = relative abundance of the two isotopes $\approx .099$

M = mass of greatest-occurring isotope = 20 atomic mass units

M' = mass of least-occurring isotope = 22 atomic mass units

The numerical values given pertain to neon.

The two terms on the right hand side of equation (2.8) represent contributions to the transmission from the two isotopes. The relationship between this equation and the qualitative discussion of the previous paragraphs may be seen with reference to Fig. 1. F_0 is close to 1 for small $k_0 l$ but

decreases rapidly with increasing $k_o \ell$. a and b are approximately equal and small if one of the isotopes is not very abundant. Therefore for small absorption (i.e. $k_o \ell$ small) the first term dominates, but at large $k_o \ell$, the argument in the second term is still small because of the factor b and the second term dominates.

Equation (2.8) is plotted in Fig. 3. For comparison $F_o(k_o \ell , \alpha)$ is plotted for several values of α (dotted line). The calculations of these functions is discussed in Appendix 2. The equation corresponding to equation (2.7) is

$$\frac{d(R^2 T)}{d(R^2)} = \frac{1}{1 + \alpha} \left[F_o(k_o(R)\ell , \alpha(R)) + \alpha F_o(b k_o(R)\ell , \alpha(R)) \right] \quad \cdots (2.9)$$

2.1.4   Analysis of Data

If k_o and α can be determined from measurement of T, the relative probabilities (or oscillator strengths), temperatures and populations can be calculated as can be see from consideration of equation (2.2). For measurements made on a single spectral line the relative temperature and number density of the lower state may be determined as a function of radial position;
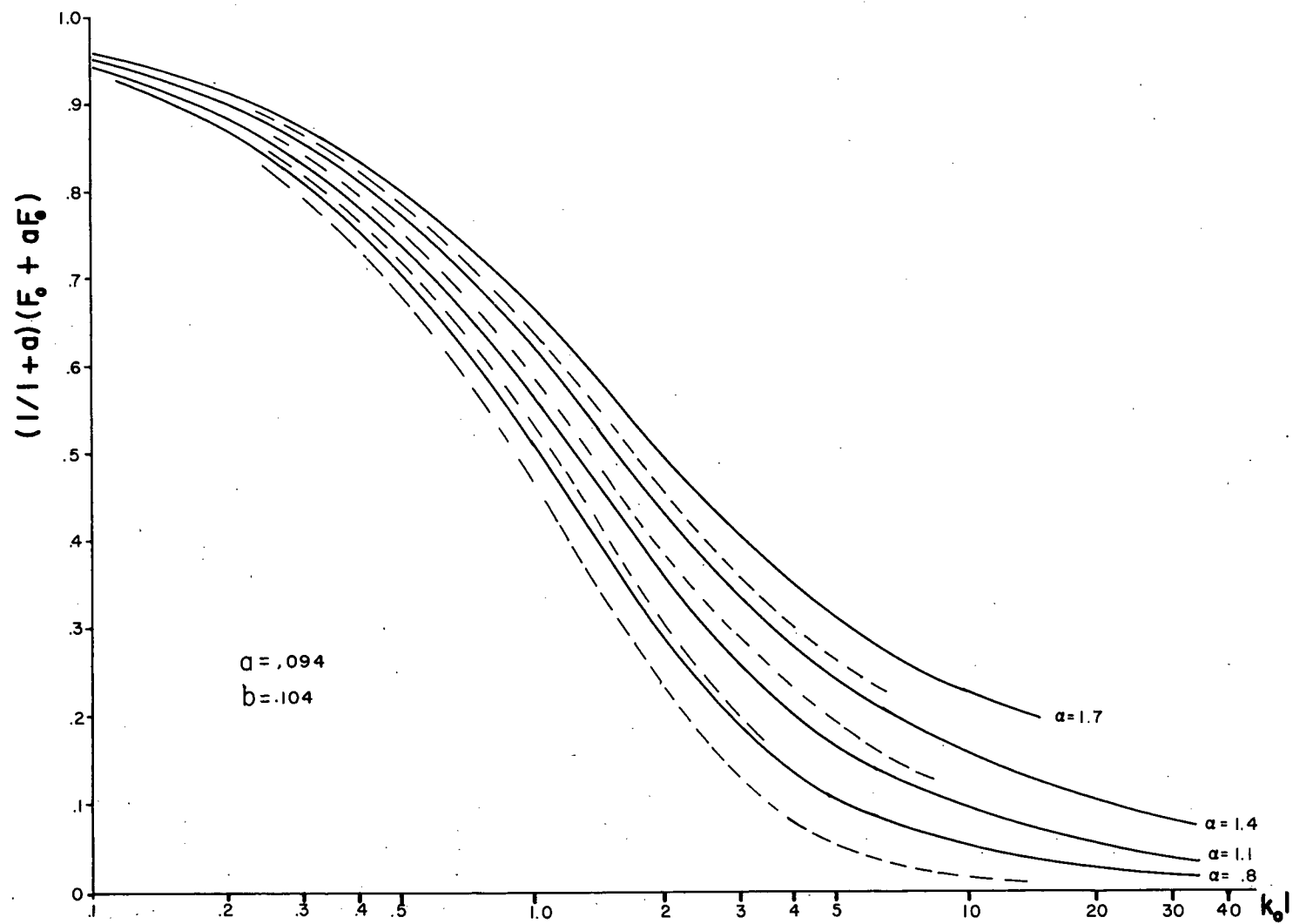
FIG. 3. Plot of $(1/1+a)(F_o(k_ol,\alpha) + aF_o(bk_ol,\alpha))$ as a function of k_ol and α

$$\frac{T_a(R)}{T_a(R')} = \left[\frac{\alpha(R')}{\alpha(R)}\right]^2$$

$$\frac{N_i(R)}{N_i(R')} = \frac{k_o(R)}{k_o(R')} \frac{T_a(R)}{T_a(R')} = \frac{k_o(R) \, \alpha(R')}{k_o(R') \, \alpha(R)} \qquad \ldots(2.10)$$

where R' is some arbitrary reference radius.

But more important, if two spectral lines having a common lower level are compared at the same radius, N_i is the same for both and

$$\frac{k_{o_1}(R)}{k_{o_2}(R)} = \frac{\lambda_1 f_1}{\lambda_2 f_2} = \frac{\lambda_1}{\lambda_2} f_{rel}(\lambda_1, \lambda_2) \qquad \ldots(2.11)$$

$$= \frac{\lambda_1^3 \, g_{j_1} A_1}{\lambda_2^3 \, g_{j_2} A_2} = \frac{\lambda_1^3 \, g_{j_1}}{\lambda_2^3 \, g_{j_2}} A_{rel}(\lambda_1, \lambda_2) \ldots(2.12)$$

2.2   Emission

Einstein /1/ showed that the power spontaneously emitted by a group of atoms is proportional to $A_{ji} h \nu$ where

A_{j1} is the spontaneous transition probability and ν is the frequency of the emitted radiation. For N_j atoms per unit volume in the upper state j emitting in a layer of thickness l the energy flux due to spontaneous emission is proportional to

$$N_j A_{j1} h \nu l \qquad \qquad \ldots(2.13)$$

Thus relative transition probabilities may be calculated from a determination of the relative intensities of lines with a common upper level since N_j is equal for both transitions and hence

$$\frac{I_1}{I_2} = \frac{\lambda_2 A_1}{\lambda_1 A_2} = \frac{\lambda_2}{\lambda_1} A_{rel}(\lambda_1, \lambda_2) \qquad \ldots(2.14)$$

If the density of atoms in the lower state is non-zero, there is a finite probability of emitted photons being reabsorbed with a consequent decrease of output intensity. This radiation imprisonment is largest for resonance line since most of the atoms are in the ground state. Ladenberg and Levy /7/ derived for a one-isotope gas a correction factor to be applied to the measured intensity for Doppler lines. They showed that the intensity of a finite layer of the luminous gas is equal to the intensity of a layer of unit thickness in the absence of self-absorption multiplied by the factor lS, where

$$S = \sum_{n=0}^{\infty} \frac{(-1)^n (k_o \ell)^n}{(n+1)! \sqrt{n+1}} \qquad \ldots (2.15)$$

When two isotopes are present, equation (2.15) must be modified to :

$$S = \frac{1}{\sqrt{\pi}} \sum_{n=0}^{\infty} \frac{(-1)^n (k_o \ell)^n}{(n+1)!} \mathscr{S}_{n+1} \qquad \ldots (2.16)$$

with

$$\mathscr{S}_n = \int_{-\infty}^{\infty} \left[e^{-\omega^2} + a\, e^{-b/a\,(\omega - \Omega)^2} \right]^n d\omega$$

where a and b are defined in equation (2.8) and Ω is the frequency separation between the isotopic components, in units of ω .

The derivation of equation (2.16) as well as a table of numerical values is given in Appendix 3.

CHAPTER 3   ABSORPTION EXPERIMENT

3.1   Apparatus

The detecting apparatus used in these studies is
based on a method described by Hamberger /16/. A brief
description of the apparatus is given with the help of Fig. 4
which illustrates schematically the experimental arrangement.

Radiation from a neon-filled Geissler tube passes
through a pinhole and is intensity-modulated at 210 cps by a
rotating disk chopper. It is then collimated by a lens and
passed through a cylindrical neon-filled absorption tube. The
absorption tube has four internal electrodes so that six
different discharge lengths may be obtained. The radiation is
then focused on the entrance slit of a monochromator set to
pass the spectral line under investigation. The cross-sectional
area of the transmitted beam is controlled by apertures placed
in the collimated beam at both ends of the absorption tube.
The intensity of the light is measured at the exit slit of the
monochromator by a photomultiplier and a narrow-band amplifier
centred at 210 cps. The resultant signal is then fed into a
phase-sensitive detector which receives a reference signal of
the same frequency. The detector only accepts signals coherent
with the reference signal and eliminates unwanted signals due
to emission of radiation from the absorption tube and noise in
the photomultiplier and amplifier. The dc signal from the
detector is measured with a chart recorder and is proportional
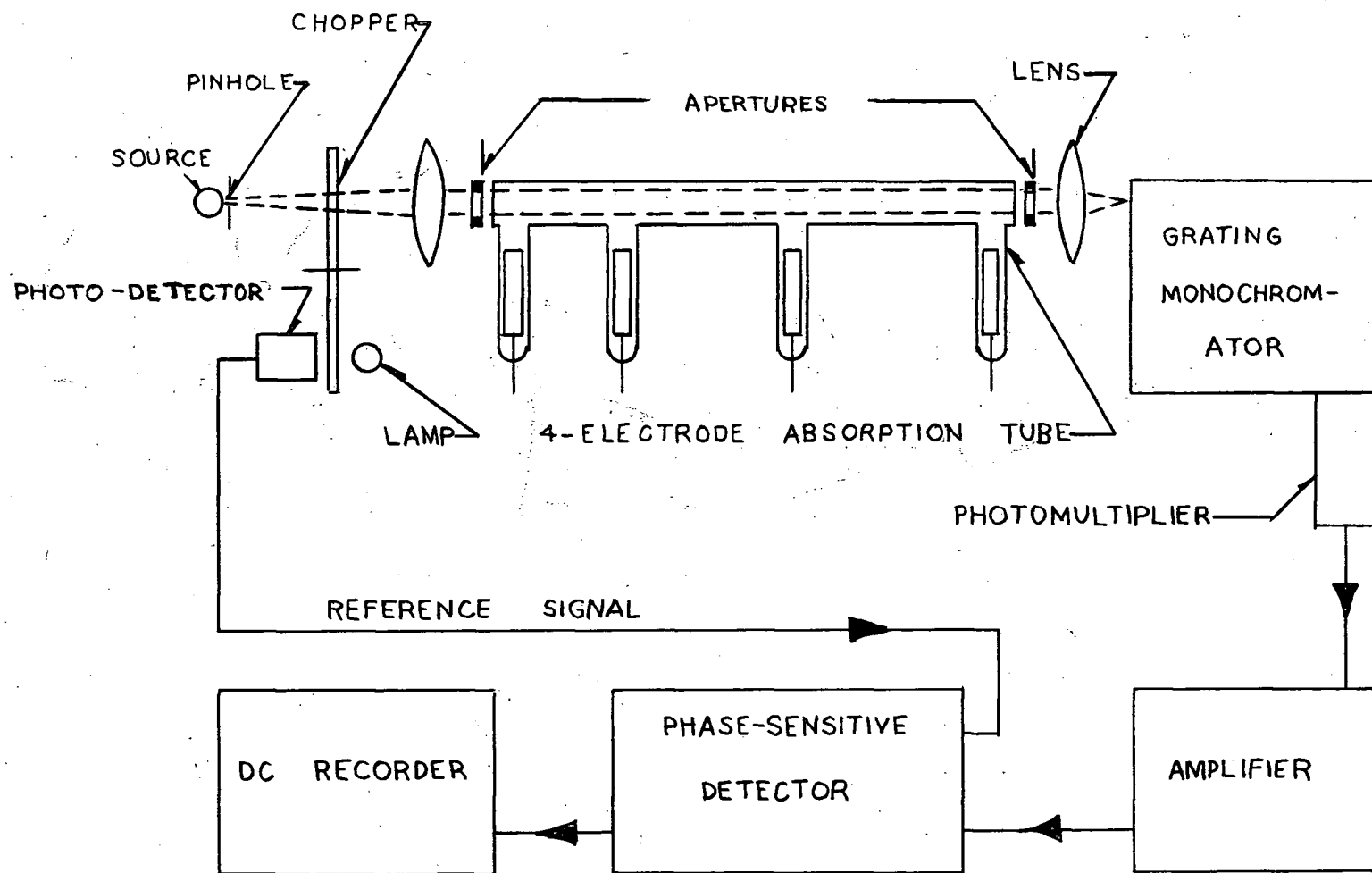
FIG. 4. SCHEMATIC OF ABSORPTION APPARATUS

to the intensity of the modulated beam falling on the photo-multiplier.   Thus the apparatus provides a means of separating the background light from the absorption tube and furnishes several absorbing lengths so that it is possible to calculate k_o and α using equation (2.9)

The apparatus will now be discussed in detail.

3.1.1   Background Light Source and Modulator

The source used was a neon-filled Geissler tube 10 cm long and approximately 2 mm inner diameter.   The tube was operated from a 600v dc power supply and current regulator. The current regulator was necessary to stabilize the intensity of the emitted radiation.   The direct current through the tube could be varied upwards from 2 ma and was operated at a maximum of 9 ma. The tube did not heat up and remained essentailly at room temperature.

The modulator was a seven-slotted circular disk placed between the Geissler tube and the collimating lens.   It was mounted on the shaft of a Bodine Electric Co. 1/25 hp, 30 cps synchronous motor, chopping the beam at a frequency of 210 cps. The modulating frequency of 210 cps was chosen to avoid harmonics of 60 cps. It was found that best overall performance was attained when the motor was driven by a 60 cps crystal oscillator and power amplifier, rather than using power from the mains.   The frequency of both the oscillator-amplifier source and the mains voltage was measured with a digital counter.   The variation of the frequency had a standard deviation of $9 \times 10^{-4}\%$ for the former source and $12 \times 10^{-4}\%$ for the latter.   This larger

deviation resulted in a 5% variation of the output signal
measured on the chart recorder. This was because the frequency
of the modulated light did not remain at the centre-frequency
of the pass-band of the amplifier. The variation of the output
signal with the oscillator-amplifier source was less than 1%.

3.1.2   Absorption Tubes and Apertures

The absorbing neon for this experiment was the plasma
of a positive column dc discharge contained in a cylindrical
absorption tube. Two absorption tubes were used for this
experiment and are illustrated in Fig. 5. Both were constructed
with glass tubing of 50 cm length, one with 25 mm inside
diameter and the other 13 mm. Optically flat windows were
mounted on each end. Four side-arms containing electrodes were
spaced along the length of the tube so that absorption lengths
of 10, 15, 20, 25, 35, and 45 cm could be obtained. The
electrodes were partially hollowed aluminum cylinders joined to
a tungsten wire sealed through the glass. The dimensions of
the electrodes are given in Fig. 5.

The glow discharge was maintained by applying 600v dc
across the pair of electrodes corresponding to the discharge
length desired. For both the absorption and emission tubes, the
discharge was initiated with a Tesla coil.

Before filling, the tubes were baked at 400°C for
several hours and then evacuated to a pressure of 10^{-9} mm Hg
on a high-vacuum system built by van Andel /21/ before being
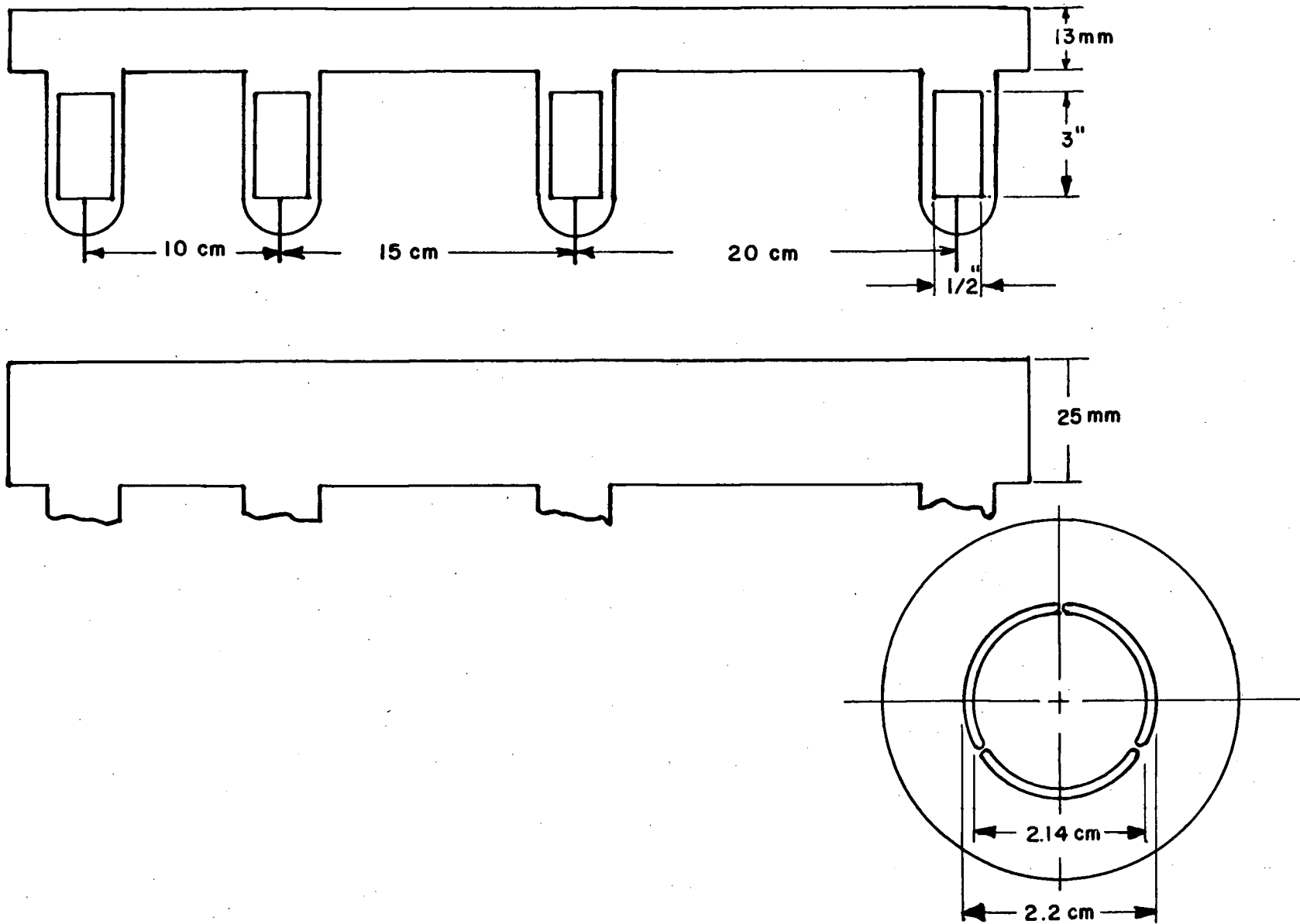
FIG. 5. ABSORPTION TUBES AND ANNULUS

filled with research grade Airco neon to a pressure of 2 mm Hg and sealed off.

Centred on each end of the narrow absorption tube were aluminum holders into which could slide short strips of aluminum with circular holes in them. By using holes of vary-ing diameter, a beam of circular cross-section of known diameter passed down the axis of the absorption tube. Mounted at each end of the larger diameter tube was a brass sheet from which was cut an annulus. This allowed a beam of 2.2 cm outer diameter and 2.14 cm inner diameter to pass through the tube. (see Fig. 5) The dimensions of the annulus was governed by experimental operating conditions. The width of the annulus had to be small for conditions to be approximately constant in the annular beam. This meant the diameter could not be too small, otherwise the cross-sectional area of the annulus and hence the intensity of the light from the background source would be small and the signal-to-noise ratio low. As well, the less highly absorbing gas well away from the axis of the absorption tube was of interest and led to the above choice of annular dimensions. Because the diameter of the annulus was larger than that of the narrow absorption tube, the annuli were only used with the large absorption tube.

It is obvious that the optical alignment for this experiment is critical and special care is necessary. For this reason a Precision Tool and Instrument Co. 2-meter optical bench with x, y, and z vernier motion saddles was used in conjunction with a Spectra-Physics He-Ne laser. The laser was

initially lined up along the axis of the monochromator and defined the optic axis for alignment of tubes, lenses, annuli, etc. Correct alignment of each component was estimated to be within .25 mm.

3.1.3   Monochromator

The monochromator used for the absorption experiment was built in this laboratory. It incorporated an f/15 3-meter spherical mirror, 10 cm diameter, and a 3-meter concave grating, 10 cm diameter. The arrangement was in a standard Wadsworth mount with the exit slit mounted on ways perpendicular to the centre of the grating. The spectrum was observed in the first order and gave a reciprocal dispersion of an almost constant 22.4 Å/mm over the total wavelength region observed (5800Å - 7300Å).

The maximum signal-to-noise resulted from maximum width of entrance and exit slits. Ideally the exit slit would be set exactly at the exit plane position corresponding to the spectral line under investigation. The slits (assuming unit magnification) could then be opened to a width equal to the distance between the centre of this spectral line and the centre of the nearest strong adjacent spectral line and the two spectral lines would then be contiguous. However because the exit slit cannot be positioned exactly there is danger of some radiation from the wrong line passing through the exit slit. To safeguard against this the width of the entrance slit

was made smaller than the exit slit by a factor of about 2/3.

Care must be taken in deciding which weak adjacent lines produce effects small enough to ignore and so can be encompassed by the exit slit; by the same reasoning as given in Chapter 2, a line which is very weak in emission can also be weak in absorption and with strong absorption of the main line, a large proportion of the energy transmitted may be due to the weak line. For this reason the spectrum from the Geissler tube was examined with a high resolving power 3.5-meter Ebert mount grating spectrograph and the approximate relative intensities of all weak lines near the main lines were measured. The criterion was set that the weak lines must have intensity less than 1% of the main line. For most lines the exit slit width was 1 mm or wider, although some had widths as small as 350 microns.

3.1.4   Photomultiplier

Affixed directly behind the exit slit in a light-tight brass container was a Philips 150 CVP end-on photo-multiplier. The circuit is shown in Fig. 6. Because the spectral response of the photomultiplier peaked in the near infra-red, the dark current was found to be excessively large at room temperature. By surrounding the brass container with crushed dry ice, the noise was reduced by a factor of approximately 50, giving an acceptable signal-to-noise ratio of approximately 5 for the less intense lines. Depending on the humidity,

a small stream of air blowing on the edges of the exit slit was
sometimes necessary to keep ice from forming on the edges.

3.1.5   Amplifier and Phase-Sensitive Detector

The signal from the photomultiplier was fed into
a four-stage amplifier with a twin-tee feed-back circuit /22/
from stage 4 to stage 2.   The resulting amplifier had a one-
half amplitude bandwidth of 13 cps centred at 210 cps and a
gain at this frequency of approximately 32,000.   The output
signal was tapped off a potentiometer and reduced in amplitude
so the resulting signal into the phase-sensitive detector was
never larger than .25v peak-to-peak to ensure linearity. The
circuit diagram is shown in Fig. 6.

The phase-sensitive detector is the same as that
described by Schuster /23/ and the circuit is drawn in Fig. 7.
Essentially it operates by having a sine-wave reference voltage
turning one triode on and the other off on each half cycle;   a
signal with the same frequency is fed through the cathodes
and alters the anode currents, but with opposite polarities in
each anode circuit. Upon rectification, the resulting dc
voltage depends sinusoidally on the phase difference between
the reference voltage and the signal. The phase difference
was set to $0°$ or $180°$ for a maximum output.   The dc output was
then monitored on a Heathkit model EUW - 20A chart recorder.
The RC time constant in the rectifying unit indicated in Fig. 7
was chosen to obtain a response time appropriate to the signal-
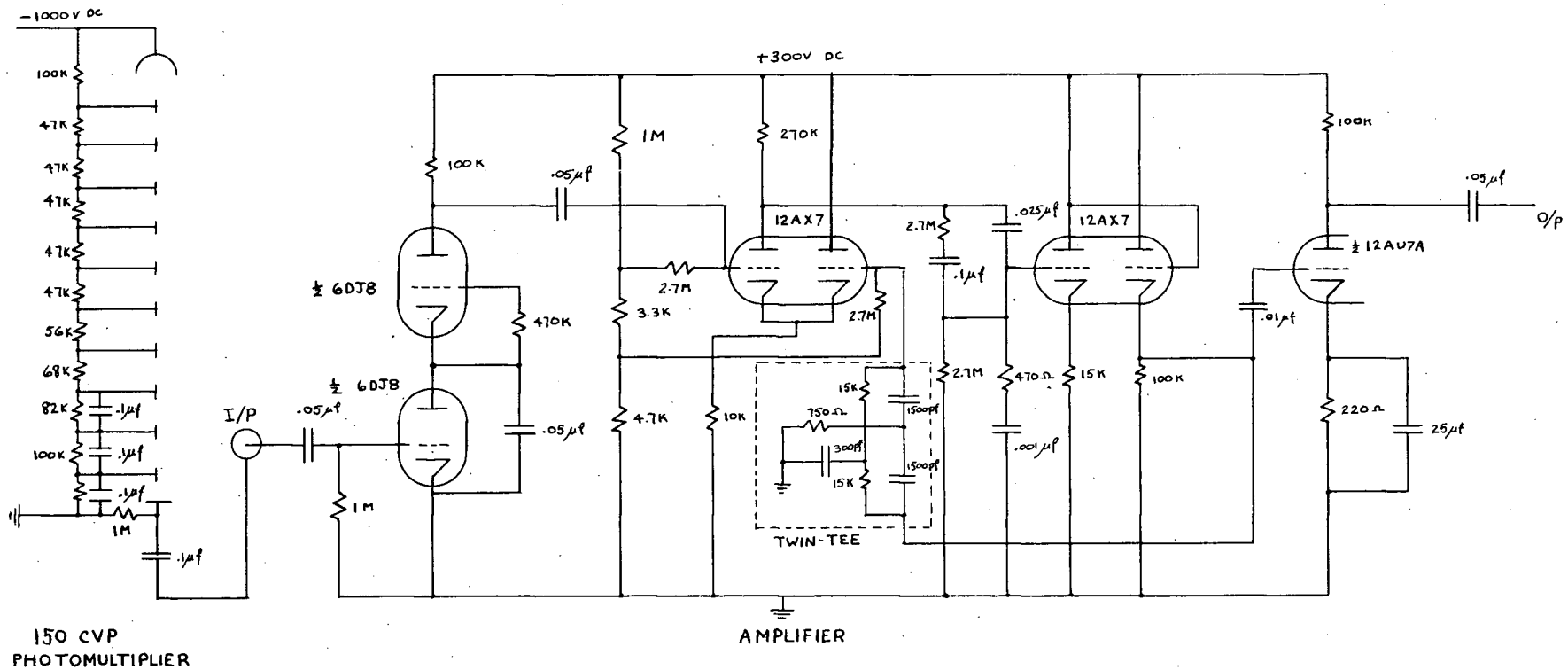
Fig. 6. Photomultiplier and Amplifier Circuit
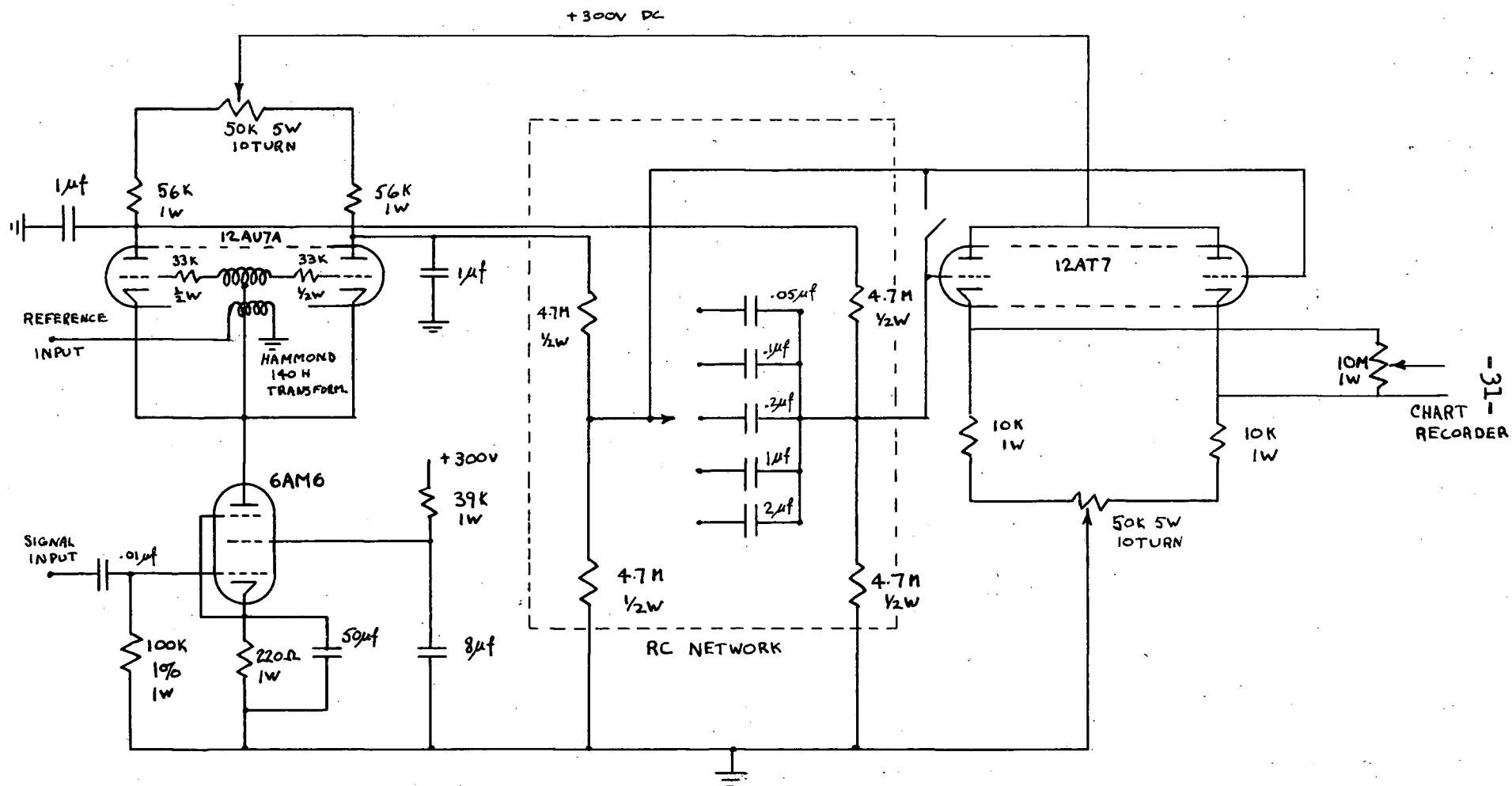
Fig. 7. Phase—Sensitive Detector Circuit

to-noise ratio at the output of the amplifier. Thus the detector acts essentially as a frequency-mixer which filters out all the resulting signals except the difference-frequency signal, which in this case happens to be a dc signal.

The reference voltage was generated by a 6v tungsten lamp illuminating a Philips OCP-71 photo-transister. The intensity was strong enough to saturate the photo-transister making the output voltage independent of variation of lamp illumination. The two components were mounted as a unit, but with the rotating disk intervening and modulating the light, as indicated in Fig. 4. The resulting square-wave signal was sent through a low-pass filter and re-shaped into a 1.4v rms sine-wave before entering the phase-sensitive detector. The phase difference between the reference signal and the signal from the amplifier could be adjusted for maximum detector output by mechanically rotating the lamp-photo-transister unit around the axis of the disk. One-seventh of a revolution was necessary for a phase-shift of 360°.

The linearity of the intensity-measuring circuit (photomultiplier, amplifier, phase-sensitive detector, and chart recorder) was measured using a 6-step neutral density filter which had transmissions varying from .06 to 1. For maximum rms voltages into the amplifier and phase-sensitive detector of 4 mv and 90 mv respectively, the system was linear to within 2%.

The entire system, including the intensity of radiation from the Geissler tube, was stable to within 3% over periods of 5 minutes or more.

3.2   Experimental Method

The procedure followed in determining absorption coefficients and oscillator strengths is outlined in the following paragraphs.

3.2.1   Circular Apertures

The circular apertures were used in conjunction with the 13 mm inner diameter absorption tube and the transmission of the gas determined for the six lengths at each diameter of aperture.   The diameters were varied from 3 mm to 13 mm in steps of 1 mm.

For a particular discharge length the transmission is determined as the ratio of the intensity of the modulated light from the source when the gas in the absorption tube is excited to the intensity when the gas is not excited. From this data of T as a function of R, R^2T can be plotted as a function of R^2 from which is to be calculated the slope $d(R^2T)/d(R^2)$ at some value of R. For this purpose, an IBM 7040 digital computer was employed to process the data and determine a least-squares fit of a second-order polynomial to the experimental points. The slope of this curve determined $d(R^2T)/d(R^2)$. A second order polynomial was chosen as it fitted the points fairly well and was simple; an example is shown in Fig. 8 of the experimental points and the calculated polynomial.

$\lambda = 5852$

$I_a = 10\,ma$

$I_s = 7\,ma$

$T R^2 = a_1 + a_2 R^2 + a_3 R^4$

$a_1 = -.1231\ (mm)^2$

$a_2 = .1366$

$a_3 = .005184(mm)^{-2}$
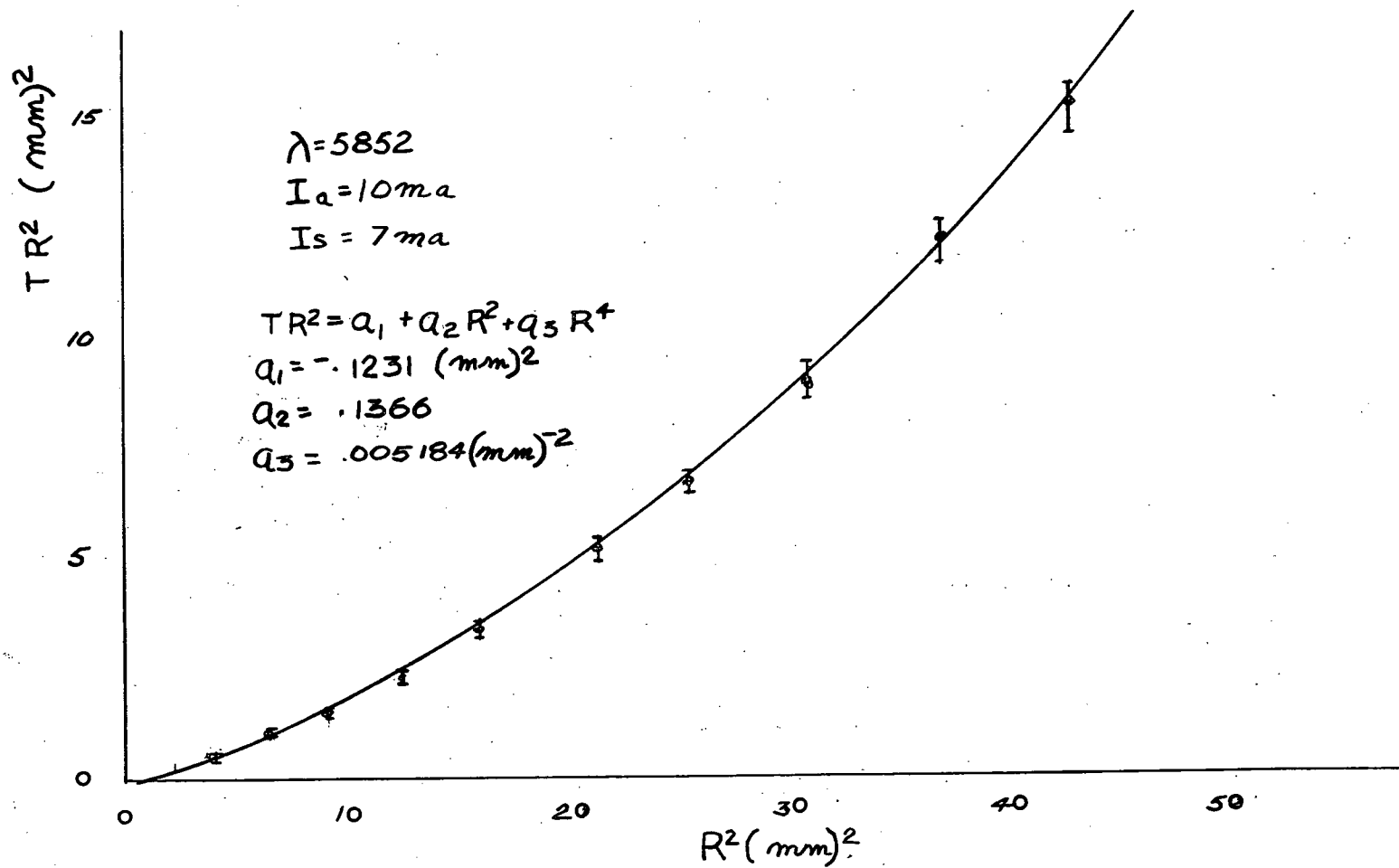
FIG. 8 POLYNOMIAL FIT OF $R^2 T$

This procedure is repeated for all six discharge lengths and a plot at a particular R of $d(R^2 T)/d(R^2)$ against log (ℓ) prepared. This differs from a plot of equation (2.9) as a function of log $(k_o \ell)$, as shown in Fig. 3, by the additive constant log (k_o). By shifting the two plots along their abscissae the theoretical curve may be found which best fits the experimental points. The curve found in this manner determines α, and the origin shift determines k_o. Thus the problem of determining the two unknowns from equation (2.9) is solved by using more than one length; six lengths allows a quick averaging graphical solution.

In this manner k_o and α were measured for each of the four series of lines; a series consists of those lines with a common lower level. The excitation current in the absorption tube had values varying from 2 to 12 ma during the course of these trials while the current in the source was kept at a constant 7 ma.

Some of the lines were extremely highly absorbing with transmissions as low as 2%. For these lines the accuracy of the measurement of T was increased by the use of an optical attenuator. This consisted of Kodak Wratten gelatin "neutral density" filters which were used to attenuate the background signal when no absorption was taking place. The sensitivity of the chart recorder was then changed until full deflection was achieved. When absorption occurred upon switching on the excitation current in the absorption tube, the filters were removed increasing the otherwise small deflection of the

recorder due to the transmitted light.

The filters were not truly neutral and the transmission
had to be measured at each wavelength for which they were used.

3.2.2   Annuli

Using the circular apertures, the transmission of
some of the highly absorbing spectral lines was less than
2%. Most of the absorption occurs near the axis of the dis-
charge tube where the atom density is higher (see section 5.2.1).
For such lines, the annulus method is useful because the region
near the axis is avoided. Conversely, more accurate measure-
ments may be performed on weakly absorbing lines by using the
circular apertures. As well, use of the annuli affords a
means of confirming the values of the transition probabilities
measured with the circular apertures.

The larger diameter absorption tube was used with an
annulus at each end and determinations of k_o made. Over a
number of measurements the current in the absorption tube was
varied from 1 to 10 ma, and the current in the source, from
5 to 9 ma. For a given set of conditions the transmission was
measured 3 times for each wavelength and an average transmission
calculated. The procedure followed to analyse the data using
the annuli was simpler than with the circular apertures; a plot
of T against log (l) was compared with the theoretical curves,
eliminating the necessity of measuring slopes from the
experimental T's.

CHAPTER 4   EMISSION EXPERIMENT

4.1   Measurement of Relative Intensities

In measuring intensities the error due to self-absorption may be eliminated either by correcting for self-absorption when the value of the absorption coefficient is known (see for example, Irwin /12/), or by lowering the gas density so the self-absorption is negligible.

Once self-absorption has been eliminated or allowed for, the variation in response of the detecting apparatus with wavelength must be taken into account. "Non-flat" response requires a calibration against a standard lamp of known spectral variation. In this case a tungsten strip filament lamp was used.

The output from the photomultiplier can be written $i(\lambda) \approx G(\lambda) \, S(\lambda) \, T(\lambda) \, P(\lambda)$ where G is a factor which accounts for the geometry of the system, S represents the sensitivity of the detector, T the transmission of the monochromator, and P the power emitted by the source. If two different sources are compared, the ratio of their power outputs at a particular wavelength can be determined by measuring the ratio of the photomultiplier outputs without knowledge of S or T. If the ratio of the P's at two different wavelengths of one source is required it may be measured if the P ratio for the other source is known.

Absolute calibration of a light-detector and deter-

mination of spectral output of a continuous light source has been described by Christensen and Ames /24/. Their theory relevant to intensity determinations is given in Appendix 4, with modification for unequal monochromator entrance and exit slits. The results of the analysis show that if the relative response of the detector at two wavelengths to the line radiation is designated R_ℓ (λ_1, λ_2) and the corresponding ratio for a continuous source is $R_c(\lambda_1, \lambda_2)$ then

$$\frac{R_\ell(\lambda_1, \lambda_2)}{R_c(\lambda_1, \lambda_2)} = \frac{I_\ell(\lambda_1) I_c(\lambda_2) K(\lambda_2) D(\lambda_1)}{I_\ell(\lambda_2) I_c(\lambda_1) K(\lambda_1) D(\lambda_2)} \qquad \ldots(4.1)$$

where I_ℓ and I_c are the intensities of the line and continuous sources, respectively, D is the dispersion of the monochromator, and K is a correction factor defined in the appendix which accounts for spectral variation of the continuous source, photomultiplier, and the monochromator transmission over the pass-band of the monochromator. In this experiment, K differs from one by an amount less than the estimated experimental error. The intensity I_ℓ includes the effect of self-absorption, if present, and must be corrected later.

For a tungsten lamp I_c can be written

$$I_c(\lambda) \equiv I_c(\lambda, T_t) = \mathcal{E}(\lambda, T_t)\, \mathcal{T}(\lambda)\, J(\lambda, T_t)$$

where $\mathcal{E}$ is the emissivity of tungsten, $\mathcal{T}$ is the transmission of the glass envelope surrounding the tungsten strip, T_t is

the temperature of the tungsten strip, and J is the blackbody spectral intensity. $\mathcal{C}$ changes very little over the range of wavelengths considered here and will be treated as a constant. Values of $\mathcal{E}$ have been measured for tungsten by de Vos /25/ and Larrabee /26/ for different λ and T_t. Although the values given in these two references differ by a few percent the ratios $\mathcal{E}(\lambda_1,T_t)/\mathcal{E}(\lambda_2,T_t)$ agreed to within .5%, and in fact were at most about 2% from the value of unity over the wavelength range 5800Å - 7000Å.

Thus equation (4.1) becomes

$$\frac{R_\ell(\lambda_1,\lambda_2)}{R_c(\lambda_1,\lambda_2)} = \frac{I_\ell(\lambda_1)\,\mathcal{E}(\lambda_2,T_t)\,J(\lambda_2,T_t)\,D(\lambda_1)}{I_\ell(\lambda_2)\,\mathcal{E}(\lambda_1,T_t)\,J(\lambda_1,T_t)\,D(\lambda_2)} \qquad \ldots(4.2)$$

from which $I_\ell(\lambda_1)/I_\ell(\lambda_2)$ may be calculated.

4.2 Preliminary Intensity Measurements

Initially it was thought that the intensity measurements could be made using the absorption tube as an emitting source, with corrections for self-absorption being determined from the measured values of k_o. Apart from the fact that the optical arrangement required for these measurements was extremely critical with respect to alignment, it turned out that the uncertainty in the value of k_o rendered the results unsatisfactory (see section 5.4.1).

The alternate method of using a discharge tube with no self-absorption was then attempted but it was found that self-absorption could not be eliminated. This preliminary experiment is described here, for although no "true" relative intensities resulted, it pointed out the difficulties involved in making intensity measurements.

Two neon sources were used. One was a discharge tube similar to the narrow absorption tube but with windows mounted perpendicular to the axis so that the discharge could be viewed transversely. This gave a discharge thickness of about 1 cm. The other source was the Geissler tube used as a background source in the absorption experiment.

The source was mounted behind the modulating chopper and imaged on the slit of the spectrograph. Beyond the source was a General Electric "Sun Gun" photographic tungsten lamp for calibrating the spectral response of the system.

Only one pair of spectral lines was investigated thoroughly. It was chosen because of the low absorption of each line, and because both transitions started from the same upper level (see equation (2.14)). The lines were $\lambda6678$ and $\lambda6096$.

First the side-on tube was used and the centre of the discharge investigated. As the discharge current was reduced from 5 ma to 1 ma in steps of 1 ma the relative response to the two spectral lines was measured at each step. If self-absorption was not present, the relative response should be independent of current. The relative response of the equipment

to the continuous radiation source was measured at these two wavelengths after each pair of line measurements. A change in this ratio would indicate a variation somewhere in the apparatus. No significant change was observed.

Two other procedures were attempted. The discharge tube operated at a current of 3 ma was moved perpendicular to the optic axis after each measurement so that succeeding measurements "saw" regions of the discharge further from the centre and nearer the cylindrical edge. Towards the outer regions, the discharge is less dense as well as being of smaller thickness. Because of this, the extreme edge of the discharge was examined where the discharge thickness is minimum as the current was again reduced in steps.

The Geissler tube was investigated in a similar manner except that only the centre of the tube was examined. Also the discharge extinguished at low currents and the intensities were measured only down to a current of 2 ma.

The reproducibility of all the measurements was extremely good. A variation between similar measurements never exceeded 2% and in most cases was less than 1%.

It was observed in all the above tests that the apparent relative intensities varied monotonically as the current or position of the discharge was changed. The total variation was approximately 10%. Fig. 9 shows a plot of the relative intensity as a function of current and discharge position.

The observed variation could have been due to the
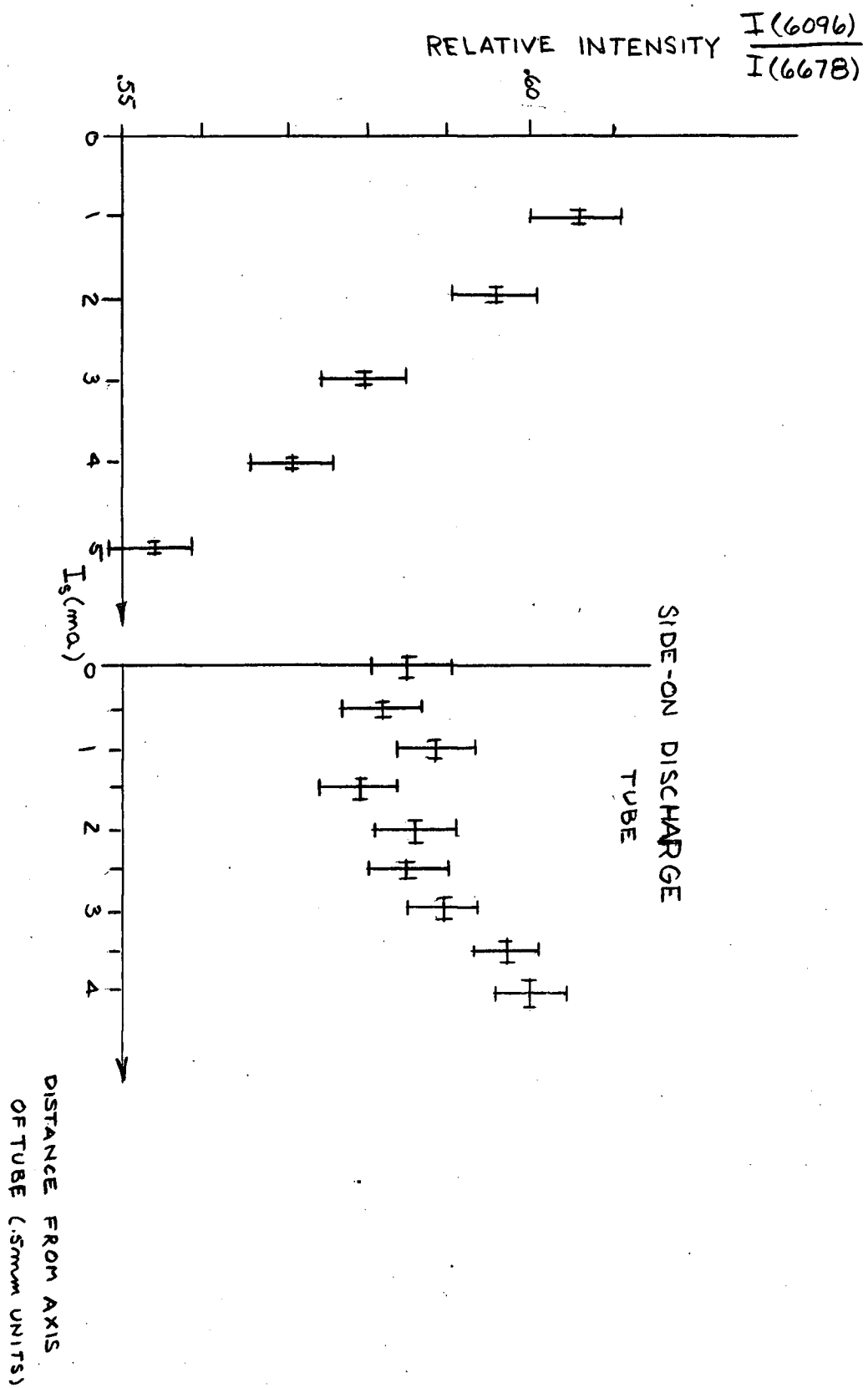
FIG. 9 RELATIVE INTENSITY OF λλ 6096, 6678

effect of self-absorption or stimulated emission. Irwin /12/
showed that stimulated emission is negligible for currents up
to 100 ma using a discharge tube similar to the side-on tube.
Ladenburg /7/ came to the same conclusion about a discharge
tube comparable to the Geissler tube used here. Thus the
observed effect must be due to self-absorption. It is also
to be noted that the variation of relative intensity is in
the direction consistent with λ6096 being the more highly
absorbing of the two lines. A decrease of the self-absorption
would increase the intensity of λ6096 by a larger proportion
than for λ6678 (see the table of self-absorption factors in
Appendix 3).

The inablility to eliminate self-absorption in the
sources prompted the use of a different type of source. The
details of the ensuing experiment are given below.

4.3   Final Intensity Measurements

The procedure finally adopted to ensure the absence of
self-absorption was to measure the emission from low density neon
which had only been in the excited state for a short time. The
low density combined with the short excitation time ensured that
the excited state population densities was small. Thus the
probability of absorption of radiation by atoms in an excited
state was small.

Because the density is low, the emission intensity is
also low and the problem consists of counting individual photons.

The average photon flux is equal to the intensity. The counting requires somewhat sophisticated apparatus and techniques which are described below.

4.3.1 Apparatus

This particular apparatus and the general techniques have been developed for lifetime measurements by van Andel /17/ who helped perform this experiment. As the apparatus is described by him in detail, only a cursory description will be given here.

.1 Sampling Technique

An electron gun situated within a bakable, ultra-high vacuum system was used to excite the neon gas which was at a pressure of .1 mm Hg. The gun was pulsed 485 times per second with a pulse duration of 200 nsec, and radiation from the emitting neon was observed with a grating monochromator and a photomultiplier. The resultant signal from the continuously monitoring RCA 7265 photomultiplier was sampled 20 nsec after the cessation of each pulse with a sample width of 0.3 nsec. The sampling was performed with a Tektronix 661 oscilloscope, which puts out a voltage proportional to the height of the sampled photomultiplier signal and was followed by an amplifier, discriminator and digital counter. The purpose of the discriminator was to isolate the counter from pulses below a certain

voltage; in this manner pulses originating from noise in the sampling circuit was eliminated. Counts were recorded over a period of ten seconds and yielded the number of samples which contained a signal. This signal indicated the arrival of one or more photo-electron pulses at time of sampling.

.2   Monochromator

The monochromator was built by van Andel /17/ for his experiment, and is a 42" focal length Ebert mount with a 6" by 8" concave grating having 300 lines/mm. The reciprocal dispersion is approximately 4 Å/mm in the fifth order and the theoretical resolving power is 300,000. Appropriate Corning filters were used to isolate the fifth order and gave an effective pass band from 5500 Å to 7500 Å. To guard against errors in positioning the spectral line image in the exit plane of the monochromater, the exit slit width was 1.75 mm and the entrance slit width 1.25 mm for all measurements. The unequal widths ensured that the image of the entrance slit was always encompassed by the exit slit.

.3   Spectral Calibration

The spectral response of the system was measured using a G. E. 6v-9A tungsten strip filament lamp placed approximately at the position occupied by the electron gun with the filament focused on the monochromater slit. The current through the lamp was 5 amps and the temperature of the tungsten

was calculated by measuring the brightness temperature with a
Hartmann and Braun filament pyrometer and then calculating
the true temperature by the method given by Rutgers and de Vos
/27/. The pyrometer in turn had been calibrated at two tempera-
tures, 1800°K and 1340°K, with a G. E. tungsten ribbon filament
standard lamp, type T-24 86-P-50. The pyrometer was found to
agree within one per cent of the calibration temperatures.
Unfortunately the standard lamp itself was too large to be used
directly to measure the response without serious modification of
the equipment.

Initially the standard source was the G. E. "Sun Gun"
used in the preliminary intensity experiment described in section
4.2. Upon measuring the intensity distribution of the Sun Gun
over the range 5800Å to 6800Å in 50Å steps, it was found that a
dip of approximately 5% in the distribution occurred at 6000Å
with a width of 100 Å. The operating voltage of the lamp for
this measurement was only 20v dc as opposed to the rated 120v dc
which had been used in the preliminary measurements. It is not
known whether this dip is present at the higher voltage as no
further investigations were made. The cause of this dip is
also uncertain; possibly it is caused by the gas(iodine)
contained in the envelope surrounding the tungsten filament for
purposes of cleansing. The strip filament lamp finally used
showed no such dip.

4.3.2   Experimental Method

The transition probabilities calculated by absorption are divided into four groups corresponding to the four lower levels on which all the spectral lines terminate. To relate the probabilities between any two groups the relative intensity of two common upper-level lines must be measured, one in each group (see equation (2.14)). The simplest way to relate all four groups is to choose one line from each group with each line having the same upper level.

In this experiment the choice of lines was governed by desireability of a high signal-to-noise ratio for the lines measured as well as the necessity of choosing from a particular group a line that had been measured in absorption. For these reasons it was not possible to choose one upper level common to the four groups and instead three separate pairs of lines were chosen to link the four groups together. They were $\lambda\lambda 6096$, 6678 (s_4 and s_2); 6163, 6599 (s_3 and s_2); 6334, 6506 (s_5 and s_3). (The level designations are in the Paschen notation (see section 5.1). Three other lines from the p_7 level were measured to give two independent self-consistancy checks; they were $\lambda\lambda 6217$, 6383, and 6533. Fig. 10 shows a partial term diagram indicating the transitions.

The intensities of the three pairs of lines were measured one pair at a time; the monochromator was set on the first line, and three ten second counts were recorded before proceeding on to the next line of the pair. This was repeated
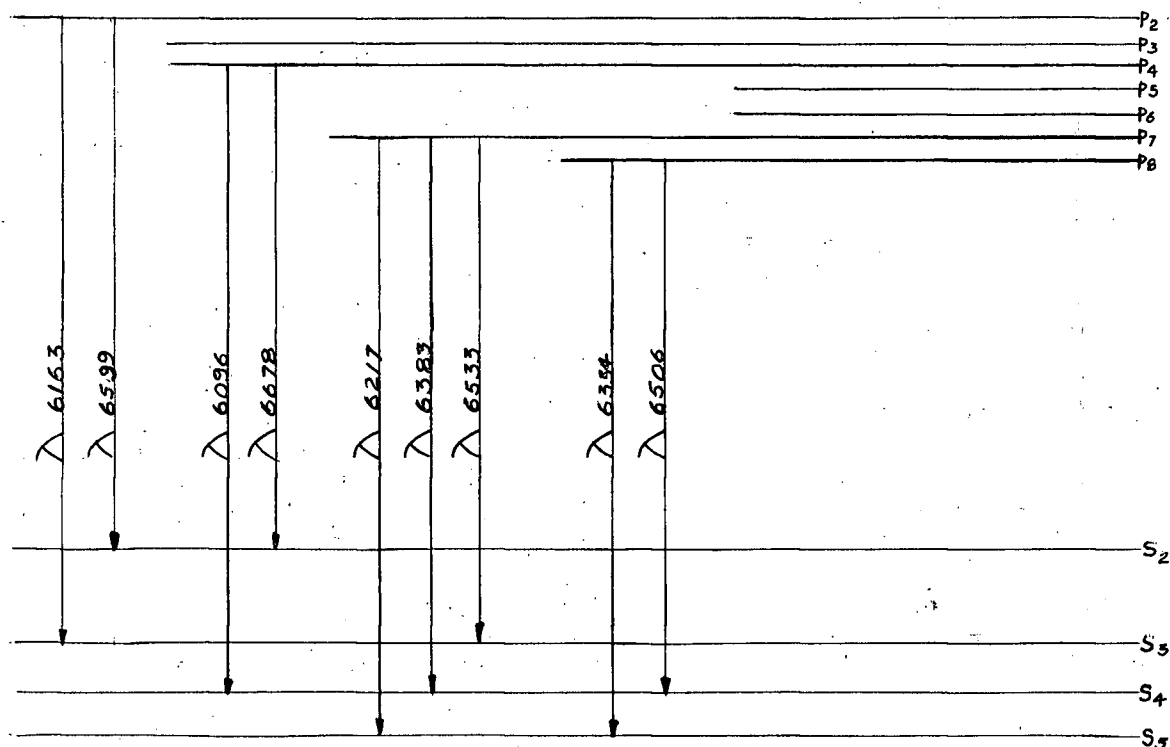
Fig. 10   Partial Term Diagram of Neon;   Intensity-
Measurement Transitions

ten times and the ratio of sums of the counts calculated as the

measured relative intensity, to be corrected for instrument

response to get the true relative intensity.   This procedure was

repeated twice more for each pair;   similar measurements were

made on the p_7 lines.

Error counts due to stray room light, photomultiplier

noise, and continuum light from the glowing cathode of the

electron gun had to be subtracted from the neon counts by

observing the counts at a time 5 microseconds after the excita-

tion pulse, when the neon excitation had decayed.

For calibrating the spectral response of the system,

an analogous procedure is followed.   The signal due to the tungsten

lamp was sampled and counted over a ten second period at each of the wavelengths for which neon measurements were made. Stray light and noise counts were made by blocking off the lamp. Fig. 11 shows the response of the system to the radiation from the tungsten lamp. $R_c(\lambda_1, \lambda_2)$ may be computed from this curve.

One of the basic systematic errors of counting methods is pile-up error; with this particular counting apparatus there can occur essentially two types of pile-up error and they will now be described.

Pile-up is the overlapping of two pulses. Consider what happens if the discriminator level is set high and the signal is sampled at a time when two pulses overlap at the anode of the photomultiplier. If individually these pulses have a height greater than one-half but less than one times the discriminator level no count is registered for separate arrival. Added together they will register a count of one, whereas there should be no count; if the intensity is assumed proportional to the count, the apparent intensity is greater than the true intensity. On the other hand, if the discriminator is set low, the arrival of the two overlapping pulses will again register as one count, although arriving separately they should give a count of two, so the apparent intensity is less than the true intensity. If the level is set low enough, the number of pulses of height less than the discriminator level is small, and the former pile-up case occurs infrequently. In both cases the error increases as the apparent count increases.

Thus for all measurements the discriminator level was
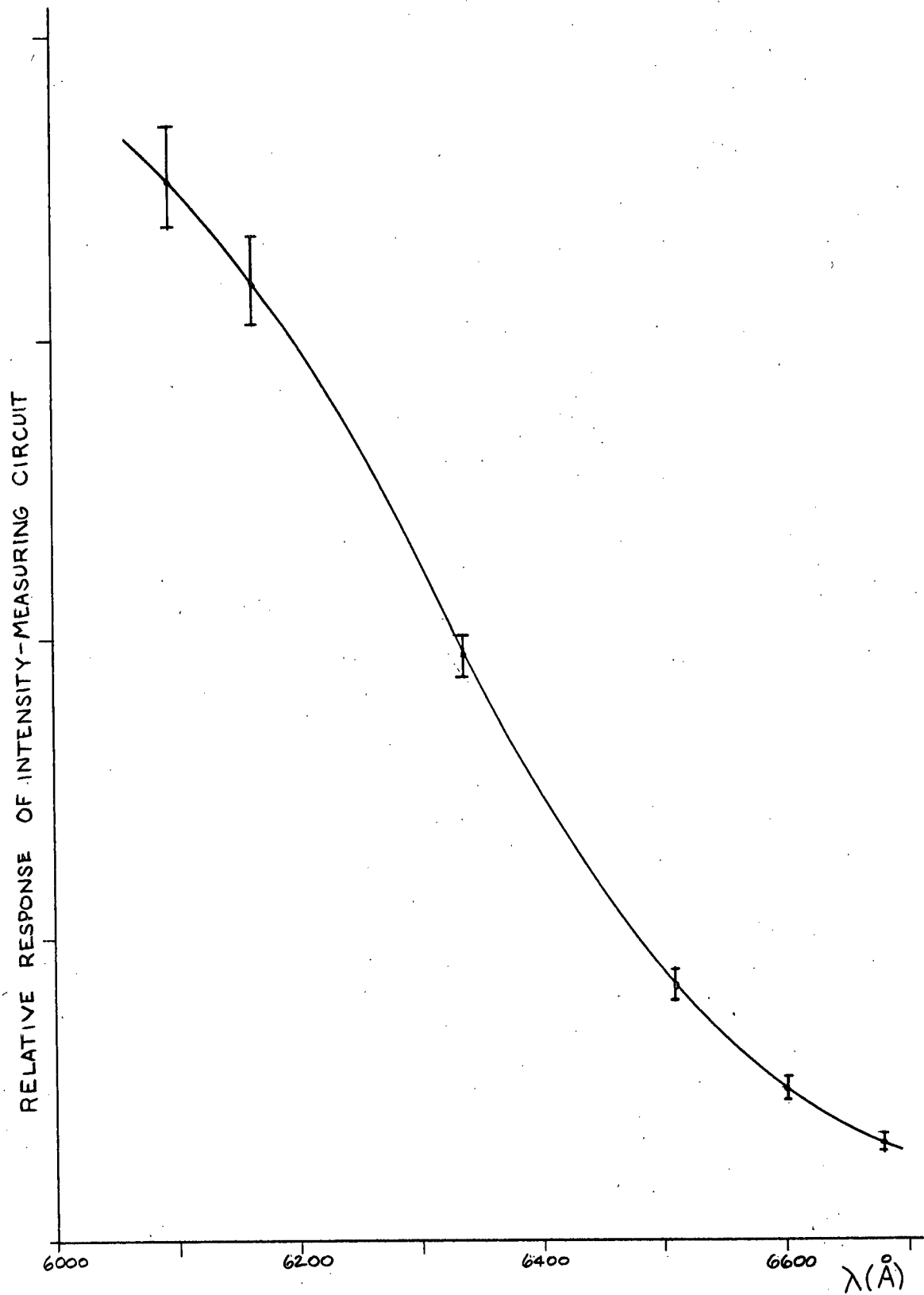
Figure 11   Relative Response of Intensity-
Measuring Circuit

kept low and the count small compared to the number of samples (4850 per 10 seconds). The neutral density filters from the absorption experiment were used on the especially "bright" lines to keep the count below 250 per 10 seconds.

The presence of pile-up at high counts was apparent when the transmission of one of the filters was measured on the apparatus. When the unfiltered count was approximately 250 per 10 seconds the transmission agreed to within 1% of the value as measured on the absorption apparatus. On the other hand an upward deviation of more than 5% was observed when the unfiltered count was approximately 700 per 10 seconds. The estimated accuracy of the transmission as measured with the absorption apparatus is about 2% so at 250 counts per 10 seconds the counting apparatus is linear.

CHAPTER 5   RESULTS AND DISCUSSION

For discussion of the results, it is appropriate to begin with a short discussion of the neon term scheme and spectra. Following this, the results are presented in two sections, one pertaining explicitly to the absorption experiment and the other to the emission. The final section of this chapter concludes with a combination of the two previous sections and presents final results. A general discussion is given in each section on the significance of the results and the validity of the theory. Errors and estimation of the accuracy of the results are also discussed.

5.1   Neon Spectrum

Thirty spectral lines emitted by neon in the visible and infra-red region result from transitions between the first and second excited states of the atom, $2p^5 3s$ and $2p^5 3p$. Fig. 12 shows the allowed transitions with the corresponding wavelengths given in Ångstroms; the full lines represent transitions on which measurements were taken in this experiment. The designation of the levels is given in both the LS /28/ and the Paschen /29/ notation; the latter notation will generally be used here.
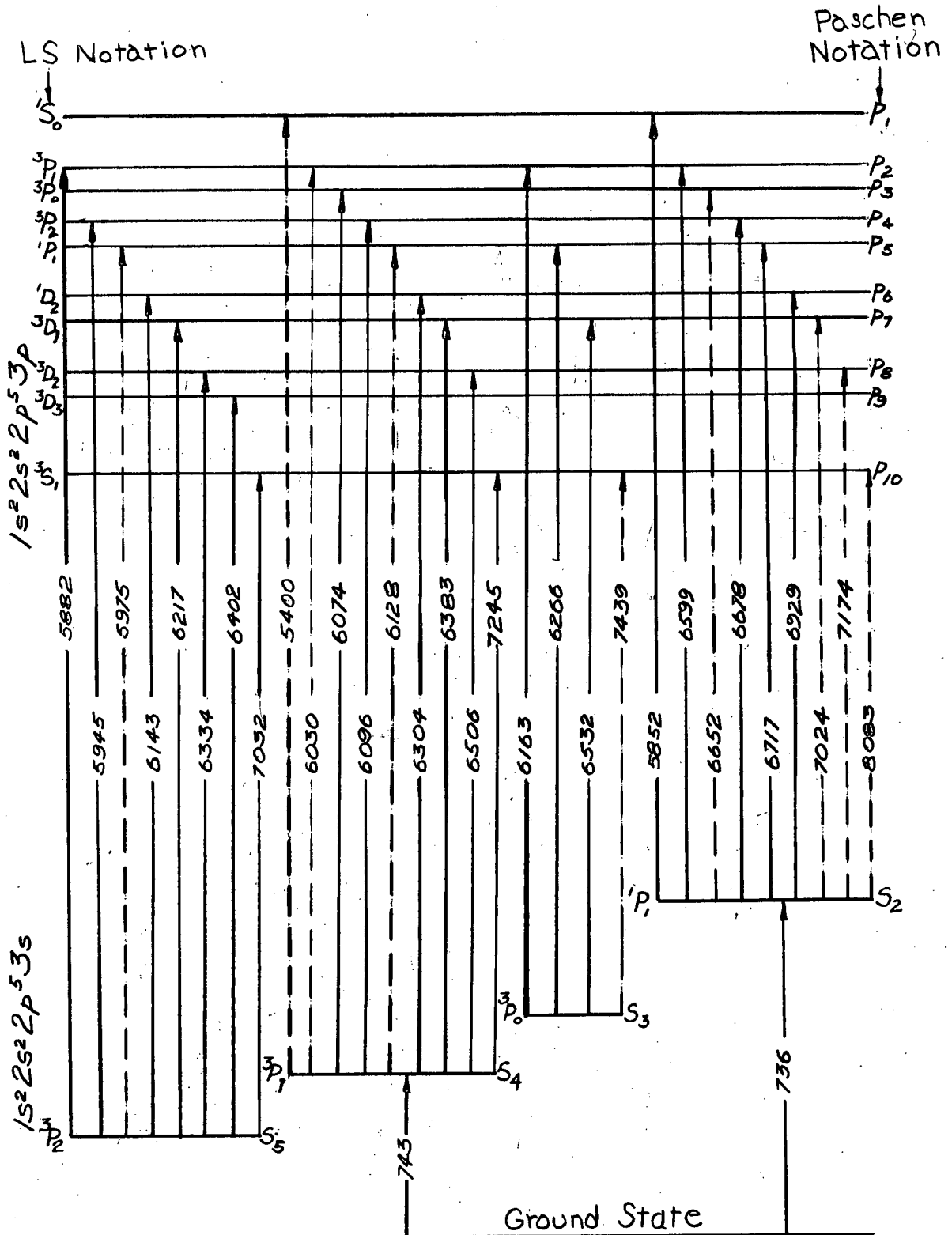
Figure 12   Neon Term Diagram;

First and Second Excited State Configuration

5.2 Absorption - Circular Apertures

As was mentioned in section 3.2.2, the circular aperture method was more applicable experimentally for lines showing small absorption. The s_2 lines were generally less absorbing than the other lines by a factor of three or more and were measured only by this method. Measurements were also made on some of the other groups of lines.

5.2.1 Cross-Sectional Variation of Transmission

If both N_1 and T_a are constant over the cross-section of the absorbing column, equation (2.3) shows that the transmission T should not vary as R, the radius of the apertures, is varied. Fig. 13 shows a typical plot of the transmission of the absorbing gas as a function of R, for the various discharge lengths. It can be seen that the shape of these curves are similar for each length, decreasing monotonically towards the centre of the tube with a corresponding tendency to level off. The curves for the other spectral lines behaved in the same manner indicating that conditions are definitely not constant over the cross-section of the absorbing column. The transmission should increase with R if N_1 decreases. Whether it increases with decreasing T_a depends on the value of k_o and α but roughly speaking an increase occurs if $k_o \ell$ is "large" and a decrease if $k_o \ell$ is "small". There is reason to believe however, that the observed increase in transmission is caused
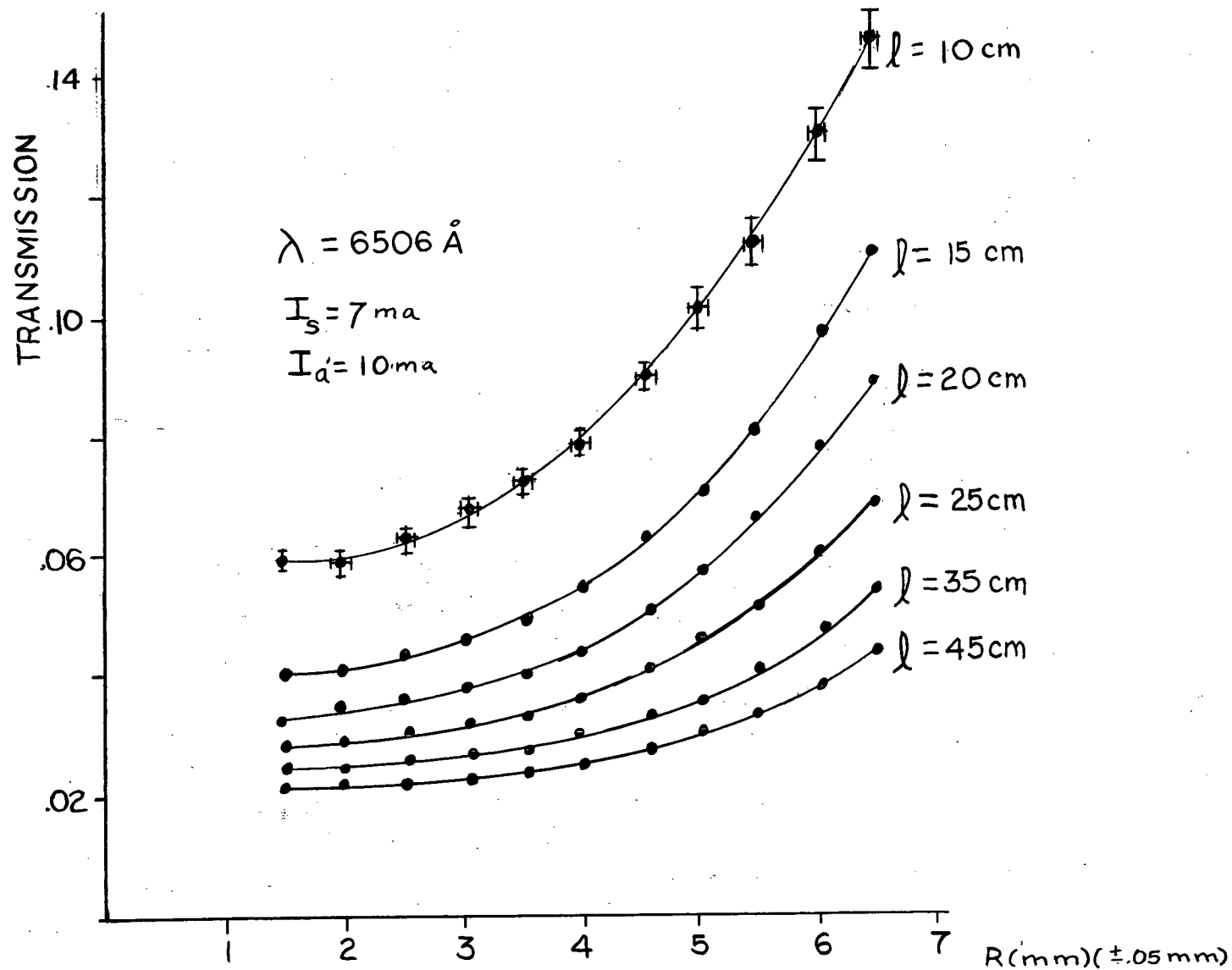
FIG 13   TRANSMISSION AS A FUNCTION OF R

$\lambda = 6506 \, \mathring{A}$

$I_s = 7 \, ma$

$I_a' = 10 \, ma$

$\ell = 10 \, cm$

$\ell = 15 \, cm$

$\ell = 20 \, cm$

$\ell = 25 \, cm$

$\ell = 35 \, cm$

$\ell = 45 \, cm$

TRANSMISSION

R(mm)(±.05 mm)

-55-

wholly by a decrease in N_1 (see discussion in section 5.4.1).

5.2.2   Curve Fitting

For the process of fitting the six values of $d(R^2T)/d(R^2)$ corresponding to the six absorption lengths to the theoretical curves (see section 3.2.1 and equation (2.9)), the slopes were calculated as a function of R, as R was varied from the minimum to the maximum diameter of aperture used, in steps of .5 mm. Generally some portion of the theoretical curves could be found which fitted the six points well although in some cases the six points showed scatter at large R (5.5 to 6.5 mm) and the fit was not as good. Fig. 14 shows an example of curve fitting where the curves of Fig. 3 are partially redrawn and the experimentally determined slopes of λ6164 for R = 4 mm, I_a = 10 ma are superimposed. a), b), and c) show fittings to the curves corresponding to α = .5, .7, and .9 respectively, with the best fit being for α = .7 giving $k_o \approx$ .245 cm^{-1}. Generally the uncertainties in estimating α and k_o from the theoretical curves were no greater than about 10% and 5% respectively. It can be seen from Fig. 3 that the curves are closely spaced for small values of $k_o \ell$, and for large $k_o \ell$ at values of $\alpha \lesssim 1$. In these regions a less precise value of α is determined.

Curve fitting was also attempted using the data of T versus log(ℓ) at a particular aperture radius. It was found that a reasonably good fit could be made but the values of α and k_o were much different from the values determined using
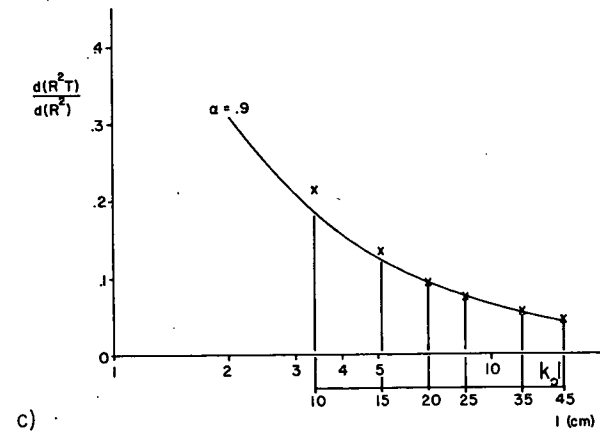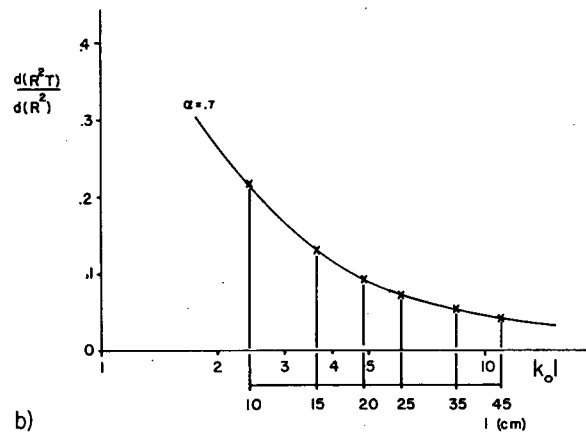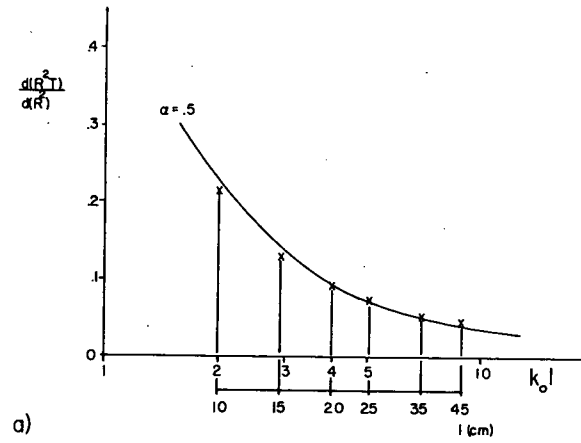
Fig. 14   Curve Fitting

$d(R^2 T)/d(R^2)$. The values of f_{rel} calculated this way were effectively the same.

5.2.3   Relative Oscillator Strengths

The relative oscillator strengths f_{rel} can be computed from equation (2.11). In this section these quantities are calculated and are converted in section 5.6 to transition probabilities.

Tables 1 - 4 list the values of f_{rel}, k_o, and α for the s_2, s_3, and s_4 lines as a function of R for various I_a. The absorption by the s_5 lines was generally greater than 90% and the experimental points did not fit the theoretical curves well so these quantities could not be determined by the circular aperture method. Fig. 15 shows some of the data for f_{rel} from Table 1 in graphical form. The error bars represent maximum possible errors due to the fitting to the theoretical curves; in most cases the best fit occurred at the same value of α for lines with the same lower level and under the same operating conditions. Sometimes it was difficult to tell which curve fitted best; in this case the average values of k_o and α were taken from the curves for which the fit was not unreasonable. It was found that even calculating f_{rel} using values of k_o determined from curves for which the fit was definitely poor, the deviation of f_{rel} from the best-fit curves was not more than 10% and often much less. The deviation of α between the best-fit and poor-fit curves was as high as 30% and indicates a slow

TABLE 1 CIRCULAR APERTURE DETERMINATION OF f_{rel}: s_2 LINES, $I_s=7ma$

I_a (ma)	R (mm)	$\lambda(\text{Å})$ 5852	6599	6678	6717	6929
6	2.0	1.00	1.32	2.23	1.34	2.02
	2.5		1.30	2.22	1.31	1.99
	3.0		1.29	2.22	1.31	1.97
	3.5		1.28	2.18	1.27	1.87
	4.0		1.26	2.13	1.23	1.82
	4.5		1.19	2.06	1.17	1.71
	5.0		1.10	1.92	1.10	1.51
Average			1.25	2.14	1.25	1.85
10	1.5	1.00	1.10	2.15	1.22	1.72
	2.0		1.10	2.17	1.24	1.72
	2.5		1.09	2.17	1.22	1.68
	3.0		1.13	2.19	1.20	1.72
	3.5		1.10	2.11	1.19	1.69
	4.0		1.10	2.04	1.18	1.65
	4.5		1.16	2.10	1.14	1.67
	5.0		1.14	1.97		1.60
Average			1.12	2.11	1.20	1.68
10	2.0	1.00	1.19	2.06	1.21	1.76
	2.5		1.18	2.04	1.18	1.74
	3.0		1.18	2.04	1.19	1.74
	3.5		1.18	2.05	1.18	1.74
	4.0		1.18	2.05	1.17	1.74
	4.5		1.17	2.05	1.18	1.74
Average			1.18	2.05	1.18	1.74
12	2.0	1.00	1.25	2.02	1.21	1.78
	2.5		1.24	2.04	1.20	1.76
	3.0		1.24	2.01	1.20	1.75
	3.5		1.23	2.02	1.19	1.74
	4.0		1.23	2.03	1.19	1.73
	4.5		1.22	2.04	1.18	1.73
	5.0		1.21	2.05	1.17	1.76
	5.5		1.20	2.05	1.16	1.74
	6.0		1.18	2.06	1.13	1.73
Average			1.22	2.04	1.18	1.75
Total Average			1.19	2.08	1.20	1.75

TABLE 2   CIRCULAR APERTURE DETERMINATION OF

k_o, α : s_2 LINES, $I_s = 7$ ma

I_a (ma)	$\lambda(\overset{\circ}{A})$ R(mm)	5852		6599		6678		6717		6929	
		$k_o(cm^{-1})$	α	$k_o(cm^{-1})$	α	$k_o(cm^{-1})$	α	$k_o(cm^{-1})$	α	$k_o(cm^{-1})$	α
6	2.0	.020	0.9	.032	1.0	.0495	0.85	.031	0.9	.0525	1.05
	2.5	.024	1.3	.031	1.1	.050	1.0	.032	1.1	.053	1.2
	3.0	.025	1.5	.034	1.4	.050	1.15	.033	1.3	.0525	1.35
	3.5	.0230	1.55	.0350	1.65	.0505	1.35	.0335	1.55	.0495	1.5
	4.0	.0235	1.85	.033	1.85	.051	1.65	.034	1.9	.047	1.7
	4.5	.0198	1.85	.0293	2.0	.0465	1.85	.0275	1.9	.0415	1.9
	5.0	.0175	2.0	.0277	2.05	.038	2.0	.021	1.9	.033	2.0
10	1.5	.052	1.05	.067	1.1	.113	0.9	.071	1.0	.103	1.0
	2.0	.050	1.1	.064	1.15	.114	1.0	.071	1.1	.098	1.05
	2.5	.052	1.25	.064	1.25	.113	1.1	.070	1.2	.098	1.15
	3.0	.050	1.35	.066	1.4	.114	1.25	.072	1.4	.089	1.3
	3.5	.050	1.5	.064	1.55	.116	1.45	.074	1.6	.096	1.45
	4.0	.050	1.7	.064	1.75	.111	1.6	.069	1.8	.091	1.6
	4.5	.046	1.9	.062	1.95	.108	1.9	.068	2.1	.087	1.8
	5.0	.040	2.0	.053	2.1	.095	2.05			.088	2.2
10	2.0	.043	1.15	.050	0.95	.0865	0.95	.054	1.0	.073	0.9
	2.5	.042	1.2	.053	1.15	.0855	1.05	.054	1.15	.078	1.1
	3.0	.046	1.5	.049	1.2	.084	1.2	.0555	1.35	.0775	1.35
	3.5	.044	1.65	.053	1.5	.084	1.4	.054	1.5	.076	1.4
	4.0	.0405	1.75	.0513	1.7	.081	1.55	.053	1.75	.074	1.6
	4.5	.0385	2.0	.0503	2.0	.075	1.75	.0523	2.0	.0715	1.85
	5.0	.0305	2.0							.062	2.05
	5.5	.0235	2.05								
12	2.0	.046	0.95	.0645	0.95	.093	0.8	.053	0.7	.085	0.8
	2.5	.047	1.1	.0635	1.05	.100	1.0	.060	1.0	.0865	0.95
	3.0	.045	1.2	.063	1.2	.0975	1.15	.0595	1.15	.0895	1.15
	3.5	.046	1.4	.063	1.4	.095	1.3	.0595	1.35	.088	1.3
	4.0	.0435	1.55	.061	1.6	.096	1.5	.059	1.55	.083	1.5
	4.5	.0405	1.75	.060	1.9	.091	1.7	.053	1.75	.079	1.7
	5.0	.037	2.0	.052	2.1	.0795	1.85	.0485	2.05	.071	1.9
	5.5	.0295	2.1	.044	2.4	.064	2.0	.035	2.1	.055	2.0
	6.0	.0238	2.5	.025	2.2	.045	2.0	.0225	2.05	.039	2.05

TABLE 3   CIRCULAR APERTURE DETERMINATION OF

f_{rel}: s_3 and s_4 LINES, I_s = 7ma

f_{rel}

I_a (ma)	$\lambda(\text{Å})$ R(mm)		s_3 LINES			
			6164	6266	6533	
10	4.0		1.22	1.73	1.00	
	4.5		1.24	1.71		
	5.0		1.20	1.85		
	5.5		1.14	1.96		
	6.0			1.91		
	6.5			2.08		
Average			1.20	1.87		

I_a (ma)	$\lambda(\text{Å})$ R(mm)	6074	6074	6096	6383	6507	7245
				s_4 LINES			
2	2.5	.714		1.00	1.16	1.69	.596
	3.0	.733	.745		1.16	1.65	.567
	3.5	.681	.744		1.16	1.71	.542
	4.0	.675	.696		1.15	1.68	.497
	4.5	.653	.678		1.18	1.70	.487
	5.0	.652	.644		1.17	1.74	.443
	5.5	.638	.626		1.16	1.69	.430
	6.0		.585		1.16	1.67	.391
	6.5		.546		1.20	1.69	
Average		.678	.658		1.17	1.69	.494
10	2.0			1.00	1.28		
	2.5				1.25		
	3.0				1.18		
	3.5		.74		1.20	1.55	.47
	4.0		.72		1.16	1.60	.46
	4.5		.72		1.16	1.59	.44
	5.0		.66		1.16	1.58	.43
	5.5		.66		1.12	1.59	.42
	6.0		.64		1.12	1.56	.40
	6.5		.65		1.11	1.60	.40
Average			.68		1.17	1.58	.43
Total Average			.673		1.17	1.64	.465

TABLE 4 CIRCULAR APERTURE DETERMINATIONS OF k_o, α : s_3 and s_4 LINES

$$I_s = 7 \text{ ma}$$

I_a (ma)	$\lambda(\overset{\circ}{A})$ R(mm)	s_3 LINES											
		6164		6266		6533							
		$k_o(cm^{-1})$	α	$k_o(cm^{-1})$	α	$k_o(cm^{-1})$	α	$k_o(cm^{-1})$	α	$k_o(cm^{-1})$	α	$k_o(cm^{-1})$	α
10	4.0	0.245	0.7	0.700	1.1	0.270	0.9						
	4.5	0.280	1.0	0.575	1.15	0.240	1.0						
	5.0	0.290	1.2	0.390	1.1	0.220	1.1						
	5.5	0.210	1.2	0.350	1.15	0.195	1.2						
	6.0			0.275	1.15	0.150	1.15						
	6.5			0.235	1.15	0.116	1.15						
		s_4 LINES											
		6074		6074		6096		6383		6507		7245	
2	2.0	.0935	0.45					0.163	0.5			0.093	0.35
	2.5	0.103	0.75			0.140	0.7	0.185	0.8	0.232	0.6	0.102	0.75
	3.0	0.114	0.95	0.110	0.9	0.148	0.9	0.182	0.95	0.260	0.9	0.112	1.0
	3.5	0.114	1.15	0.110	1.05	0.151	1.1	0.193	1.1	0.250	1.0	0.114	1.2
	4.0	0.106	1.25	0.098	1.15	0.151	1.2	0.170	1.15	0.230	1.1	0.106	1.35
	4.5	0.111	1.5	0.098	1.35	0.137	1.3	0.170	1.3	0.212	1.2	0.096	1.5
	5.0	0.093	1.55	0.083	1.45	0.121	1.4	0.148	1.4	0.200	1.3	0.076	1.55
	5.5	0.075	1.6	0.061	1.4	0.106	1.5	0.133	1.5	0.165	1.35	0.055	1.5
	6.0			0.046	1.45	0.084	1.5	0.098	1.45	0.135	1.4	0.039	1.5
	6.5					0.0615	1.45	0.079	1.5	0.103	1.35		
10	2.0					0.500	0.65	0.710	0.7				
	2.5			0.280	0.5	0.740	1.0	0.500	0.65			0.240	0.6
	3.0			0.280	0.7	0.720	1.1	0.520	0.85			0.250	0.85
	3.5			0.290	0.8	0.570	1.1	0.645	1.05			0.260	1.0
	4.0			0.270	1.0	0.450	1.1	0.500	1.05	1.00	1.2	0.245	1.1
	4.5			0.260	1.1	0.360	1.1	0.440	1.1	0.75	1.2	0.220	1.2
	5.0			0.230	1.2	0.300	1.1	0.430	1.2	0.55	1.15	0.205	1.3
	5.5			0.185	1.2	0.245	1.1	0.315	1.15	0.455	1.15	0.165	1.3
	6.0			0.150	1.2	0.205	1.1	0.280	1.2	0.375	1.15	0.130	1.3
	6.5			0.120	1.2	0.185	1.15	0.230	1.2	0.315	1.15	0.103	1.3
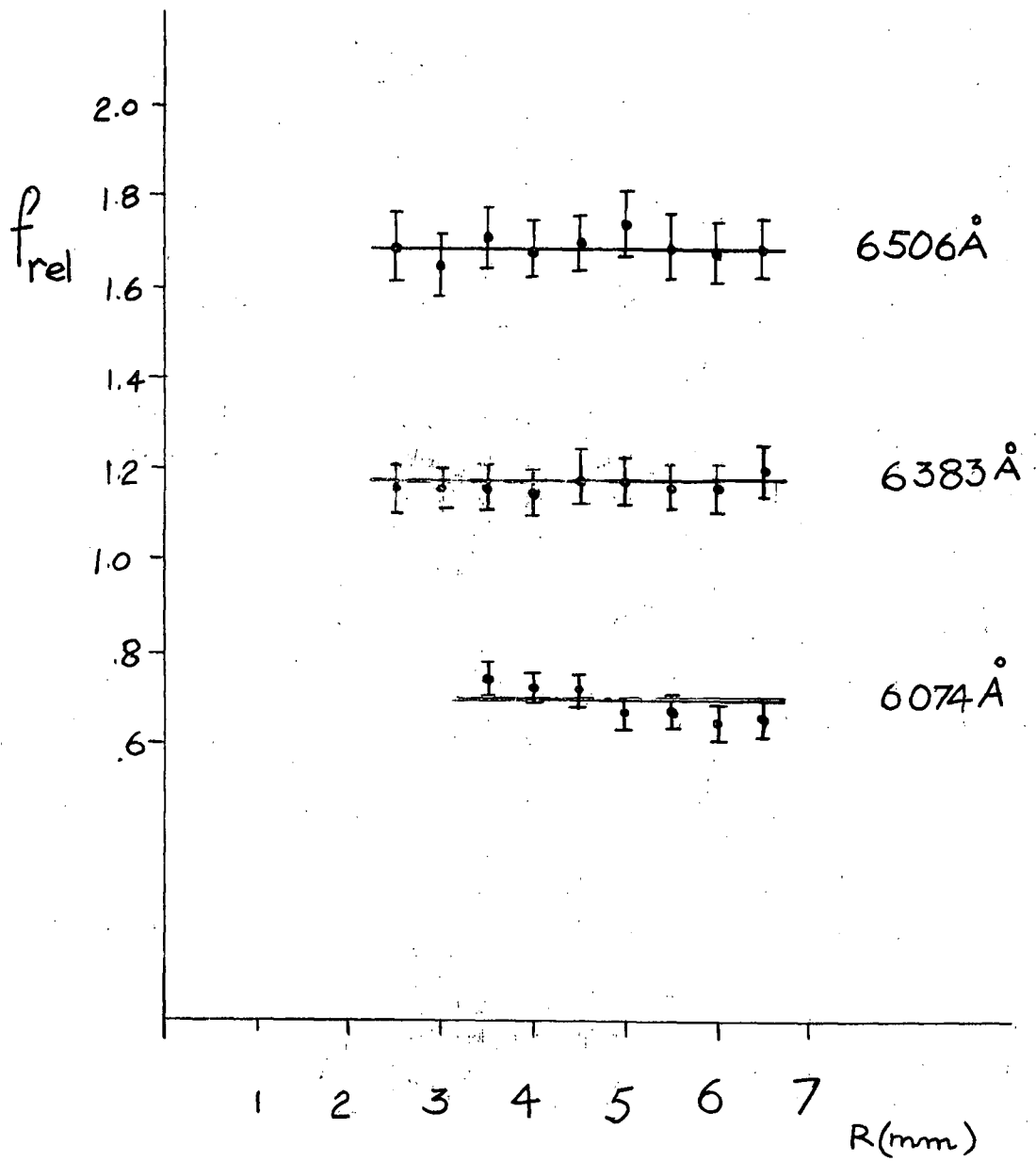
Fig. 15 f_{rel} as a Function of R

dependence of f_{rel} with α.

It can be seen upon comparing Tables 2 and 4 that the values of α are significantly higher for the s_2 lines than the other series. The pressure in the source was 5 mm Hg which is slightly higher than in the absorber. Lang /30/ has shown that pressure broadening of the s_2 lines is much more prevalent than the other lines; it is conceivable that if there is pressure broadening of the s_2 lines in the source the effective α measured could be higher than for other lines. The significance of the values of α obtained will be discussed in section 5.4.

5.3   Absorption - Annuli

The larger absorption tube was used with the annulus configuration. This allowed the transmission of the more strongly absorbing lines in the less dense regions away from the axis of the tube to be accurately measured. The absorption of the s_2 lines was consequently too small to measure accurately and fit to the k_o - α curves.

Tables 5 and 6 list the values of f_{rel}, k_o, and α for measurements made on the s_3, s_4, and s_5 lines for various values of I_a and I_s. It can be seen that there seems to be no definite systematic variation of f_{rel} with I_a or I_s. The remarks made previously concerning the fitting of the points to the curves (in the circular aperture method) are generally applicable here also. It was observed that in some trials, the experimental value of T was less than the theoretical value

TABLE 5 ANNULUS DETERMINATION OF

f_{rel}: s_2, s_4 and s_5 LINES

I_a (ma)	$\lambda(\text{Å})$ / I_s (ma)	f_{rel}: s_3 LINES		
		6164	6266	6533
8	7.6	1.19	1.82	1.00
10	7	1.21	1.88	
10	7	1.14	1.84	
10	7	1.18	1.83	

I_a (ma)	$\lambda(\text{Å})$ / I_s (ma)	f_{rel}: s_4 LINES					
		6074	6096	6305	6383	6507	7245
2	7				1.00	1.44	.401
4	7					1.44	.402
6	7	.592	.852			1.41	.423
8	7	.600	.860	.271		1.41	.448
8	7.6			.265			
10	7	.611	.869	.266		1.43	.440
10	7.6			.251			

I_a (ma)	$\lambda(\text{Å})$ / I_s (ma)	f_{rel}: s_5 LINES						
		5882	5945	6143	6217	6334	6402	7032
1	7.6	.347	.592	1.43	.244	1.00	2.79	.988
1	8						2.71	
2	7			1.38			2.60	1.01
2	9.2			1.40				
2	9.2			1.40				
2	6			1.42				
2	7.0						2.52	
2	6.0						2.59	
2	5.0						2.60	

TABLE 6 ANNULUS DETERMINATION OF k_o, α : s_3, s_4, and s_5 LINES

s_3 LINES

I_a (ma)	I_s (ma)	6164 $k_o(cm^{-1})$	α	6266 $k_o(cm^{-1})$	α	6533 $k_o(cm^{-1})$	α
8	7.6	.0187	.45	.0293	.5	.0168	.5
10	7	.0164	.65	.0261	.65	.0144	.65
10	7	.0176	.7	.0289	.65	.0163	.65
10	7	.0177	.55	.0276	.5	.0156	.5

s_4 LINES

I_a (ma)	I_s (ma)	6074 $k_o(cm^{-1})$	α	6096 $k_o(cm^{-1})$	α	6305 $k_o(cm^{-1})$	α	6383 $k_o(cm^{-1})$	α	6507 $k_o(cm^{-1})$	α	6245 $k_o(cm^{-1})$	α
2	7							.0133	1.45	.0195	1.45	.0060	1.4
4	7							.0196	1.3	.0288	1.3	.0095	1.4
6	7	.0118	.85	.0157	.7			.0199	.75	.0296	.8	.0099	.8
8	7	.0135	.5	.0190	.4	.0064	.5	.0244	.5	.0425	.85	.0129	.6
8	7.6					.0090	1.0	.0343	1.0				
10	7	.0161	.65	.0216	.55	.0073	.7	.0277	.7	.0518	1.05	.0135	.6
10	7.6					.0096	1.0	.0386	1.0				

s_5 LINES

I_a (ma)	I_s (ma)	5882 $k_o(cm^{-1})$	α	5945 $k_o(cm^{-1})$	α	6143 $k_o(cm^{-1})$	α	6217 $k_o(cm^{-1})$	α	6334 $k_o(cm^{-1})$	α	6402 $k_o(cm^{-1})$	α	7032 $k_o(cm^{-1})$	α
1	7.6	.0205	1.35	.0356	1.35	.0807	1.35	.0153	1.35	.0638	1.35	.163	1.3	.077	1.45
1	8									.0625	1.4	.174	1.35		
2	7					.0790	1.15			.059	1.15	.165	1.2	.072	1.25
2	9.2					.102	1.35			.0755	1.35				
2	9.2					.101	1.3			.0734	1.3				
2	6					.104	1.3			.0755	1.3				
2	7.0									.0700	1.25	.193	1.3		
2	6.0									.0726	1.25	.190	1.25		
2	5.0									.0735	1.25	.194	1.25		

when $\ell = 10$ cm. Since the other experimental points agreed well with the theoretical predictions the discrepancy may be due to the effect in the discharge as it "rounds the corner" in the tube (see section 5.4.2). When the above discrepancy occurred, k_o was measured from the curves with and without inclusion of the 10 cm point; the value of f_{rel} calculated by these two methods was substantially the same. Again in calculating f_{rel} from curves which definitely were not the best fit, variations of 5% at most were observed. It is apparent also, in comparing lines common to Tables 1 and 5, that there is essentially no difference in the values of f_{rel} obtained by the annulus and the circular aperture method.

If the experimental points were fitted to the theoretical curves calculated for the presence of only a single isotope, portions of the curves could be found which fitted adequately. The values of α were approximately the same, while k_o was lower. Qualitatively it can be seen that this should be so, since the one-isotope curves tend to zero more quickly with increasing $k_o\ell$; fitting the points to a curve of the same α "pushes" the experimental T versus log(ℓ) plot to the left, i. e. smaller k_o. The fractional decrease of k_o between the one-isotope and two-isotope fits depends on the absorption of the spectral line and is larger the higher the absorption. The value of f_{rel} depends on the k_o values from two spectral lines. Thus f_{rel} for the one-isotope fit will be greater or less than the value computed from the two-isotope curves depending on whether the absorption of the reference line is

greater or less than the other line. This observed difference in f_{rel} was no greater than approximately 5% and was less for low k_o.

5.4   Discussion of Results and Errors of Absorption Method

5.4.1   Fictitious Line-Shapes

One of the things to be noticed from Tables 2 and 4 is the variation of the value of α over the cross-section of the absorption tube. Under the conditions of this experiment, the relative increase of α from R = 1.5 mm to R = 6.5 mm was generally about two, going from approximately 1 to 2 for the s_2 lines and approximately .6 to 1.3 for the s_3 and s_4 lines; apparently the temperature changes by a factor of about four in this distance. Hamberger /31/ has measured the Doppler widths of spectral lines emitted by a hydrogen-helium-filled Geissler tube and concluded the temperature of the emitting gas corresponded to the wall temperature of the tube. Assuming, therefore that both the source and the outer regions of the absorber are at room temperature, a four-fold increase in temperature in the absorber would yield a temperature of $1200^{\circ}K$ at the centre. This seems hardly possible. Irwin /12/ did not observe this in his line-width measurements on a similar absorption tube.

Ecker and Zöller /32/ have considered theoretically the temperature variations across a cylindrical positive column

and for the column used in this experiment, a current of about 4 amps would be required to get such a variation; they predict a constant temperature, equal to the wall temperature, with the operating conditions used here. Granting that both the absorber and emitter should have temperatures close to room temperature, the values of α should then be approximately unity, contrary to what was found in fitting the data to the theoretical curves.

The reason for these results is probably that the spectral lines do not have a pure Doppler profile. Lang /33/ has measured the spectral distribution of the neon λ5852 line as a function of pressure and showed that at pressures of the order of 1 mm Hg, Doppler broadening is the dominant process. It is expected, however, that there will be some deviation, particularly at the edges of the spectral line, due to various combinations of natural broadening, and collision and Stark broadening, as well as some self-absorption of radiation from the source. Indeed, self-absorption seems to be present, as mentioned in section 4.2. Slight deviations from a pure Doppler distribution in the wings of the line can be significant when absorption is large; most of the centre of the line is "absorbed out" and a large part of the total amount of the light transmitted comes from the non-Doppler wings. (The isotope effect discussed in section 2.1.3 is a comparable process.)

A solution of this problem would be to measure the spectral distribution by the standard methods such as a high-resolution spectrograph or Fabry-Perot interferometer. In

actual practice it would be a time-consuming and tedious pro-
cedure that would have to be undertaken on each line and for
each operating condition. Also it is doubtful whether, with the
equipment at hand, the accuracy of the measurements would be
sufficiently high to allow more accurate analysis than has been
done here. Lang apparently has an accuracy of only about 20%
in the wings of the line.

A reasonable explanation of the good fit of the exper-
imental points to the Doppler theoretical curves could be that
there is non-Doppler broadening processes prevailing which
approximately match a transmission curve for pure Doppler broaden-
ing having the parameters k_o and α corresponding to those cited
in Tables 2, 4, and 6.

That this could happen is seen by considering two
specific examples of non-Doppler line-shapes: a self-absorbed
Doppler distribution, and a Voigt (i. e. Doppler plus natural)
distribution. Numerical calculations for a single-isotope gas
have been performed for these two distributions and the results
are given in Appendix 5. It is shown in the appendix that Voigt
and self-absorbed Doppler profiles can be found which fit the
transmission curves of a pure Doppler profile.

Because of the uncertainty in the actual line-shapes
and parameters pertaining to the source and the absorber, no
quantitative conclusions can be drawn from these calculations.
Qualitatively they show the possibility of equivalence between
non-Doppler line-shapes and "fictitious" Doppler line-shapes. A
more detailed calculation pertaining to a self-absorbed Doppler

source was undertaken in the appendix. The results indicate that f_{rel} obtained from fitting transmissions using a self-absorbed source is not very dependent on deviations from a pure Doppler line-shape, although the k_o and α for the two profiles differ markedly. This is in accordance with observation, since in the experiment the value of f_{rel} was generally independent of absorber and source current, and method of measurement. This is the main justification in the acceptance of the values of f_{rel} while rejecting the values of k_o and α; with variation of conditions and consequent variation of the "fictitious" values of k_o and α, f_{rel} remained constant and generally independent of these variations. The results of the intensity measurements discussed in section 4.2 show that most lines emitted by the source have some self-absorption so that the lines are definitely not pure Doppler. The effect of the deviations from a non-Doppler distribution is smaller the less the absorption so that more weight should be placed on f_{rel} for lines which are least absorbing.

Because of the uncertainty in the value of k_o, values of the relative densities of the atoms in the lower states as a function of R calculated from equation (2.10) are in doubt and computations have not been carried out.

5.4.2   Discussion of Errors

The estimation of errors is usually difficult and the situation here is no exception. The most likely and most

important causes of error in this experiment are discussed below, and estimations of the magnitude of the errors are made.

.1   Stimulated Emission

It has been assumed that stimulated emission in the absorption tubes is negligible. If it is not, k_o (see equation (2.2) must be corrected by multiplying by the factor (see for example, Mitchell and Zemansky /19/) $Q_{ji} = 1 - N_j g_i/N_i g_j$. N_i and N_j are the atom densities of the lower and upper levels, respectively, and g_i and g_j the corresponding statistical weights. Irwin /12/ has measured the ratio N_j/N_i in a discharge tube of dimensions similar to that used here and containing neon at the same pressure (2 mm Hg). At $I_a =$ 15 ma, he found the largest correction for stimulated emission was for the $\lambda 5852$ line which amounted to $Q_{ji} = .996$. This correction is negligible compared to the accuracy of the measurement of k_o.

As mentioned in section 4.2, Ladenburg's /7/ results indicate the absence of stimulated emission in the Geissler tube.

.2   Transmission Accuracy

Throughout the course of this experiment the linearity of the intensity-measuring circuit was checked periodically by varying the light intensity into the monochromator using neutral density filters. The output was never found to deviate from linearity by more than 2%. The chart recorder could usually be

read to better than 2% and transmissions were measured three times
for each discharge length and the average taken for subsequent
analysis.   Errors here should be random and less than about 2%.

.3   Curve Fitting and Slopes

In fitting the experimental points of T or $d(R^2T)/d(R^2)$
to the theoretical curves, it was found that the uncertainty
of the fitting was usually less than 5% of k_o so that maximum
uncertainty of f_{rel} would be less than 10% for a single calcula-
tion of f_{rel}. Over several measurements the standard deviation
of f_{rel} should be no greater than 5%. The error involved in
computing $d(R^2T)/d(R^2)$ in the circular aperture method is hard
to estimate and depends on the quality of the approximation to
a second order polynomial assuming accurate experimental
points. The apparent variation of f_{rel} at large R for some
wavelengths (see Table 1) and the poor fitting is no doubt due
in part to calculating the slopes by the polynomial method.

.4   Optical Alignment

When measurements were repeated on a series of spec-
tral lines after a short period of time such as the order of a
day, without changing the alignment of the absorption tube,
source, or the optics, it was found that the values of k_o would
generally agree within 5%, whereas if repetition took place after
a period of a few weeks or the equipment was disturbed and

realigned, there would be a larger deviation between the values of k_o. It can be seen, however, that the values of f_{rel} corresponding to these cases do not deviate in nearly as drastic a manner, systematically or otherwise, indicating an independence to alignment. Therefore the variation of f_{rel} due to alignment should be generally of a statistical nature and the error is diminished by increasing the number of measurements, realigning the optics between each measurement.

.5   End-Window Reflections

Frish and Bochkova /34/ measured absorption coefficients of a gaseous discharge by placing the discharge tube between two parallel mirrors and measuring the light output after the emitted radiation had undergone multiple reflections through the absorbing gas. Conceivably in this experiment the radiation from the source could be reflected back and forth between the end-windows undergoing absorption with each pass and introduce an error in the analysis as given previously.

If the windows are considered as singly-reflecting plane surfaces of reflectivity r, and are positioned perpendicular to the axis of the tube, a procedure similar to that given in the above reference shows that the transmission is given by

$$ T = \frac{\int_{line} \frac{1-r^2}{1-r^2 e^{-2k(\nu)\ell}} I(\nu) \, d\nu}{\int_{line} I(\nu) \, d\nu} \qquad \ldots (5.1) $$

For glass, $r = .04$ and the factor $(1-r^2)/(1-r^2 e^{-2k(\nu)\ell})$ thus approaches .998 for high absorption close to the centre of the line and is effectively unity elsewhere. Even if the windows of the actual absorption tube were parallel and perpendicular to the axis, which is probably not the case, the error due to multiple reflections is negligible.

.6   Uniform Discharge Conditions

The configuration of the absorption tube was chosen with the electrodes located away from the main column (see Fig. 5). This ensured that the various glow and dark space regions associated with the anode and cathode would not penetrate into the absorbing column, and only the positive column region would be associated with the absorbing process.

Uniform conditions along the length of the absorption tube have been assumed; this assumption depends on the conditions occurring in the positive column. In a low-pressure glow discharge this positive column is generally considered as a region of constant and equal concentrations of positive ions and electrons and is characterized by a constant low voltage-gradient. This situation is not always so, however, and under certain conditions alternate bright and dark striations appear which may be stationary or move along the column /35/. Generally the motion of these running striations is so rapid that the column appears uniform. Donahue and Dieke /36/ contend that these striations are only exceptionally absent and play

an essential part in the mechanism of the glow discharge.
Krebs /37/ found, using neon in a similar tube to that used here,
that the striations only disappeared above a current of 2 amps.

Rudimentary examination of the positive column with
a photocell confirmed the existence of running striations in
this absorption tube. A relatively large slit (approximately 2mm)
in front of the photocell limited the resolution but yielded a
period of oscillation of approximately 1.8 msec and an intensity-
modulation of no less than 25%. Because of the relatively short
period of the striations compared to the absorption time ($\approx$10
seconds or greater), local variations of conditions in the
positive column would be averaged out in any measurements.

One other variation of conditions in the positive
column was observed when a photograph of the tube was taken;
when the discharge had an unused electrode situated between
the two conducting electrodes, a slight diffusion of the
discharge into the unused side-arm took place. Although not
noticeable by eye, this manifested itself by a slight decrease
of intensity above the side-arm when observed with a camera.
Fig. 16 shows this intensity decrease. The effect of this would
be to yield a shorter effective absorption length, although
in the analysis, its presence was ignored.

.7   End-Effects of Absorption Column

So far no mention has been made concerning the
error introduced by the rounding of the discharge at the ends.

(see Fig. 16). It is evident from Fig. 17 that incident rays
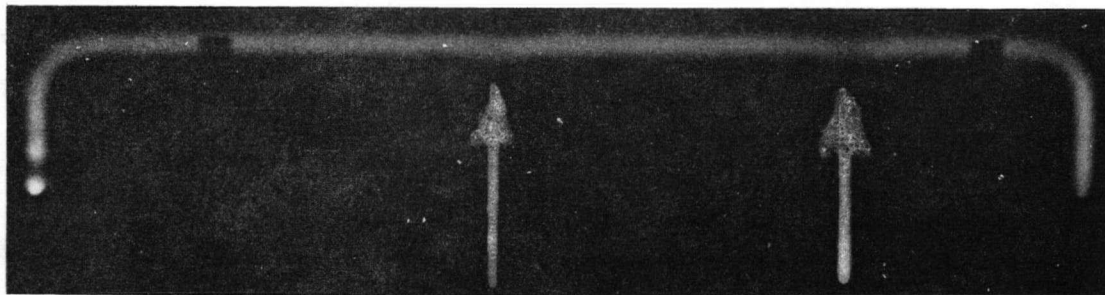
Arrows indicate position of side-arms. (opaque
segments near ends of discharge are clamps).

Fig. 16   Photograph of Discharge

such as CD are more strongly absorbed in the end regions than
the diametrically opposite rays such a AB. This is due to the
more dense end region that CD passes through and the longer
absorbing length. By assuming an absorption length l equal
to the distance between the centres of the electrodes, the errors
for the two rays shown in the diagram are in opposite directions
and tend to cancel each other. However using this absorption
length may lead to an error for the total effect of all the rays
passing through the absorption tube.

For the annular incident beam, two attempts have been
made to calculate the effect the ends have on the transmission.
The details of these calculations are given in Appendix 6. It
is assumed that the discharge bends through 90° in a circular
path at each end, and as a first approximation that k_o and α are
constant in the end region.

With these simplifying assumptions the results of the
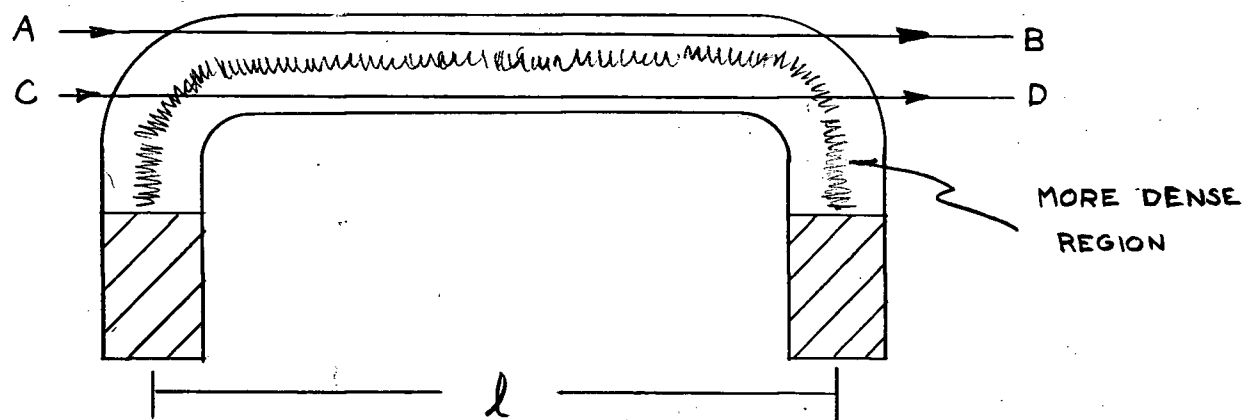
FIG. 17   END-EFFECTS OF DISCHARGE

calculations show that no correction for the ends is necessary. Consequently no correction was applied.

The basic fault in this analysis is that k_o is not constant in the end zone. A better approximation if the profile of k_o across the diameter of the tube were known would be to assume this profile is preserved in "going around the corner" and perform a triple numerical integration over the frequency, length, and angular position on the annulus to calculate the error. Because the form and magnitude of k_o is not well known and because of the complexity of the calculations, no attempts were made in this direction.

It is likely that for the less highly absorbing lines the end-effect error is small and of course is highest for the 10 cm discharge length. As mentioned previously the 10 cm point sometimes did not seem to fit very well in the curve-fitting, although whether this point was included or not made little difference in the value of f_{rel} determined.

As a result of the analysis, no corrections for end-effects for the method of circular apertures was applied either.

.8   Estimated Errors

The averaged values of the relative oscillator strength and a numerical estimate of the errors are given in Table 7. The values of the errors given represent the ratio of the standard deviation of f_{rel} to the value of f_{rel}, in percent. These hopefully account for contributions to random errors from such

TABLE 7 f_{rel} AND ESTIMATED ERRORS

(The number in parentheses following the error is the number of measurements)

	$\lambda(\text{Å})$	f_{rel}	Estimated Error
s_2 Lines	5852	1.00	Reference
	6599	1.19	5.5%(4)
	6678	2.08	2.3%(4)
	6717	1.20	2.6%(4)
	6929	1.75	4.0%(4)
s_3 Lines	6163	1.18	2.3%(5)
	6266	1.85	1.5%(5)
	6533	1.00	Reference
s_4 Lines	6074	.589	2.9%(6)
	6096	.861	0.9%(5)
	6304	.263	3.3% (4)
	6383	1.00	Reference
	6506	1.42	1.6%(7)
	7245	.416	6.1%(7)
s_5 Lines	5882	.347	10 %(1)
	5945	.592	10 %(1)
	6143	1.41	1.4%(5)
	6217	.244	10 %(1)
	6334	1.00	Reference
	6402	2.64	3.7%(6)
	7032	1.00	7.5%(2)

causes as alignment, curve fitting, transmission accuracy etc. and are made from a purely statistical approach. The standard deviation σ representing the error is the best estimate to the standard deviation of an infinite number of measurements of f_{rel}. The standard deviation s calculated from the n measurements of f_{rel} actually made is related to σ by the relation $\sigma^2 = (n/(n-1))s^2$ (see for example, Topping /38/). The value of n for each spectral line is indicated in brackets following the error. For lines which were measured only once or twice the values of 10% and 7.5% respectively were assigned to the error.

For most lines systematic errors are believed to be small and are not included in this analysis. Non-Doppler line-shapes and incomplete isotope separation (see Appendix 1) could contribute a significant systematic error if absorption is high. By far the most highly absorbing line is $\lambda6402$ so that the error estimate given here may be optimistic. Futher discussion is given in section 5.6.

5.5 Emission

5.5.1 Relative Transition Probabilities

For the calculation of relative transition probabilities equations (2.14) and (4.2) yield

$$A_{rel}(\lambda_1,\lambda_2) = \frac{A_{ji}(\lambda_1)}{A_{ji}(\lambda_2)} = \frac{\lambda_1\,\mathcal{E}(\lambda_1,T_t)R_\ell(\lambda_1,\lambda_2)J(\lambda_1,T_t)}{\lambda_2\,\mathcal{E}(\lambda_2,T_t)R_c'(\lambda_1,\lambda_2)J(\lambda_2,T_t)} \quad \ldots(5.2)$$

where

$$R'_c(\lambda_1, \lambda_2) = R_c(\lambda_1, \lambda_2) \, D(\lambda_1)/D(\lambda_2)$$

Table 8 gives the values of the factors in equation (5.2) for each line pair and the final two columns lists A_{rel} and the estimated error. Only two of the last three pairs of lines are independent so $A_{rel}(6383/6533)$ is merely calculated from the two values immediately preceeding it.

5.5.2   Discussion of Errors

The error analysis is more amenable to numerical estimation here than in the absorption experiment; the main sources of error are discussed below and estimates given.

.1   Intensity-Ratio Error

The errors involved in measureing $R_\ell (\lambda_1, \lambda_2)$ and $R_c(\lambda_1, \lambda_2)$ for each wavelength pair were estimated from the fractional standard error of the three sets of measurements. This amounted from between 1% and 3% for R_ℓ , and 4% to 5% for R_c. R_c for $\lambda\lambda 6217$, 6383, and 6533 was derived from the curve of Fig. 11 rather than by direct measurement and the error was estimated at 6% to 9%.

.2   Emissivity and Temperature Error

The errors in $\mathcal{E}(\lambda, T_t)$ as given by Larrabee /26/ amd de Vos /25/

TABLE 8   RELATIVE TRANSITION PROBABILITIES FROM INTENSITY MEASUREMENTS

$\lambda_1 : \lambda_2$	λ_1 / λ_2	$\dfrac{\varepsilon(\lambda_1)}{\varepsilon(\lambda_2)}$	$R_\ell(\lambda_1,\lambda_2)$	$R_c'(\lambda_1,\lambda_2)$	$\dfrac{J(\lambda_1,T_t)}{J(\lambda_2,T_t)}$	$A_{rel}(\lambda_1,\lambda_2)$	$\dfrac{\Delta A_{rel}}{A_{rel}}$
6096/6678	.913	1.02	17.5	10.8	.535	.802	4.5%
6164/6599	.934	1.01	6.47	6.49	.626	.591	4.1%
6334/6506	.974	1.00	1.63	2.32	.834	.572	5.6%
6217/6383	.974	1.00	.542	1.83	.832	.241	6.2%
6217/6533	.952	1.01	3.87	3.95	.711	.668	8.0%
6383/6533						2.77	8.9%

are both approximately .5%; although their values differ
by about 2.5%, it is estimated here that the error in the ratio
$\mathcal{E}(\lambda_1, T_t)/\mathcal{E}(\lambda_2 T_t)$ is no greater than 1%. The brightness
temperature of the tungsten lamp measured with the pyrometer
was found to be $1768°K \pm 14K$ where the uncertainty factor is the
standard deviation of 10 measurements. The true temperature T_t
was calculated to be $1900°K \pm 16° K$ where the difference between
using Larrabee's or de Vos's values of $\mathcal{E}$ amounted to only $4° K$.
From this temperature and its uncertainty, the uncertainty in
$J(\lambda_1, T_t)/J(\lambda_2, T_t)$ was less than 1% for all wavelengths used.

.3 Pile-Up Error

The second type of pile-up error discussed in section
4.3.2 can be roughly estimated in the following way. $\bar{n}$ is
the average number of photo-electron pulses arriving at the
anode of the photomultiplier per sampling period, and hence is
proportional to the intensity. Gadsden /39/ has shown that the
time distribution of the arrival of pulses is closely Poisson,
so that the probability of no pulses arriving during the
sampling period is $e^{-\bar{n}}$. The proability of one or more arriving
is $1-e^{-\bar{n}}$. The apparatus used here counts how many samples contain
one or more pulses. If there are C counts for the normal
4850 samples, then it follows from above that

$$1-e^{-\bar{n}} = C/4850 \qquad \ldots (5.3)$$

This equation may be solved exactly for $\bar{n}$ but for a low count
(and therefore low $\bar{n}$) equation (5.3) becomes approximtely

$$\bar{n}(1-\bar{n}/2) = C/4850$$

and for the C = 250 the error in assuming $\bar{n} = C/4850$ is approximately 2%. The more equal the counts are for each wavelength pair, the less is the error of the ratios of the counts; by using the optical filters to do this and to keep the count below 250, the pile-up error was expected to have been kept below 1%.

An objection may be raised that a Poisson distribution is invalid for this analysis because the sampling width (.3 nsec) is smaller than an individual photo-electron pulse width (approximately 5 nsec). However if the width of the pulses at the voltage level set by the discriminator has an average value $\bar{w}$, on average a count is registered whenever the centre of a pulse falls within $\bar{w}/2$ of either edge of the sampling gate. This gives an effective sampling width of $\bar{w} + w$, where w is the width of the sampling gate, and the Poisson distribution is valid.

.4 Radiation Trapping

One fact which has been tacitly assumed in measuring the emission intensities is the absence of self-absorption of the lines. This demands that the number density of atoms of the lower level of the transition be small.

Consideration of the excitation and de-excitation processes occurring in the gas after switching on the electron

beam can give an upper bound on the number densities of the lower levels of the transitions in the following way. The important processes which populate the four levels of the $2p^5 3s$ configuration are excitation of atoms in the ground state by collision with electrons in the electron beam and decay from upper levels. The processes which de-populate the levels are spontaneous transitions to the ground state with accompanying emission of radiation, diffusion to walls of the container and subsequent de-excitation, and absorption of radiation of appropriate frequency. As well, because the energy differences between the four levels are small, collisions with neutral atoms can bring about transitions between these excited states. This redistributes the populations among the four levels but does not change the total population of the configuration. The upper bound on the number density can be obtained by considering only the populating processes mentioned above and disregarding the de-populating processes. Imprisonment of the resonance radiation need not be considered as a population process since every atom raised to an excited energy state by self-absorption requires the transition of at least one atom in the reverse direction, and that atom will have already been "counted".

For population by electron collision the total number density of the configuration is governed by the following equation

$$\frac{dN_T}{dt} = N_e N_o Q_T \qquad \qquad \ldots (5.4)$$

where $N_T = \sum_{i=1}^{4} N_i$ is the number density of all four levels, Q_T is

the total cross-section for excitation to any of the levels in the configuration, N_o is the number density of atoms in the ground state, and N_e is the flux of excitation elctrons per unit area in the electron beam.

The other populating process is cascading from higher levels and in neon the only direct cascading is from the $2p^5 3p$ configuration. The cross-sections for each of the ten levels in this configuration has been measured by Frish and Revald /40/ and are all approximately $10^{-19} cm^2$. If all these atoms cascade into the $2p^5 3s$ configuration the effective cross-section for populating the lower configurations by this method is approximately $10^{-18} cm^2$. According to Revald /41/ the configuration cross-section for direct excitation is approximately $10^{-17} cm^2$ so that cascading contributes an effect which is one order of magnitude smaller. Detailed values of cross-sections for the higher configurations are not known, but it is probable that the total effect of cascading for the excitation time used here can at best make a contribution which is comparable to that from direct excitation. Thus for rough calculations, equation (5.4) is valid for estimating population densities. From this equation it follows $N_T \approx N_e N_o Q_T t$ and under the experimental conditions used here, the approximate values $N_e \approx 10^{17} cm^{-2} sec^{-1}$, $N_o \approx 10^{15} cm^{-3}$, $Q_T \approx 10^{-17} cm^2$, and the excitation time t = 200 nsec yields $N_T(t) \lesssim 10^8 cm^{-3}$ for the maximum number density of the lower configuration. N_i for each level will of course be smaller.

For Doppler lines, the effect of self-absorption is

given by the factor S of equations (2.15) or (2.16). Rough calculations give k_o from equation (2.2) as

$$k_o \approx \frac{(6\times10^{-5})^2 \; 10^7 \, N_i}{8\pi^{3/2} \, 7\times\sqrt{2} \times 10^8} \approx 10^{-12} N_i$$

and as ℓ for the electron gun is approximately 1 cm, $k_o\ell \lesssim 10^{-4}$. Reference to the table in Appendix 2 shows that for this value of $k_o\ell$ the self-absorption is negligible.

5.6   Absolute Transition Probabilities

As mentioned before, by combining the relative transition probabilities between lines having the same lower level (absorption) with those having the same upper level (emission) a complete set of relative transition probabilities may be obtained. Here, only three relative emission probabilities are needed to tie the four lower-level groups of lines together. There were however, five independent measurements made in emission thus allowing a self-consistency check. It was found that the results were consistent within the estimated experimental error and so a weighted averaging method was employed to arrive at the final relative transition probabilities (see section 5.6.1). The final set of relative probabilities are placed on the absolute scale using one lifetime measurement recently made in this laboratory and the absolute values are discussed and compared with those of other workers in sections 5.6.2 and 5.6.3.

5.6.1 "Multi-Path" Method of Relative Transition Probabilities

With five independent relative intensity measurements
it is possible to obtain up to five independent ways of calcu-
lating A_{rel} for one particular line, with $\lambda 5852$ chosen as the
reference line. The different "routes" are best seen when the
spectral lines investigated are layed out in a transition array
with the lower levels labeling the rows, and the upper levels
labeling the columns. Fig. 18 shows this array with the
wavelengths marked at the intersection of the appropriate
rows and columns. The vertical arrows connect the line-pairs
involved in the emission measurement and hence indicate the
the interconnection between the rows.

To utilize completely the information gained from
the intensity measurements, the following method was adopted
to calculate the entire set of transition probabilities, relative
to $\lambda 5852$. Starting at the wavelength in question, one proceeds
to $\lambda 5852$ by moving horizontally along the rows and vertically
along the arrows of Fig. 18 by as many independent paths as
possible. Since the transition probabilities in a particular
row are calculated relative to an arbitrarily chosen spectral
line in the row, a path which jumps to more than two squares
without leaving the row first is not independent. Also no
path may pass through the same square more than once although
it may "jump" over a previously used square. The number in
parentheses following the wavelengths in Fig. 18 indicates the
number of independent paths for that wavelength. The individual

UPPER / LOWER	P_1	P_2	P_3	P_4	P_5	P_6	P_7	P_8	P_9	P_{10}
S_2	5852 REFERENCE LINE	6599(3)		6678(3)	6717(5)	6929(5)				
S_3		6163(3)			6266(3)		6533(3)			
S_4			6074(5)	6096(3)		6304(5)	6383(4)	6506(4)		7245(5)
S_5		5882(4)		5945(4)		6143(4)	6217(4)	6334(4)	6402(4)	7032(4)

FIG.18 TRANSITION ARRAY FOR MULTI-PATH METHOD

relative transition probabilities of each step in a path are
used to calculate the probability relative to $\lambda 5852$. A weighted
average is then calculated from these independent values of
the transition probabilities. The weight given to a value
obtained along a particular path is derived from the estimated
errors of the transition probabilities of which the path is
composed. Table 9 lists these errors, where the number at the
intersection of a row and column indicates the standard deviation
of the relative transition probability for the wavelengths at
the head of the column and row. These deviations have been
obtained from the absorption and emission error analysis and
only those which are required here have been calculated.

An example of one independent calculation for the
$\lambda 5882$ line is given here for the path $5882 \longrightarrow 6334 \longrightarrow 6506 \longrightarrow$
$6096 \longrightarrow 6678 \longrightarrow 5852$. The standard deviation σ_i for each step
is 10% 5.6%, 1.2%, 4.5%, and 2.3% respectively, as given in
Table 9. The product of the relative probabilities derived
from Tables 1, 3, 5, and 8 yield $A_{rel_j}(5882/5852) = .144$
while $s_j = (\sum_i \sigma_i^2)^{1/2}$ gives a standard deviation of 12.6%.

The weighting factor to be given the A_{rel_j} associated
with a particular path j is $w_j = 1/s_j^2$ where s_j is the standard
deviation associated with the path. The weighted average is
thus computed using the formula

$$\bar{A}_{rel}(\lambda) = \sum_{j=1}^{n} w_j A_{rel_j} \Big/ \sum_{j=1}^{n} w_j$$

(see for example, Topping /38/). The standard deviation of the

λ(Å)	5852	5882	5945	6074	6096	6143	6163	6217	6266	6304	6334	6383	6402	6506	6533	6599	6678	6717	6929	7032	7245
5852																5.5%	2.3%	2.6%	4.0%		
5882								10%			10%										
5945								10%			10%										
6074					2.5%							2.9%		4.1%							
6096				2.5%						7.5%		0.9%		1.2%			4.5%				7.6%
6143								10%			1.4%										
6163									2.3%						2.3%	4.5%					
6217		10%	10%			10%					10%	6.2%	10%	8.0%						10%	
6266							2.3%							1.5%							
6304					7.5%							3.3%		7.5%							
6334		10%	10%			1.4%		10%					3.7%	5.6%						7.5%	
6383				2.9%	0.9%			6.2%		3.3%				1.6%	8.9%						6.1%
6402								10%			3.7%										
6506				4.1%	1.2%					7.5%	5.6%	1.6%									5.7%
6533							2.3%	8.0%	1.5%			8.9%									
6599	5.5%						4.1%											4.2%	2.2%		
6678	2.3%				4.5%													1.8%	3.7%		
6717	2.6%															4.2%	1.8%				
6929	4.0%															2.2%	3.7%				
7032								10%			7.5%										
7245					7.6%							6.1%		5.7%							

TABLE 9

ESTIMATED ERRORS OF TRANSITION PROBABILITIES

(EMISSION AND ABSORPTION)

TABLE 10   RELATIVE AND ABSOLUTE NEON TRANSITION
PROBABILITIES AND OSCILLATOR STRENGTHS

$\lambda(\text{Å})$	A_{rel}	$A_{abs}(\text{sec}^{-1})$ $\times 10^{-7}$	f_{abs}	ERROR %
5852	10.0	6.58	.113	1.6
5882	1.44	.948	.0295	13.0
5945	1.44	.948	.0503	13.0
6074	8.54	5.62	.104	10.7
6096	2.50	1.64	.152	7.0
6143	3.17	2.09	.118	11.3
6163	1.90	1.25	.214	7.6
6217	.948	.624	.0216	13.0
6266	2.87	1.89	.334	7.5
6304	.691	.455	.0449	12.4
6334	2.11	1.39	.0832	11.2
6383	4.33	2.85	.174	8.4
6402	3.91	2.57	.221	11.7
6506	3.68	2.42	.256	9.1
6533	1.43	.941	.181	8.0
6599	3.17	2.09	.136	6.0
6678	3.20	2.11	.235	3.9
6717	3.01	1.98	.134	5.3
6929	2.50	1.64	.197	7.3
7032	2.88	1.90	.0845	12.6
7245	1.39	.915	.0720	12.5

values of A_{rel_j} is used as an estimation of the error of $\bar{A}_{rel}(\lambda)$ and is computed by the formula

$$\left[\sum_j w_j (A_{rel_j} - \bar{A}_{rel})^2 / \sum_j w_j \right]^{1/2}$$

The final relative transition probabilities and errors determined in this manner are listed in Table 10. The determination of the absolute probabilities also listed in the table is discussed in the next section.

5.6.2 Lifetime Measurement

The lifetime of level i is connected to the spontaneous transition probabilities through the relation

$$\tau_i = 1 / \sum_{k<i} A_{ik} \qquad \dots(5.7)$$

For the p_1 level of neon there are only two allowed downward transitions, $\lambda 5852$ and $\lambda 5400$. Recent measurements by van Andel /17/ gives the value of $15.2 \pm .25$ nsec. for the lifetime of this level. The intensity of $\lambda 5400$ was measured to be less than 10^{-2} of the intensity of $\lambda 5852$ so that neglecting the contribution of the $\lambda 5400$ transition to the lifetime would amount to an error of less than 1%. Consequently the value of $A_{abs}(5852)$ was taken to be $(15.2 \times 10^{-9})^{-1} = (6.58 \pm .11) \times 10^7$ sec.$^{-1}$. From this absolute value, the complete set of absolute values may be computed and are shown in Table 10. Also included are the possible errors associated with them and the oscillator strengths.

TABLE 11   COMPARISON OF ABSOLUTE TRANSITION
PROBABILITIES $(X10^{-7})$ sec^{-1}

$\lambda(\text{Å})$	THIS EXP'T	IRWIN /12/	DOHERTY /10/	FRIEDRICHS /11/	LADENBURG /7/
5852	6.58	6.8	3.51	6.0	12.8
5882	.948	1.15	.69	.96	2.12
5945	.948	1.05	.61	.93	1.70
6074	5.62	4.8	3.0	5.90	7.8
6096	1.64	1.6	.89		2.4
6143	2.09	2.75	1.34		3.25
6163	1.25	1.5	.78	1.5	2.44
6217	.624	.61	.35	.77	1.46
6266	1.89	2.2	1.20		3.84
6304	.455	.38	.27	.4	.93
6334	1.39	1.4	.84		2.07
6383	2.85	2.65	1.5		4.17
6402	2.57	5.3	2.7		5.78
6506	2.42	2.22	1.3		3.4
6533	.941	1.2	.7		2.14
6599	2.09	2.35	1.2		4.32
6678	2.11	2.35	1.1		4.10
6717	1.98	2.4	1.1		4.17
6929	1.64	1.8	.8		3.56
7032	1.90	2.0	1.06		3.24
7245	.915	.72	.42		1.80

TABLE 12   COMPARISON OF RELATIVE TRANSITION PROBABILITIES

λ	THIS EXP'T		IRWIN /12/		DOHERTY /10/(30%)	FRIEDRICHS /11/(20-30%)	LADENBURG /7/(20-30%)
5852	10.0	(1.6%)	10.0	(10%)	10.0	10.0	10.0
5882	1.44	(13.0%)	1.69	(15%)	1.97	1.60	1.66
5945	1.44	(13.0%)	1.54	(15%)	1.74	1.55	1.33
6074	8.54	(10.7%)	7.06	(10%)	8.55	9.85	6.09
6096	2.50	(7.0%)	2.35	(10%)	2.54		1.87
6143	3.17	(11.3%)	4.04	(20%)	3.82		2.54
6163	1.90	(7.6%)	2.20	(15%)	2.22	2.50	1.91
6217	.948	(13.0%)	.897	(15%)	.997	1.29	1.14
6266	2.87	(7.5%)	3.24	(15%)	3.42		3.00
6304	.691	(12.4%)	.559	(10%)	.769	.668	.726
6334	2.11	(11.2%)	2.06	(15%)	2.39		1.62
6383	4.33	(8.4%)	3.68	(10%)	4.27		3.26
6402	3.91	(11.7%)	7.79	(25%)	7.98		4.51
6596	3.68	(9.1%)	3.26	(10%)	3.70		2.66
6533	1.43	(8.0%)	1.76	(15%)	1.99		1.67
6599	3.17	(6.0%)	3.45	(10%)	3.42		3.37
6678	3.20	(3.9%0	3.45	(10%0	3.13		3.20
6717	3.01	(5.3%)	3.53	(10%)	3.13		3.26
6929	2.50	(7.3%)	2.65	(10%)	2.28		3.78
7032	2.88	(12.6%)	3.21	(15%)	3.02		2.53
7245	1.39	(12.5%)	1.13	(10%)	1.20		1.41

5.6.3   Comparison and Discussion of Absolute Probabilities

For comparison with the results of other workers /7/, /10/, /11/, /12/ by different methods, Tables 11 and 12 list both the absolute and relative transition probabilities measured here with those from the references cited above. The errors as given by the authors are also included.

It can be seen that Ladenburg's absolute values are generally higher whereas Doherty's are lower than those of the present work. Friedrichs shows general agreement as does Irwin, who claims the best accuracy to date.

However on the relative scale Ladenburg and Doherty agree with the present work within experimental error. This indicates that the differences may be attributed to the fixing of the absolute scale. Ladenburg places his relative values on an absolute basis by adopting the value $f = .5$ for $\lambda 6402$, after computing the bounds of .85 and .21 by the f-sum rule. The uncertainty of this value can explain the discrepancies, while from van Andel's measurement of the lifetime of $\lambda 5852$, Doherty's absolute values must be considered to be in error.

Because of its extremely high absorption, $\lambda 6402$ seems to be one of the most difficult lines to measure and there is a large variance between the value measured here and those of the others. Irwin cites evidence that his value is somewhat high but nevertheless this large difference seems to indicate the presence of systematic errors so that the error estimate given in the present work is too optimistic for this line.

The lifetimes of the $2p^5 3p$ levels may be computed from absolute transition probabilities by means of equation (5.7). This has been done and is contained in Table 13 and includes similar data computed by Irwin /12/ and Klose /15/. Several of the lifetimes computed from this work do not contain all the probabilities, but the ones missing are small and contribute an error less than 15%. Again agreement is good except for the p_9 level, for which the lifetime is due only to the $\lambda 6402$ transition.

TABLE 13   COMPARISON OF UPPER-LEVEL LIFETIMES $(\times 10^9)$ sec.

LEVEL	THIS EXP'T	IRWIN /12/	KLOSE /15/
p_1	15.2*	14.7*	14.7
p_2	23.6*	18.1	16.3
p_3	17.7*	20.7*	23
p_4	21.3	20.0	22
p_5	25.8**	20.1*	18.9
p_6	23.5	20.3	22
p_7	23.0*	23.2*	20.3
p_8	26.5*	25.4	24.3
p_9	37.7	19	22.5
p_{10}	35.3**	37**	

* Missing 1 transition probability

** Missing 2 transition probabilities

CHAPTER 6   CONCLUSIONS

Relative transition probabilities for transitions
between the excited state configurations $2p^53s$ and $2p^53p$ of
Ne I have been successfully measured by a new method. Measure-
ments were made on both a variable length cylindrical dc glow
discharge absorber and a pulsed electron gun emitter to
obtain a complete set of relative probabilities.

The transmission of the glow discharge absorber
varied over the cross-section of the column; this is attributed
mainly to a variation of the excited atom density. The trans-
mission was compared with that which would be obtained from
Doppler-broadened spectral lines and a generally good comparison
was found. The values of the parameter α were anomolous however
and subsequent numerical calculations showed the possibility of
equivalence between non-Doppler and "fictitious" Doppler line-
shapes. The relative transition probabilities computed from this
method are valid although the accuracy is less with highly
absorbing lines due to both non-Doppler line-shapes and approxi-
mations used to account for the presence of isotopes. Experi-
mental evidence exists for the presence of self-absorption in
the Geissler tube source.

Use of a pulsed electron gun emitter has been found
feasible for measurement of relative line intensities. The
advantage is that self-absorption in the emitting neon is
negligible.

Finally a lifetime measurement by van Andel /17/

allowed absolute transition probabilities to be calculated as well as lifetimes of the upper levels of the transitions.

APPENDIX 1.   ISOTOPE CORRECTION

Equation (2.9) was given in section 2.1.3 for the case of a gas containing two isotopes. The derivation of this equation is contained in this appendix.

Consider the case of a gas having two isotopes occurring in the ratio $K(K \leq 1)$. If both the isotopes have Doppler-shaped spectral lines then in the notation of Chapter 2, with primed and unprimed quantities referring to the two isotopes:

$$I(\nu) = I_o \, e^{-\omega^2} \quad , \quad k(\nu) = k_o \, e^{-\omega^2 \alpha^2}$$

with $\quad \omega = \dfrac{\nu - \nu_o}{.6 \Delta \nu_{DS}} \quad , \quad \alpha^2 = \dfrac{T_s}{T_a} \quad , \quad k_o = \dfrac{\sqrt{\pi} \, e^2 N_i f_{ij}}{mc^2 \, .6 \Delta \nu_{Da}}$

and $\quad I'(\nu) = I_o' \, e^{-\omega'^2} \quad , \quad k'(\nu) = k_o' \, e^{-\omega'^2 \alpha'^2}$

with $\quad \omega' = \dfrac{\nu - (\nu_o + \delta)}{.6 \Delta \nu_{DS}'} = (\omega - \Omega) \dfrac{\Delta \nu_{DS}}{\Delta \nu_{DS}'} \quad , \quad \alpha'^2 = \dfrac{T_s'}{T_a'} \quad , \quad k_o' = \dfrac{\sqrt{\pi} \, e^2 N_i' f_{ij}'}{mc^2 \, .6 \Delta \nu_{Da}'}$

where δ is the centre frequency separation of the spectral lines of the two isotopes.

The energy into the absorber per unit time is thus

$$E_i = \int_A \int_o^\infty \left(I(\nu) + I'(\nu) \right) d\nu \, dA$$

and the energy transmitted per unit time is

$$E_o = \int_A \int_o^\infty (I(\nu) + I'(\nu)) e^{-(k(\nu) + k'(\nu))l} \, d\nu \, dA \qquad \ldots (A1.1)$$

If the ratio $|\delta|/\Delta\nu_{D\alpha}$ is large enough, the two components may be considered as separate and equation (A1.1) becomes

$$E_o = \int_A \int_o^\infty (I(\nu) e^{-k(\nu)l} + I'(\nu) e^{-k'(\nu)l}) \, d\nu \, dA$$

so that the transmission is

$$T = \frac{\int_A [\int_o^\infty I(\nu) e^{-k(\nu)l} \, d\nu + \int_o^\infty I'(\nu) e^{-k'(\nu)l} \, d\nu] \, dA}{\int_A [\int_o^\infty (I(\nu) + I'(\nu)) \, d\nu] \, dA}$$

Differentiation with respect to the area for axially symmetric geometry yields

$$\frac{d(R^2 T)}{d(R^2)} = \frac{\int_o^\infty (I(\nu) e^{-k(\nu)l} + I'(\nu) e^{-k'(\nu)l}) \, d\nu}{\int_o^\infty (I(\nu) + I'(\nu)) \, d\nu} \qquad \ldots (A1.2)$$

The following assumptions are now made:

1. There is no preferential thermal heating between the isotopes, so that $T_a = T_a'$, $T_s = T_s'$, and therefore $\alpha = \alpha'$.

2. The populations of corresponding levels of the isotopes are in the ratio K and the transition probabilities for corresponding transitions are equal, or less stringently, $A_{j1}' N_{i,j}' = K A_{j1} N_{i,j}$.

From these assumptions, and the fact that

$$\frac{\nu_0 + |\delta|}{\nu_0} = 1 + O(10^{-5}) \approx 1 \quad , \text{ it can be seen that}$$

$$\frac{k_0'}{k_0} = \frac{N_i' A_{ji}'}{N_i A_{ji}} \sqrt{\frac{M'}{M}} = K \sqrt{\frac{M'}{M}} = b \qquad \qquad \text{...(A1.3)}$$

$$\frac{\Delta \nu_{DS}'}{\Delta \nu_{DS}} = \sqrt{\frac{M}{M'}} \frac{\nu_0 + \delta}{\nu_0} \approx \sqrt{\frac{M}{M'}}$$

and since $I_0 \sim A_{ji} N_j$

$$\frac{I_0'}{I_0} = K \qquad \qquad \text{...(A1.4)}$$

so that equation (A1.2) becomes:

$$\frac{d(R^2 T)}{d(R^2)} = \frac{\int_{-\infty}^{\infty} e^{-\omega^2} e^{-k_0 \ell e^{-\omega^2 \alpha^2}} + \frac{\Delta \nu_{DS}'}{\Delta \nu_{DS}} K \int_{-\infty}^{\infty} e^{-\omega'^2} e^{-b k_0 \ell e^{-\omega'^2 \alpha'^2}} d\omega'}{\int_{-\infty}^{\infty} e^{-\omega^2} d\omega + \frac{\Delta \nu_{DS}'}{\Delta \nu_{DS}} K \int_{-\infty}^{\infty} e^{-\omega'^2} d\omega'}$$

$$= \frac{1}{1+a} \left[F_0(k_0 \ell, \alpha) + a F_0(b k_0 \ell, \alpha) \right] \qquad \text{...(A1.5)}$$

which is identical with equation (2.9).

A few comments about the assumptions are appropriate here. In this experiment the times of observation and measurement are of the order of minutes. A rough calculation of the collision frequency between the isotopes gives a value of 10^6 collisions per second. With the energy transfer fraction

being .5 for elastic collisions, ample time occurs for equili-
brium to be established between the isotopes.

Half of assumption 2. has been experimentally
verified by Conner and Biondi /42/, as well as Lang /33/, who
observed for neon the relation given by equation (Al.4). It
seems reasonable that this should hold for all levels and
particularly the lower level i, justifying the assumption.

The errors introduced in considering the two Doppler
lines completely separated can be estimated by considering the
ratio of the Doppler width to the splitting. Nagaoka and
Mishima /43/ have measured the isotope splitting of neon, and
found it to be between .02 and .035 Å. Irwin /12/ measured the
Doppler widths of the neon lines using a radiation source
similar to that used here, and found the widths to correspond to
room temperature, or approximately .017A. This gives an isotope
separation to Doppler line-width ratio greater than 1 to approxi-
mately 2.

Knowing this ratio, equation (Al.1) may be integrated
numerically as a function of $k_o \ell$ and α, and T (or $d(R^2R)/d(R^2)$)
calculated exactly. This has been done using an IBM 7040
digital computer and the error between equations (Al.1) and
(Al.5) is shown graphically in Fig. Al as a function of $k_o \ell$.
For those lines that are highly absorbing, the value of k_o is no
doubt in error due to this cause, particularly for high absorber
currents and near the axis of the tube where absorption is
greater. This, could be one of the reasons for the poor fit to
the curves that was observed for some strong lines (see remarks
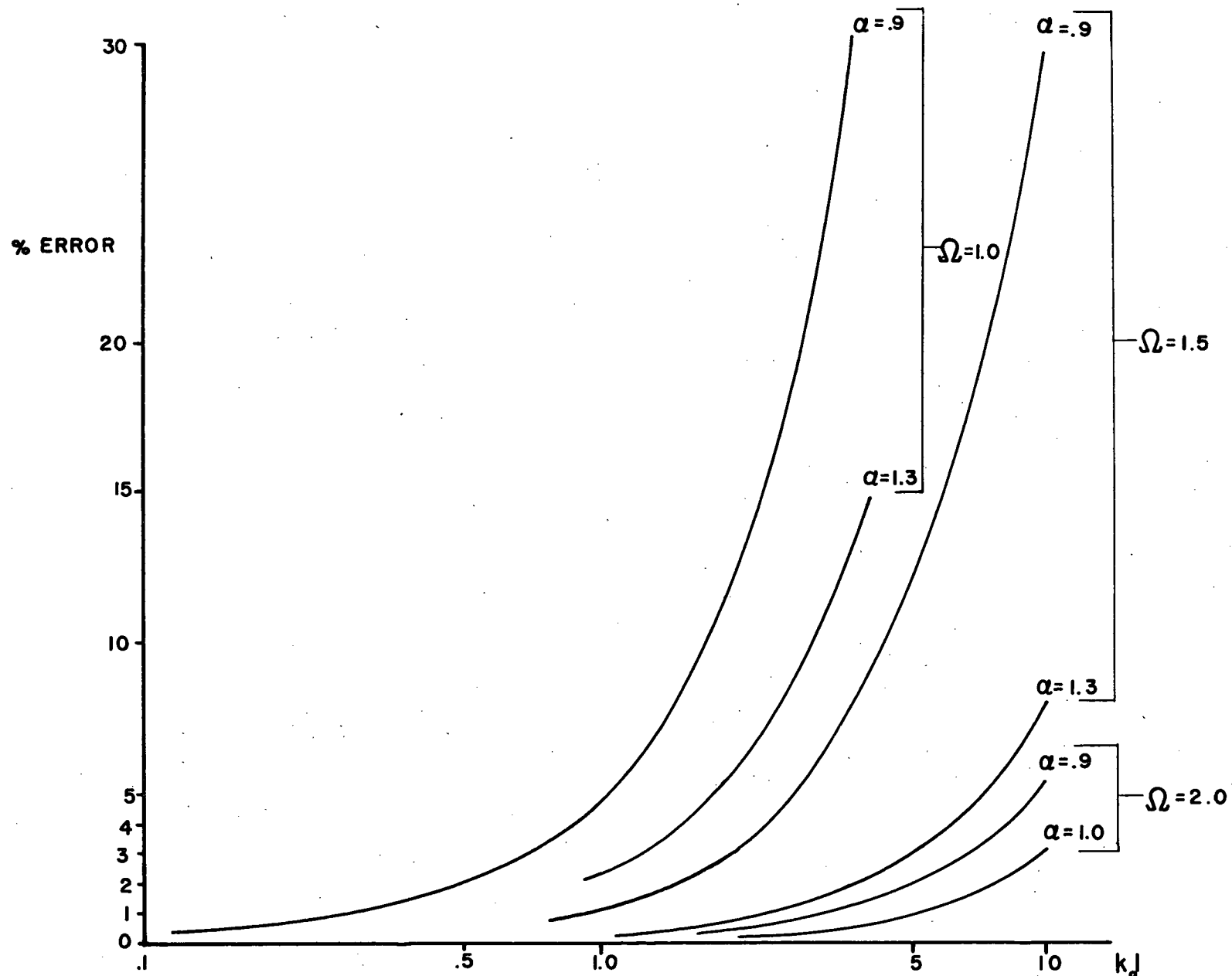
FIG. AI. ISOTOPE SPLITTING ERROR

in section 5.2.3). Generally most lines had a $k_o \ell$ of less than 3 and an Ω of 1.5 or greater making the error in assuming separated curves to be less than 5%. The error in determining f_{rel} can be considerably less than this however, since f_{rel} depends on the ratio of two k_o's (see equation (2.11)). For two lines having comparable absorption and values of Ω, the error in the values of k_o will tend in the same direction and make the error in f_{rel} less.

APPENDIX 2.   EVALUATION OF TRANSMISSION EQUATION

The method of computing the right-hand side of
equation (2.8) is outlined in this appendix.

Equation (2.8) can be evaluated either by numerical
integration of equation (A1.5) or by use of the infinite series
form of equations (2.8) and (2.3):

$$T = \frac{1}{1+a} \left[\sum_{n=0}^{\infty} \frac{(-1)^n x^n}{n! \sqrt{1+n\alpha^2}} + a \sum_{n=0}^{\infty} \frac{(-1)^n (bx)^n}{n! \sqrt{1+n\alpha^2}} \right] \quad \ldots (A2.1)$$

with $x = k_0 \ell$, $a = 0.094$, and $b = 0.104$. For small x the series
converges rapidly and the number of terms necessary in order to
evaluate it is small. For large x the opposite is true and
recourse to numerical integration is best.

The problem in calculating the series for large x
is that the terms are not small until $n > x$ and evaluation
consists of computing the difference between pairs of large
numbers. With a finite "word length" such as is present in a
computer, truncation and round-off of the terms becomes critical.
Using an IBM 7040 digital computer with double precision, it
was found that for the T's encountered in this experiment, the
values of x necessary were low enough to use this series. How-
ever for the larger x used it probably would have been quicker
to call on numerical integration.

The FORTRAN IV program is given below. The first

sum in equation (A2.1) is called the major series and the second sum the minor series. The procedure in calculating these sums for a given x is to evaluate successive terms until their absolute value is less than 10^{-4}, after which computation ceases. For speed of computation and minimization of round-off error, terms are evaluated from preceeding terms, thus:

$$T_{n+1} = -T_n \frac{1}{n+1} \sqrt{\frac{1+n\alpha^2}{1+(n+1)\alpha^2}} \; x$$

It was found that the major series becomes unstable above x = 35, at which value the number of terms computed was approximately 100. A spot-check of the values was carried out using a Simpsons Rule numerical integration and was found to agree to three significant figures.

```
IBFTC   SUM
        DOUBLE PRECISION T,TERM,RATIO,R,A2,AI,XI,R1,XF,DSQRT,X1,X2,T2,T3
        DIMENSION RATIO(500),R(500)
        READ(5,1)XI,XF,DELX,A,AF,AD,M1
   1    FORMAT(6F8.4,I4)
C   XI=X(INITIAL),XF=X(FINAL),DELX=INCREMENT IN X, DITTO FOR A,AF,AD WRT ALPHA
C   M1=MAX. NO. OF TERMS IN SERIES
        DO 12 I1=1,NN
   99   WRITE(6,4)
   4    FORMAT(1H1,7X,3HSUM,6X,2H X,6X,5HALPHA)
        AI=A**2
        R(1)=1.D0+A2
        RATIO(1)=1.D0/DSQRT(R(1))
        M2=M1
        DO 6 I=2,M2
        AI=I
        R(I)=R(I-1) +A2
   6    RATIO(I)=DSQRT(R(I-1)/R(I))/AI
C
C                CALCULATION OF MAJOR SERIES
C
        X1=XI
   7    T=1.D0
        N=1
        TERM=-RATIO(1)*X1
   3    IF(ABS(TERM).LT..0001) GO TO 175
        T=T+TERM
        IF(N.GT.M2) GO TO 189
        N=N+1
        R1=RATIO(N)*X1
        TERM=-TERM*R1
        GO TO 3
C
C          CALCULATION OF MINOR SERIES
C
  175   X2=0.104*X1
        T2=1.D0
        N=1
        TERM=-RATIO(1)*X2
  30    IF(ABS(TERM).LT..0001) GO TO 170
        T2=T2+TERM
        IF(N.GT.M2) GO TO 180
```

```
        N=N+1
        R1=RATIO(N)*X2
        TERM=-TERM*R1
        GO TO 30
170     T3=(T+.094*T2)/1.094
        GO TO 18
180     WRITE(6,183)
183     FORMAT(1X,41HNUMBER OF TERMS IN MINOR SERIES TOO LARGE)
        GO TO 12
189     WRITE(6,184)
184     FORMAT(1X,41HNUMBER OF TERMS IN MAJOR SERIES TOO LARGE)
        GO TO 12
18      WRITE(6,2) T3,X1,A
2       FORMAT(5X,3F8.3
        IF(X1.GE.XF) GO TO 10
        X1=X1+DELX
        GO TO 7
10      IF(A.GE.AF) GO TO 12
        A=A+AD
        GO TO 99
12      STOP
        END
```

APPENDIX 3.   SELF-ABSORPTION CORRECTION FACTOR

Self-absorption reduces the intensity emitted by a gaseous source. The correction factor S to be applied to the measured intensity for Doppler-broadened lines is derived in the following paragraphs (see section 2.2).

By considering the equation of transfer of radiation it can be shown that the total line intensity emitted by an optically thick layer of length ℓ can be represented by (see for example, Irwin /12/)

$$I = B\int_{line} (1 - e^{-k(\nu)\ell})\, d\nu \qquad \ldots(A3.1)$$

where, if stimulated emission is negligible

$$B = \frac{2h\nu^3 N_j g_i}{c^2 N_i g_j}$$

Substitution of the simple Doppler profile for $k(\nu)$ results in the correction factor given by equation (2.15). However when two isotopes are present, $k(\nu)$ has the form given in Appendix 1.

$$k(\nu) = k_0 e^{-\omega^2} + k_0' e^{-\omega'^2}$$

$$= k_0(e^{-\omega^2} + b e^{-b/a(\omega-\Omega)^2})$$

$$\therefore \quad 1 - e^{-k(\nu)\ell} = 1 - \sum_{n=0}^{\infty} \frac{(-1)^n}{n!} \left\{ k_0 \ell \left(e^{-\omega^2} + b e^{-b/a(\omega - \Omega)^2} \right) \right\}^n$$

$$= k_0 \ell \sum_{n=0}^{\infty} \frac{(-1)^n (k_0 \ell)^n}{(n+1)!} \left\{ e^{-\omega^2} + b e^{-b/a(\omega - \Omega)^2} \right\}^{n+1}$$

Substituting for k_0 from equation (2.2) and B from above into equation (A3.1), and changing the integration variable from ν to ω then yields equation (2.16).

A table of numerical values of S for several values of the isotope separation are given in Table A3. The value of S is defined such that S = 1.0 for no self-absorption when only one isotope is present; for two isotopes in the ratio 9.9 :100, S = 1.099 when the optical thickness is zero. As well, the correction factor for a single isotope has been calculated from equation (2.15) and has been included. It agrees with the values given by Ladenburg and Levy /7/ for the values of $k_0 \ell$ which are common to both.

The computer program used to evaluate equation (2.16) is given below. To calculate the factor

$$\mathscr{S}_n = \int_{-\infty}^{\infty} \left[e^{-\omega^2} + a e^{-b/a(\omega - \Omega)^2} \right]^n d\omega$$

numerical integration was resorted to. The method of integration chosen was Simpson's Rule because of its simplicity, as well as the fact that the accuracy needed was not high — only to three significant figures. After computation of $\mathscr{S}_n$,

the series was evaluated in a manner entirely analogous to that used in the program given in Appendix 2. The single-isotope self-absorption factor was computed by putting $K = 0$ (and therefore $a = b = 0$) in the program.

TABLE A3   SELF-ABSORPTION CORRECTION FACTOR FOR A
ONE AND TWO ISOTOPE GAS

$k_o \ell$	S(TWO ISOTOPES)			S
	$\Omega = 1.0$	$\Omega = 1.5$	$\Omega = 2.0$	(ONE ISOTOPE)
0.0	1.099	1.099	1.099	1.000
.02	1.091	1.091	1.092	.993
.04	1.083	1.084	1.084	.986
.06	1.075	1.077	1.077	.979
.08	1.068	1.069	1.070	.972
.1	1.060	1.062	1.063	.966
.2	1.023	1.027	1.030	.933
.3	.988	.994	.998	.902
.4	.956	.962	.967	.873
.5	.924	.933	.938	.845
.6	.895	.904	.911	.818
.7	.867	.877	.884	.793
.8	.840	.852	.860	.769
.9	.915	.827	.836	.747
1.0	.791	.804	.813	.725
1.2	.746	.761	.771	.685
1.4	.705	.721	.733	.648
1.6	.668	.685	.698	.615
1.8	.635	.653	.666	.584
2.0	.604	.622	.636	.556
2.4	.550	.569	.584	.507
2.8	.504	.524	.540	.466
3.2	.466	.485	.502	.430
3.6	.432	.451	.469	.399
4.0	.403	.422	.440	.372

```
$IBFTC   ISOABS
         REAL OMEGA,OMEGAF
         DOUBLE PRECISION SUM,TERM,RATIO,AI,DSQRT,S
         DIMENSION RATIO(100),S(100)
         READ(5,10) X,XF,DX,OMEGA,DOMEGA,OMEGAF
10       FORMAT(6F8.1)
         IF(XF.GT.35.)STOP
         IF(XF.LE.35.)N=120
         IF(XF.LT.20.)N=60
         IF(XF.LT.10.)N=35
         IF(XF.LT.5.0)N=20
         IF(XF.LT.1.3)N=10
         N1=20
         N2=40
         N3=20
         B=2.5
         A=2.5
         RT=SQRT(1.1)
         HK=.099
         HK1=RT*HK
         XI=X
23       WRITE(6,11)
11       FORMAT(1H1,7X,1HS,11X,4HK0*L,3X,8HNO.TERMS,5X,5HOMEGA)
C
C   COMPUTE S(J)
C
         J1=1
7        DO 50 J=J1,N
C
C        INTEGRATION FROM -INF. TO -B
         BN1=N1
         H=1./(BN1*B)
         SUME=0.
         SUMO=0.
         L=1
         K=1
         N11=N1-1
         DO 100 I=1,N11
         AI=I
         Y=AI*H
103      Y=1./Y
         Y2=Y*Y
```

```
      BRAK=(EXP(-Y2)+HK1*EXP(-1.1*((Y+OMEGA)**2)))
      F1=Y2*((BRAK)**J)
      IF(L.EQ.2) GO TO 101
      IF(K.EQ.1)SUMO=SUMO+F1
      IF(K.EQ.0)SUME=SUME+F1
      IF(I.EQ.N11)GO TO 102
      GO TO 100
  201 Y=1./B
      L=2
      GO TO 103
  101 FF1=F1
  100 K=1-K
      SUM1=(1.33333*SUMO+.66667*SUME+.33333*FF1)*H
C
C     INTEGRATION  FROM -B TO A
      BN2=N2
      H=(A+B)/BN2
      L=1
      K=0
      SUME=0.
      SUMO=0.
      DO 200 I=1,N2
      AI=I-1
      W=-B+AI*H
  204 W2=W*W
      BRAK=(EXP(-W2)+HK1*EXP(-1.1*((W-OMEGA)**2)))
      F2=BRAK**J
      IF(I.EQ.1)GO TO 201
      IF(L.EQ.2)GO TO 202
      IF(K.EQ.1)SUMO=SUMO+F2
      IF(K.EQ.0)SUME=SUME+F2
      IF(I.EQ.N2)GO TO 203
      GO TO 200
  201 FI2=F2
      GO TO 200
  203 W=A
      L=2
      GO TO 204
  202 FF2=F2
  200 K=1-K
      SUM2=(1.33333*SUMO+.66667*SUME+.33333*(FF2+FI2))*H
C
```

R. L. CRAIN LIMITED

```fortran
C     INTEGRATION  FROM A TO INF.
      BN3=N3
      H=1./(A*BN3)
      SUME=0.
      SUMO=0.
      L=1
      K=1
      N31=N3-1
      DO 300 I=1,N31
      AI=I
      Y=AI*H
      Y=1./Y
303   Y2=Y*Y
      BRAK=(EXP(-Y2)+HK1*EXP(-1.1*((Y-OMEGA)**2)))
      F3=Y2*((BRAK)**J)
      IF(L.EQ.2)GO TO 301
      IF(K.EQ.1)SUMO=SUMO+F3
      IF(K.EQ.0)SUME=SUME+F3
      IF(I.EQ.N31)GO TO 302
      GO TO 300
302   Y=A
      L=2
      GO TO 303
301   FF3=F3
300   K=1-K
      SUM3=(1.33333*SUMO+.66667*SUME+.33333*FF3)*H
50    S(J)=SUM1+SUM2+SUM3
C
C     S(J) NOW COMPUTED
C
18    J2=J1+1
      DO 55 I=J2,N
      AI=I
55    RATIO(I)=(S(I)/S(I-1))/AI
      IF(J1.GE.2)GO TO 8
      TERM=-S(2)*X/2.
      SUM=S(1)
8     J3=J2+1
      DO 2 I=J3,N
      IF(ABS(TERM).LT.1.D-4)GO TO 3
      SUM=SUM+TERM
2     TERM=-TERM*RATIO(I)*X
```

```fortran
3        IF(I-N)5,6,6
6        J1=N+1
         N=N+10
         GO TO 7
5        SUM=SUM/1.77245
         WRITE(6,4)SUM,X,I,OMEGA
4        FORMAT(5X,F7.4,5X,F5.3,5X,I3,5X,F4.1)
         X=X+DX
         IF(X-XF)16,16,17
16       J1=1
         GO TO 18
17       X=XI
         OMEGA=OMEGA+DOMEGA
         IF(OMEGA-OMEGAF)23,23,19
19       STOP
         END
```

R. L. CRAIN LIMITED

APPENDIX 4.   RELATIVE INTENSITY MEASUREMENT OF SPECTRAL LINES

The theory developed in this appendix derives equation (4.1) for the quantitative measurement of relative intensities of spectral lines (see section 4.1).

Consider the case in which the illumination covers the slit of a monochromator and is of uniform intensity. The transmission pass-band is then triangular or trapeziodal, depending on the relative sizes of exit and entrance slit.

If the monochromator is set on wavelength λ_M and the width of the exit slit is denoted by W_{xt}, then it encompasses a wavelength region $\Delta\lambda_{xt}$ given by

$$\Delta\lambda_{xt} = W_{xt} / D(\lambda_M)$$

where $D(\lambda_M)$ is the linear dispersion. The corresponding region which the image of the entrance slit covers, $\Delta\lambda_{nt}$, is given by

$$\Delta\lambda_{nt} = M(\lambda_M) W_{nt} / D(\lambda_M)$$

where $M(\lambda)$ is the lateral magnification of the instrument in the exit plane and W_{nt} is the width of the entrance slit. It is assumed here that $\Delta\lambda_{nt} \leqq \Delta\lambda_{xt}$ so the transmission of an ideal monochromator is trapezoidal of width $\Delta\lambda_{xt}$. This is shown in Fig. A4.a.

$t(\lambda,\lambda_M)$ is the transmission of the monochromator and reaches a maximum, $T(\lambda_M)$ in the region

$$\lambda_M - \frac{\Delta\lambda_{xt} - \Delta\lambda_{nt}}{2} \leqq \lambda \leqq \lambda_M + \frac{\Delta\lambda_{xt} - \Delta\lambda_{nt}}{2}$$

The detector output current due to radiation in a small band of wavelengths $d\lambda$, centred at λ is

$$di = \Omega t(\lambda,\lambda_M) S(\lambda) I(\lambda) d\lambda \qquad \dots(A4.1)$$

where Ω is the solid angle subtended at the source by the monochromator and input lens, $S(\lambda)$ is the sensitivity of the detector, and $I(\lambda)$ is the intensity per unit solid angle per unit wavelength interval of the source.
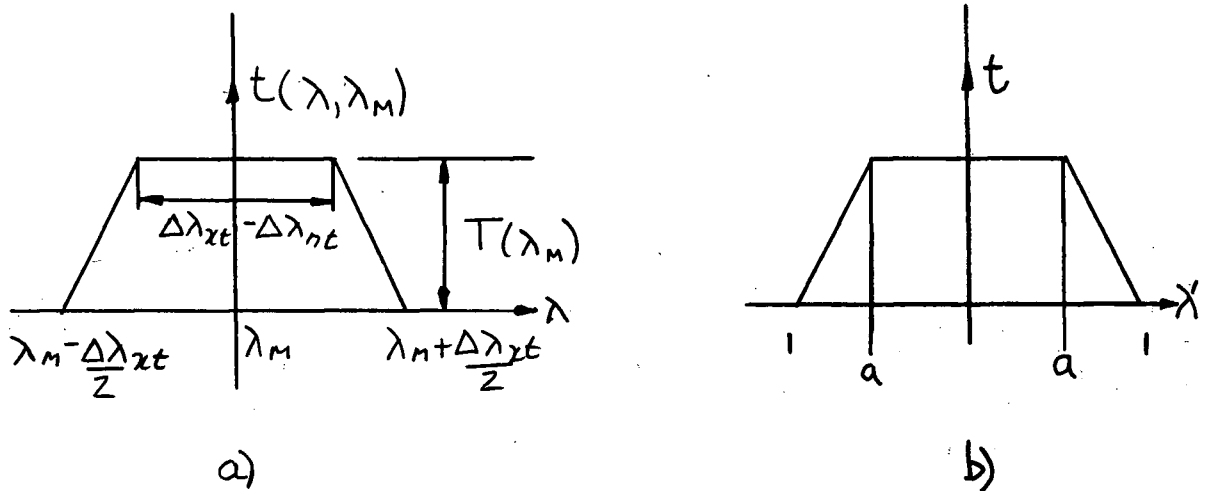
Fig. A4   Pass-Band of Monochromator

Integrating over all wavelengths yields the total response, thus:

$$i = \int_{\lambda=0}^{\lambda=\infty} di = \int_{\lambda_m-\frac{\Delta\lambda_{2t}}{2}}^{\lambda_m+\frac{\Delta\lambda_{2t}}{2}} \Omega t S I d\lambda \qquad \dots(A4.2)$$

For a spectral line of width $\delta\lambda \ll \Delta\lambda_{2t}$ and wavelength λ_M

$$\ell(\lambda_M) = \Omega_\ell \, T(\lambda_M) \, S(\lambda_M) \, I_\ell(\lambda_M) \, \delta\lambda$$

where the subscript ℓ indicates line radiation. Therefore for two lines λ_1, λ_2 of the same line-width

$$\frac{\ell(\lambda_1)}{\ell(\lambda_2)} = R_\ell(\lambda_1, \lambda_2) = \frac{T(\lambda_1) \, S(\lambda_1) \, I_\ell(\lambda_1)}{T(\lambda_2) \, S(\lambda_2) \, I_\ell(\lambda_2)}$$

For a continuous source, the variation of I and S over $\Delta\lambda_{2t}$ must be taken into account. Introducing a new variable $\lambda' = (\lambda-\lambda_M)/\dfrac{\Delta\lambda_{2t}}{2}$ and writing a Taylor series expansion for I and S about $\lambda' = 0$

$$I(\lambda') = I(0) + I'(0)\lambda' + I''(0)\frac{\lambda'^2}{2!} + \cdots$$

$$S(\lambda') = S(0) + S'(0)\lambda' + \cdots$$

Now $I'(0) \approx (I(1) - I(0))/1$ and if only the first two terms in the expansion are retained, then

$$I(\lambda') \approx I(0)[1 + (\varepsilon-1)\lambda']$$

$$S(\lambda') \approx S(0)[1 + (\sigma-1)\lambda']$$

with $\quad \varepsilon = I(1)/I(0) \quad , \quad \sigma = S(1)/S(0)$

and the transmission is given by (see Fig. A4.b)

$$
t(\lambda') = \begin{cases} (1+\lambda')\dfrac{T(0)}{1-a} & , \quad -1 \le \lambda' \le -a \\[2mm] T(0) & , \quad -a \le \lambda' \le a \\[2mm] (1-\lambda')\dfrac{T(0)}{1-a} & , \quad a \le \lambda' \le 1 \end{cases}
$$

where

$$
a = 1 - \frac{\Delta\lambda_{nt}}{\Delta\lambda_{xt}}
$$

Equation (A4.2) then becomes

$$
i(\lambda_M) = \Omega_c\, S(\lambda_M)\, I_c(\lambda_M) \int_{-1}^{1} t(\lambda')(1+(\varepsilon-1)\lambda')(1+(\sigma-1)\lambda')\frac{\Delta\lambda_{xt}}{2}\,d\lambda'
$$

or $i(\lambda_M) = \Omega_c T(\lambda_M) S(\lambda_M) I_c(\lambda_M) K(\lambda_M) \dfrac{\Delta\lambda_{xt}}{2}$

with $K(\lambda) = \left\{ \dfrac{1}{1-a}\left[1 + \frac{1}{6}(\varepsilon-1)(\sigma-1) - a^2 - \frac{a^4}{6}(\varepsilon-1)(\sigma-1)\right]\right\}$

and a, ε, and σ are functions of λ.

Therefore if two wavelengths λ_1, λ_2 are compared,

$$
\frac{i(\lambda_1)}{i(\lambda_2)} = R_c(\lambda_1,\lambda_2) = \frac{\Delta\lambda_{xt}(\lambda_1) T(\lambda_1) S(\lambda_1) I_c(\lambda_1) K(\lambda_1)}{\Delta\lambda_{xt}(\lambda_2) T(\lambda_2) S(\lambda_2) I_c(\lambda_2) K(\lambda_2)}
$$

but $\dfrac{\Delta\lambda_{xt}(\lambda_1)}{\Delta\lambda_{xt}(\lambda_2)} = \dfrac{D(\lambda_2)}{D(\lambda_1)}$

where D is the linear dispersion. The ratio

$$\frac{R_\ell}{R_c} = \frac{I_\ell(\lambda_1)\, I_c(\lambda_2)\, K(\lambda_2)\, D(\lambda_1)}{I_\ell(\lambda_2)\, I_c(\lambda_1)\, K(\lambda_1)\, D(\lambda_2)}$$

is then identical with equation (4.1).

APPENDIX 5. CURVE-FITTING OF NON-DOPPLER SPECTRAL DISTRIBUTION
TO DOPPLER SPECTRAL DISTRIBUTION

Attempts are made here to equate the transmissions
of pure Doppler-broadened spectral lines to two types of non-
Doppler spectral lines, as discussed in section 5.4.1.

1. Self-Absorbed Doppler Distribution

The intensity distribution of a gaseous source of
length ℓ_e in which self-absorption takes place is given by
(see Appendix 3).

$$I(\nu) = B(1 - e^{-k_e(\nu)\ell_e})$$

...(A5.1)

which, for $k(\nu)$ given by a Doppler distribution and $k_0\ell \ll 1$
reduces to the form given in Chapter 2.

For a uniform, mono-isotopic emitter and absorber
gas with a pure Doppler absorption coefficient, the trans-
mission T is actually given by

$$T = \frac{\int (1 - EXP(-k_e(\nu)\ell_e)) \, EXP(-k_a(\nu)\ell_a) \, d\nu}{\int (1 - EXP(-k_e(\nu)\ell_e)) \, d\nu}$$

$$= \frac{\int_{-\infty}^{\infty} (1 - e^{-y e^{-\omega^2}}) \, e^{-x e^{-\omega^2 \alpha^2}} \, d\omega}{\int_{-\infty}^{\infty} (1 - e^{-y e^{-\omega^2}}) \, d\omega}$$

$$= \sum_{n=0}^{\infty} \sum_{m=0}^{\infty} \frac{(-1)^{n+m} y^n x^m}{(n+1)! \, m! \sqrt{n+1+m\alpha^2}} \Bigg/ \sum_{n=0}^{\infty} \frac{(-1)^n y^n}{n!(n+1)^{3/2}}$$

$$= T_s(y, x, \alpha) \qquad\qquad \ldots(A5.2)$$

where $y = k_{oe}\ell_e$ and $x = k_{oa}\ell_a$, and the subscripts e and a refer to emitter and absorber, respectively.

The question is raised, can this be equated to a Doppler transmission with no self-absorption ? i. e. for the six absorption lengths ℓ_{a_i}, is there some value of x' and α' such that

$$T_s(y, x_i, \alpha) = T'(x_i', \alpha'), i = 1, \cdots, 6 ? \quad \ldots(A5.3)$$

where $x_i = k_{oa}\ell_{a_i}$ and $x' = k'_{oa}\ell_{a_i}$, and

$$T'(x', \alpha') = \sum_{n=0}^{\infty} \frac{(-1)^n (k_{oa}\ell_a)^n}{n! \sqrt{1+n\alpha'^2}} \qquad \ldots(A5.4)$$

as given in equation (2.3).

An attempt has been made to solve equation (A5.3) numerically in the IBM 7040 digital computer; values of k'_{oa} and α' determined experimentally (see sections 3.2.1 and 3.2.2) were used to compute $T'(x_i', \alpha')$. $T_s(y, x_i, \alpha)$ was evaluated as k_{oa} was increased in steps using assumed

values of the parameters y and α until the root-mean-square deviation between T' and T_S for the six absorption lengths was a minimum.

Some examples of T_S and T' for two wavelengths are shown in Table A5.1. It can be seen that a fit with a low rms error is possible; the error is better than some of the experimental fits to the theoretical curves in determining k'_{oa} and α'. Another point to be noticed is that k_{oa} substantially differs from k'_{oa} when $\alpha \neq \alpha'$ indicating a large uncertainty in approximating the 'fictitious' k'_{oa} to k_{oa}. Further computations were carried out on the two lines in Table A5.1; since f_{rel} is proportional to $k_{oa}(rel)$, this latter ratio was computed as $k_{oe}\ell_e$ was varied, for $\alpha = .9$ and 1.0 , and compared with the measured value of $.0285/.0193 = 1.48$. The results of these computations are shown in Table A5.2. The value of $k_{oe}\ell_e$ for $\lambda 6383$ was increased in steps of $.01$. The corresponding value for $\lambda 6505$ was assigned by assuming $k_{oe}(rel) = k'_{oa}(rel)$.

Exact values of $k_{oe}\ell_e$ for the Geissler tube are not known although from measurements of k_o made by Irwin /12/ $k_{oe}\ell_e$ could be of the order of $.3$ for some of the strongly absorbing lines; as well, in the present calculations the determined value of k_{oa} is uncertain to 5 units in the last figure. Both these facts do not allow any quantitative conclusions to be made from the above tables, but the variation of $k_{oa}(rel)$ appears to be much less than that of "absolute" k_{oa} as a function of $k_{oe}\ell_e$.

TABLE A5.1 SELF-ABSORBED DOPPLER LINE-SHAPE FIT

λ	k'_{oa} (cm^{-1})	α'	$k_{oe}\ell_e$		ABSORPTION LENGTH (CM)						k_{oa} (cm^{-1})	α	RMS ERROR
					10	15	20	25	35	45			
6506	.0285	1.3	.05	T'	.844	.778	.719	.666	.575	.501	.0230	1.0	.003
				T_s	.845	.780	.722	.668	.575	.497			
6383	.0193	1.3	.05	T'	.891	.842	.797	.755	.679	.614	.0157	1.0	.006
				T_s	.886	.838	.792	.750	.673	.605			

TABLE A5.3 VOIGT LINE-SHAPE FIT

λ	k'_{oa} (cm^{-1})	α'	a		ABSORPTION LENGTH (CM)						k_{oa} (cm^{-1})	α	RMS ERROR
					10	15	20	25	35	45			
6506	.0285	1.3	.01	T'	.844	.778	.719	.666	.575	.501	.0238	1.0	.004
				T_v	.854	.783	.723	.681	.575	.497			

TABLE A5.2 CALCULATION OF k_{oa}(rel) FOR SELF-ABSORBED DOPPLER LINE-SHAPES

		$k_o'(cm^{-1})$	α'	k_{o2}'/k_{o1}'
$\lambda_1(Å)$	6383	.0193	1.3	1
$\lambda_2(Å)$	6506	.0285	1.3	1.48

	6383		6506		
α	$(k_o\ell)_e$	$k_o(cm^{-1})$	$(k_o\ell)_e$	$k_o(cm^{-1})$	k_o/k_{o1}
.9	.01	.0152	.0148	.0220	1.45
.9	.02	.0152	.0295	.0220	1.45
.9	.03	.0150	.0443	.0218	1.45
.9	.04	.0149	.0591	.0216	1.45
1.0	.01	.0161	.0140	.0234	1.45
1.0	.02	.0160	.0295	.0232	1.45
1.0	.03	.0159	.0443	.0230	1.45
1.0	.04	.0159	.0591	.0230	1.45
1.0	.05	.0157	.0738	.0228	1.45
1.0	.06	.0156	.0886	.0226	1.45
1.0	.07	.0154	.1034	.0224	1.45
1.0	.08	.0154	.1181	.0222	1.44
1.0	.09	.0153	.1329	.0220	1.44

The computer program used to evaluate equation (A5.3) and compose Tables A5.1 and A5.2 is given below. T' is computed using the FUNCTION TFALS subprogram, while T_s is computed from the FUNCTION TTRUE subprogram as k_{oa} is varied for some α until $T' = T_s$ for minimum rms error.

2. Voigt Distribution

When the line-broadening processes are a combination of Doppler and natural broadening, the spectral line shape is given by the Voigt profile   (see for example, Mitchell and Zemansky /19/)

$$k(\nu) = k_o \frac{a}{\pi} \int_{-\infty}^{\infty} \frac{e^{-y^2} dy}{a^2 + (\omega - y)^2} \qquad \ldots (A5.5)$$

where $a = \frac{\Delta\nu_N}{\Delta\nu_D} \sqrt{\ln 2}$

and $\Delta\nu_N$ is the natural half-width of the spectral line, and the other parameters are as defined previously. It should be pointed out that this distribution is perhaps a more "real" distribution, as most individual broadening processes are Gaussian or Lorentzian.

For the case of negligible self-absorption in the source and a line-shape given by equation (A5.5), the corresponding transmission becomes, again for uniform and mono-

isotopic emitter and absorber

$$T = \frac{\int_{-\infty}^{\infty} VOIGT(\omega,a)\, e^{-\chi VOIGT(\alpha\omega,\alpha a)}\, d\omega}{\int_{-\infty}^{\infty} VOIGT(\omega,a)\, d\omega} = T_v(\chi,\alpha,a) \quad \cdots (A5.6)$$

where VOIGT(ω,a) is defined from equation (A5.5) as $k(\nu)/k_o$ and x is defined as before.

Again, can this be equated to a pure Doppler trans-mission for some values of k_o' and α'? i. e. can

$$T_v(\chi_i,\alpha,a) = T'(\chi_i',\alpha'),\, i = 1, \cdots, 6 ? \quad \cdots (A5.7)$$

This equation has been evaluated in a manner equivalent to equation (A5.3) for k_{oa} using an assumed value of α and a, to see whether a solution does exist; Table A5.3 shows the results of this computation. It is seen that an approximate solution is possible for a k_{oa} and α much different than k_o' and α'; excessive computing time as well as the gaining of informa-tion of little value precluded further computational investiga-tion.

The program used to evaluate equation (A5.7) is also given below and is similar in form to the program in the previous section. FUNCTION TPKA evaluates T', but by numerical integration rather than by the infinite series, and FUNCTION TKAA calculates T_v. The VOIGT integral is evaluated in FUNCTION VOIGT from a program written by Young /44/.

```
$IBFTC FALST1
       REAL KPO,L,KPOL,KOLE,KO,KOI,KOL,KOF,KOMIN
       DIMENSION L(6),TP(6),T(6),E(6)
       DATA L/10.,15.,20.,25.,35.,45.
       READ(5,1)KPO,ALFAP
C    KPO,ALFAP = FICTITIOUS VALUES OF K AND ALPHA
1      FORMAT(2F6.3)
       KO=KPO/5.5
       READ(5,1)KOLE,ALFA
C    KOLE =K*L FOR EMITTING SOURCE,   ALFA = ?TRUE? ALPHA
       KOF=10.*KO
       KOI=KO
       DK=KO
       DO 7 I=1,6
       KPOL=KPO*L(I)
7      TP(I)=TFALS(KPOL,ALFAP)
77     WRITE(6,5)KOLE,ALFA
5      FORMAT(1X//1X,7H(KOL)E=,F7.4,3X,5HALFA=,F5.2)
       J=1
9      E2=0.
       DO 10 I=1,6
       KOL=KO*L(I)
       T(I)=TTRUE(KOLE,KOL,ALFA)
       E(I)=T(I)-TP(I)
10     E2=E2+E(I)*E(I)
       ERMS=SQRT(E2/6.)
       WRITE(6,8)(T(I),I=1,6),KO,ERMS
6      FORMAT(1X///1X,22HMEASURED TRANSMISSIONS,5X,6F9.3)
       WRITE(6,6)(TP(I),I=1,6)
8      FORMAT(1X,22HSELF-ABS TRANSMISSIONS,5X,6F9.3/1X,3HKO=,F9.4,5X,5HER
      1MS=,3X,F6.3)
       IF(J.EQ.1)GO TO 15
       IF(ERMS.GE.EMIN) GO TO 11
       EMIN=ERMS
       KOMIN=KO
       GO TO 11
15     EMIN=ERMS
       KOMIN=KO
       J=2
11     KO=KO+DK
       IF(KO.LE.KOF)GO TO 9
       IF(KOMIN.EQ.KOF)GO TO 20
```

```
      IF(KOMIN.EQ.KOI)GO TO 20
      KO=KOMIN-DK
      KOI=KO
      KOF=KOMIN+DK
      DK=DK/5.
      IF(DK.LE.1.E-4)STOP
      GO TO 77
20    WRITE(6,21)
21    FORMAT(1X/1X,22HEND-PT. MINIMUM,BEWARE)
      STOP
      END




      FUNCTION TFALS(X1,ALFA)
      DOUBLE PRECISION T,TERM,RATIO,R,A2,AI,RI,DSQRT
      DIMENSION RATIO(100),R(100)
      IF(X1.GT.10.)M1=100
      IF(X1.LE.10.)M1=35
      IF(X1.LE.6.5)M1=25
      IF(X1.LE.4.5)M1=20
      IF(X1.LE.3.) M1=15
      IF(X1.LE.1.) M1=10
      IF(X1.LE..2) M1=5
      A2=ALFA*ALFA
      R(1)=1.D0+A2
      RATIO(1)=1.D0/DSQRT(R(1))
      DO 6 I=2,M1
      AI=I
      R(I)=R(I-1)+A2
6     RATIO(I)=DSQRT(R(I-1)/R(I))/AI
      T=1.D0
      N=1
      TERM=-RATIO(1)*X1
      R1=RATIO(1)*X1
3     IF(ABS(TERM).LT..0001)GO TO 17
      T=T+TERM
      N=N+1
      R1=RATIO(N)*X1
      TERM=-TERM*R1
      GO TO 3
```

R. L. CRAIN LIMITED

```
17        TFALS=T
          RETURN
          END



          FUNCTION TTRUE(X,Y,ALFA)
          REAL NUM
          IF(X.GT.1.5)MMAX=25
          IF(X.LE.1.5)MMAX=10
          IF(Y.GT.10.)MAX=100
          IF(Y.LE.10.)MAX=35
          NMAX=50
9         DENOM=SUM1(X,MMAX)
8         SUM=SUM2(Y,ALFA,0,MAX)
          TERM=-SUM2(Y,ALFA,1,MAX)*X/2.
          DO 2 N=2,NMAX
          IF(ABS(TERM).LT.1.E-4)GO TO 3
          AN=N+1
          SUM=SUM+TERM
2         TERM=-TERM*SUM2(Y,ALFA,N,MAX)*X/AN
3         NUM=SUM
          TTRUE=NUM/DENOM
          RETURN
          END



          FUNCTION SUM1(X,MMAX)
12        DIMENSION R(50),RATIO(50)
11        R(1)=2.
10        RATIO(1)=(1./R(1))**1.5
9         DO 1 I=2,MMAX
8         AI=I
7         R(I)=R(I-1)+1.
1         RATIO(I)=(R(I-1)/R(I))**1.5/AI
5         SUM1=1.
4         TERM=-RATIO(1)*X
3         DO 2 I=2,MMAX
          IF(ABS(TERM).LT.1.E-4) RETURN
```

```
            SUM1=SUM1+TERM
      2     TERM=-TERM*RATIO(I)*X
            END


            FUNCTION SUM2(X,ALFA,M,MAX)
            DOUBLE PRECISION TERM,RATIO,R,A2,DSQRT,AI,AM,DABS
            DIMENSION R(100),RATIO(100)
            A2=ALFA*ALFA
            AM=M
            R(1)=AM+1.D0+A2
            RATIO(1)=1.D0/DSQRT(R(1))
            DO 1 I=2,MAX
            AI=I
            R(I)=R(I-1)+A2
      1     RATIO(I)=DSQRT(R(I-1)/R(I))/AI
      5     SUM2=1.D0
            TERM=-RATIO(1)*X
            DO 2 I=2,MAX
            IF(DABS(TERM).LT.1.D-4)GO TO 3
            SUM2=SUM2+TERM
      2     TERM=-TERM*RATIO(I)*X
      3     RETURN
            END
```

```
$IBFTC   FALST6
         REAL KPO,L,KPOL,KOLE,KO,KOI,KOL,KOF,KOMIN
         DIMENSION L(6),TP(6),T(6),E(6)
         DATA L/10.,15.,20.,25.,35.,45.
         READ(5,1)KPO,ALFAP
C    KPO,ALFAP = FICTITIOUS VALUES OF K AND ALPHA
1        FORMAT(2F6.3)
         READ(5,1)ALFA,A
C    ALFA = @TRUE@ ALPHA, A = (NATURAL TO DOPPLER LINE-WIDTH RATIO)*SQRT(ALOG(2))
         KO=KPO/5.5
         KOF=10.*KO
         KOI=KO
         DK=KO
         DO 7 I=1,6
         KPOL=KPO*L(I)
7        TP(I)=TPKA(KPOL,ALFAP)
77       WRITE(6,3)A,ALFA
3        FORMAT(1X//1X,17HLINE WIDTH RATIO=,F6.3,3X,5HALFA=,F5.2)
         J=1
9        E2=0.
         DO 10 I=1,6
         KOL=KO*L(I)
         T(I)=TKAA(KOL,ALFA,A)
         E(I)=T(I)-TP(I)
10       E2=E2+E(I)*E(I)
         ERMS=SQRT(E2/6.)
         WRITE(6,6)(TP(I),I=1,6)
6        FORMAT(1X//1X,22HMEASURED TRANSMISSIONS,5X,6F9.3)
         WRITE(6,8)(T(I),I=1,6),KO,ERMS
8        FORMAT(1X,22H DOPPLER TRANSMISSIONS,5X,6F9.3/1X,3HKO=,F9.4,5X,5HER
        1MS=,3X,F6.3)
         IF(J.EQ.1)GO TO 15
         IF(ERMS.GE.EMIN) GO TO 11
         EMIN=ERMS
         KOMIN=KO
         GO TO 11
15       EMIN=ERMS
         KOMIN=KO
         J=2
11       KO=KO+DK
         IF(KO.LE.KOF)GO TO 9
         IF(KOMIN.EQ.KOF)GO TO 20
```

```fortran
      IF(KOMIN.EQ.KOI)GO TO 20
      KO=KOMIN-DK
      KOI=KO
      KOF=KOMIN+DK
      DK=DK/5.
      IF(DK.LE.1.E-4)STOP
      GO TO 77
20    WRITE(6,21)
21    FORMAT(1X/1X,22HEND-PT. MINIMUM,BEWARE)
      STOP
      END



      FUNCTION TPKA(X,Y)
      N=10
      A1=2.
      AN=N
7     H=A1/AN
      SUME=0.
      SUMO=0.
      L=1
      K=0
      DO 2 I=1,N
      AI=I-1
      W=AI*H
3     WA=W*Y
      W2=W*W
      WA2=WA*WA
      E=EXP(-WA2)
      E2=EXP(-W2)
      F=E2*EXP(-X*E)
      IF(I.EQ.1)GO TO 4
      IF(L.EQ.2)GO TO 5
      IF(K.EQ.0)GO TO 74
      SUMO=SUMO+F
      GO TO 75
74    SUME=SUME+F
75    IF(I.EQ.N)GO TO 6
      GO TO 2
4     FI=F
```

```fortran
      GO TO 2
6     W=A1
      L=2
      GO TO 3
5     FF=F
2     K=1-K
      SUM1=(1.33333*SUMO+.66667*SUME+.33333*(FI+FF))*H
      H=1./(A1*AN)
      SUME=0.
      SUMO=0.
      L=1
      K=1
      N1=N-1
      DO 10 I=1,N1
      AI=I
      W=AI*H
      W=1./W
13    W2=W*W
      WA=W*Y
      WA2=WA*WA
      E=EXP(-WA2)
      E2=EXP(-W2)
      F=E2*EXP(-X*E)*W2
      IF(L.EQ.2)GO TO 11
      IF(K.EQ.0)GO TO 76
      SUMO=SUMO+F
      GO TO 77
76    SUME=SUME+F
77    IF(I.EQ.N1)GO TO 12
      GO TO 10
12    W=AI
      L=2
      GO TO 13
11    FF=F
10    K=1-K
      SUM2=(1.33333*SUMO+.66667*SUME+.32333*FF)*H
      SUM=SUM1+SUM2
      TPKA=2.*SUM/1.77245
      RETURN
      END
```

```
      FUNCTION TKAA(X,Y,Z)
      N=10
      A1=2.
      AA=Y*Z
      AN=N
    7 H=A1/AN
      SUME=0.
      SUMO=0.
      L=1
      K=0
      DO 2 I=1,N
      AI=I-1
      W=AI*H
    3 WA=W*Y
      W2=W*W
      WA2=WA*WA
      V=VOIGT(WA,AA)
      VV=VOIGT(W,Z)
      F=VV*EXP(-X*V)
      IF(I.EQ.1)GO TO 4
      IF(L.EQ.2)GO TO 5
      IF(K.EQ.0)GO TO 74
      SUMO=SUMO+F
      GO TO 75
   74 SUME=SUME+F
   75 IF(I.EQ.N)GO TO 6
      GO TO 2
    4 FI=F
      GO TO 2
    6 W=A1
      L=2
      GO TO 3
    5 FF=F
    2 K=1-K
      SUM1=(1.33333*SUMO+.66667*SUME+.33333*(FI+FF))*H
      H=1./(A1*AN)
      SUME=0.
      SUMO=0.
      L=1
      K=1
```

```
        N1=N-1
        DO 10 I=1,N1
        AI=I
        W=AI*H
        W=1./W
13      W2=W*W
        WA=W*Y
        WA2=WA*WA
        V=VOIGT(WA,AA)
        VV=VOIGT(W,Z)
        F=VV*EXP(-X*V)*W2
        IF(L.EQ.2)GO TO 11
        IF(K.EQ.0)GO TO 76
        SUMO=SUMO+F
        GO TO 77
76      SUME=SUME+F
77      IF(I.EQ.N1)GO TO 12
        GO TO 10
12      W=AI
        L=2
        GO TO 13
11      FF=F
10      K=1-K
        SUM2=(1.33333*SUMO+.66667*SUME+.33333*FF)*H
        SUM=SUM1+SUM2
        TKAA=SUM/.8862
        RETURN
        END



        FUNCTION VOIGT(XIN,YIN)
        DIMENSION A(42),HH(10),XX(10)
        DIMENSION RA(32),CA(32),RB(32),CB(32),B(44),AK(5),AM(5),DY(4)
        DATA HH(1),HH(2),XX(1),XX(2),A/0.80491409E-00,0.81312835E-01,0.524
       164762,1.65068012,0.,0.19999999E 0,0.,-0.184E 0,0.,0.15583999,0.,-0
       2.121664,0.,0.87708159E-1,0.,-0.58514124E-1,0.,0.3621573E-1,0.,-0.
       320849765E-1,0.,0.11196011E-1,0.,-0.56231896E-2,0.,0.26487634E-2,0.
       4,-0.1173267E-2,0.,0.48995199E-3,0.,-0.19336308E-3,0.,0.72287745E-4
       5,0.,-0.25655512E-4,0.,0.86620736E-5,0.,-0.27876379E-5,0.,0.8566873
       66E-6,0.,-0.25184337E-6,0.,0.70936022E-7
```

R. L. CRAIN LIMITED

```
401     X=XIN
        Y=YIN
        X2=X*X
        Y2=Y*Y
        IF(X-7.) 200,201,201
200     IF(Y-1.) 202,202,203
203     RA(1)=0.
        CA(1)=0.
        RB(1)=1.
        CB(1)=0.
        RA(2)=X
        CA(2)=Y
        RB(2)=.5-X2+Y2
        CB(2)=-2.*X*Y
        CB1=CB(2)
        CA1=0.
        UV1=0.
        DO 250 J=2,31
        JMINUS=J-1
        JPLUS=J+1
        FLOATJ=JMINUS
        RB1=2.*FLOATJ+RB(2)
        RA1=-FLOATJ*(2.*FLOATJ-1.)/2.
        RA(JPLUS)=RB1*RA(J)-CB1*CA(J)+RA1*RA(JMINUS)-CA1*CA(JMINUS)
        CA(JPLUS)=RB1*CA(J)+CB1*RA(J)+RA1*CA(JMINUS)+CA1*RA(JMINUS)
        RB(JPLUS)=RB1*RB(J)-CB1*CB(J)+RA1*RB(JMINUS)-CA1*CB(JMINUS)
        CB(JPLUS)=RB1*CB(J)+CB1*RB(J)+RA1*CB(JMINUS)+CA1*RB(JMINUS)
        UV=(CA(JPLUS)*RB(JPLUS)-RA(JPLUS)*CB(JPLUS))/(RB(JPLUS)*RB(JPLUS)+
       1CB(JPLUS)*CB(JPLUS))
        IF(ABS(UV-UV1)-1.E-7) 251,250,250
250     UV1=UV
251     VOIGT=UV/1.772454
        RETURN
202     IF(X-2.) 301,301,302
301     ARNT=1.
        MAX=12.+5.*X2
        KMAX=MAX-1
        DO 303 K=0,KMAX
        AJ=MAX-K
303     ARNT=ARNT*(-2.*X2)/(2.*AJ+1.)+1.
        U=-2.*X*ARNT
        GO TO 304
```

R. L. CRAIN LIMITED

```
302     IF(X-4.5) 305,306,306
305     B(43)=0.
        B(44)=0.
        J=42
        DO 307 K=1,42
        B(J)=.4*X*B(J+1)-B(J+2)+A(J)
307     J=J-1
        U=B(3)-B(1)
        GO TO 304
306     ARNT=1.
        MAX=2.+40./X
        AMAX=MAX
        DO 308 K=1,MAX
        ARNT=ARNT*(2.*AMAX-1.)/(2.*X2)+1.
308     AMAX=AMAX-1.
        U=-ARNT/X
304     V=1.772454*EXP(-X2)
        H=.02
        JM=Y/H
        IF(JM) 310,311,310
311     H=Y
310     Z=0.
        L=0
        DY(1)=0.
312     DY(2)=H/2.
        DY(3)=DY(2)
        DY(4)=H
318     AK(1)=0.
        AM(1)=0.
        DO 313 J=1,4
        YY=Z+DY(J)
        UU=U+.5*AK(J)
        VV=V+.5*AM(J)
        AK(J+1)=2.*(YY*UU+X*VV)*H
        AM(J+1)=-2.*(1.+X*UU-YY*VV)*H
        IF(J-3) 313,314,313
314     AK(4)=2.*AK(4)
        AM(4)=2.*AM(4)
313     CONTINUE
        Z=Z+H
        L=L+1
        U=U+.1666667*(AK(2)+2.*AK(3)+AK(4)+AK(5))
```

```
        V=V+.1666667*(AM(2)+AM(3)+AM(3)+AM(4)+AM(5))
        IF(JM) 315,320,315
315     IF(L-JM) 318,317,220
317     AJM=JM
        H=Y-AJM*H
        GO TO 312
320     VOIGT=V/1.772454
        RETURN
201     F1=0.
        DO 330 J=1,2
330     F1=F1+HH(J)/(Y2+(X-XX(J))*(X-XX(J)))+HH(J)/(Y2+(X+XX(J))*(X+XX(J))
       1)
        VOIGT=Y*F1/3.1415927
        RETURN
        END
```

APPENDIX 6.   END CORRECTION ATTEMPTS

An investigation is undertaken here into the effects the ends of the absorbing column have on the transmission (see section 5.4.2.7).

The geometry of the ends of the discharge are drawn in Fig. A6.1. The cylindrical discharge has an outer radius R and bends circularly at the ends through 90° with an inner and outer radius of curvature D and D + 2R respectively. It is assumed k_o and α are constant in the ends of the discharge. Consider a single ray of light which leaves the straight portion of the discharge at position r,θ in the cross-section of the annulus of radius r(r = 1.07 cm). It emerges from the curved portion of the discharge at point B after traversing a distance $\mathcal{L}(\theta)$ on plane A. $\mathcal{L}$ may be computed from the geometry on the end as a function of θ. The total distance travelled is $\ell_o + 2\mathcal{L}$, ℓ_o being the length of the straight portion of the discharge. Let $\mathcal{L}(\theta)$ be divided into two segments, z and $\Delta z(\theta)$, where z is independent of θ. Therefore for each parallel ray of light the intensity out of the discharge is

$$I(\nu)e^{-k(\nu)\ell} = I(\nu)e^{-k(\nu)(L+2\Delta z(\theta))}$$

where L = ℓ_o + 2z, and the transmission is then

$$T = \frac{\int_A \int_{-\infty}^{\infty} I(\nu)e^{-k(\nu)\ell}d\omega dA}{\int_A \int_{-\infty}^{\infty} I(\nu)d\omega dA} \qquad \ldots(A6.1)$$
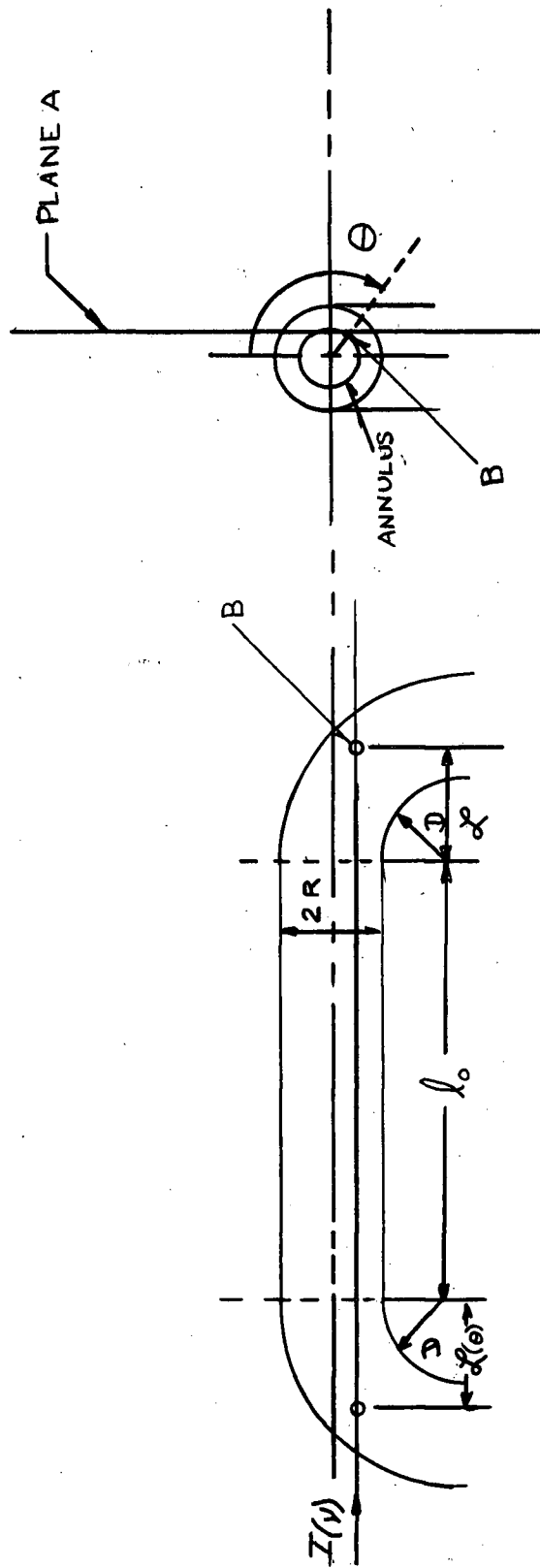
FIG. A 6.1 GEOMETRY OF ENDS OF ABSORBING COLUMN

If the bottom of the annulus (i. e. the side toward the electrodes) is symmetrically blocked off at an angle θ_M, (see Fig. A6.2) and the usual assumption of Doppler line-shapes holds, equation (A6.1) becomes,

$$T = \frac{2 \int_0^{\theta_M} \int_{-\infty}^{\infty} e^{-\omega^2} e^{-k_0 L e^{-\omega^2 \alpha^2}} (1 - 2k(\nu)\Delta g + \cdots) d\omega \, r \Delta r \, d\theta}{\sqrt{\pi} \, 2\theta_M r \Delta r}$$

...(A6.2)

$$= \sum_{m=0}^{\infty} \frac{(-2)^m \overline{\Delta g^m}}{m!} F_m(k_0 L, \alpha) = \sum_{m=0}^{\infty} T_m$$

where $\overline{\Delta g^m} = \frac{1}{\theta_M} \int_0^{\theta_M} (\Delta g)^m d\theta$

and $F_m(k_0 L, \alpha) = k_0^m \int_{-\infty}^{\infty} e^{-\omega^2(1 + m\alpha^2)} e^{-k_0 L e^{-\omega^2 \alpha^2}} d\omega$

$$= \sqrt{\pi} \, k_0^m \sum_{n=0}^{\infty} \frac{(-1)^n (k_0 L)^n}{n! \sqrt{1 + (n+m)\alpha^2}}$$
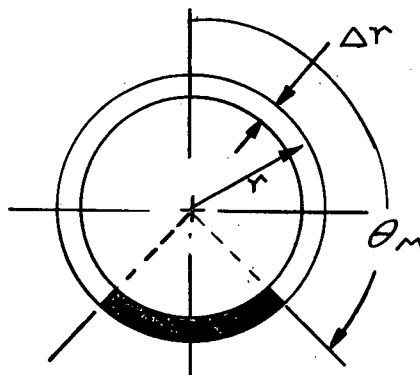

Fig. A6.2   Annulus with Portion Blocked Off

That F_m tends to zero rapidly as m increases can be seen for $k_o \ll 1$, where the presence of the term k_o^m ensures the rapid decrease; on the other hand the same tendency is present as k_o increases because although the k_o^m factor is then not so small, the integral (or sum) F_m is. At any rate it seems advantageous to try to choose conditions so that the first correction term (T_1) is small or zero by making $\overline{\Delta z}$ as small as possible.

The first case which was tried was to choose L equal to the distance between the centres of the electrodes, i. e. z = D + R and calculate θ_M on the computer such that $\overline{\Delta \zeta} = 0$. The results of this calculation are shown in Table A6.1 using some experimentally determined values of k_o and α for the case in which the end-effects should be the greatest, which corresponds to L = 10 cm. It was found that $\overline{\Delta \zeta} < 0$ for $0 \le \theta \le \pi$ which means the effective absorption length for the first order correction is less than the distance between the electrodes for any θ, although $|\overline{\Delta \zeta}|$ is a minimum at $\theta = \pi$ where $\overline{\Delta \zeta}$ has the value -.08 cm. Also included in this table are the succeeding terms (T_m) of equation (A6.2) up to m = 4. It can be seen that even for the highest value of k_o, the correction necessary is not greater than .003. For absorption lengths greater than 10 cm the correction terms rapidly decrease. Table 6 shows that k_o attains this highest value only for $\lambda 6402$. Because the value of k_o is uncertain due to its "fictitious" quality (see section 5.4.1), as well as the unjustified but simplifying assumption of constant conditions in the ends, it is apparent

TABLE A6.1 END-CORRECTION ATTEMPT #1: $\theta = \pi$, $L = 10$ cm

m	$(-2)^m \overline{\Delta g^m}/m!$	$k_o = .0217$ cm^{-1}		$k_o = .082$ cm^{-1}		$k_o = .193$ cm^{-1}	
		$F_m/\sqrt{\pi}$	T_m	$F_m/\sqrt{\pi}$	T_m	$F_m/\sqrt{\pi}$	T_m
1	$-.16$	.019	$-.003$	.03	$-.005$	.04	$-.006$
2	2.26	.0005	.001	.001	.002	.004	.009
3	$-.16$	$\approx 10^{-5}$	$\approx -10^{-6}$	.0001	$\approx -10^{-5}$	.0006	$\approx -10^{-4}$
4	.82	$\approx 10^{-7}$	$\approx 10^{-7}$	$\approx 10^{-6}$	$\approx 10^{-6}$	$\approx 10^{-4}$	$\approx 10^{-4}$

TABLE A6.2 END-CORRECTION ATTEMPT #2: $= 1.99$ cm, R + D = 2.03 cm, L = 10 cm

m	$(-2)^m \overline{\Delta g^m}/m!$	T_m		
		$k_o = .0217$	$k_o = .082$	$k_o = .193$
1	0	0	0	0
2	2.26	.001	.002	.009
3	$-.35$	$\approx -10^{-6}$	$\approx -10^{-5}$	$\approx -10^{-4}$
4	.63	$\approx 10^{-7}$	$\approx 10^{-6}$	$\approx 10^{-4}$

that these corrections cannot be quantitatively applied. It is likely however, that those spectral lines Table 6 indicates as having a small value of k_o do not need end-effect corrections; this cannot be said of lines like $\lambda 6402$ quite so definitely.

The second correction attempt sought an effective absorption length for a fixed value of Θ_M , which in this case was chosen as π . Again T_1 was to be as small as possible so a value of z was looked for such that $\overline{\Delta z} = 0$. For this equality to occur, z has the value 1.99 cm. D + R for the absorption tube (see Fig. A6.1) is 2.03 cm so the effective absorption length is essentially equal to the distance between the electrodes. This of course follows from the first correction attempt if $\Theta_M = \pi$ and the general comments given concerning that attempt are generally applicable here also. The first four terms of the correction series are given in Table A6.2.

The three computer programs used to compute F_m and $\overline{\Delta g^m}$ are given below; the first two were used in the first end-correction attempt, and the first and the third in the second attempt. The only remarks necessary concerning these programs is that the presence of two isotopes was taken into account, and that numerical integrations were done using Simpson's Rule.

```
$IBFTC   NDCOR1
1        FORMAT(3I4)
2        FORMAT(2F10.3)
76       FORMAT(1X,F6.4,2X,F6.2,2X,F4.0,2X,F6.4,2X,3I4)
         DOUBLE PRECISION T,TERM
         DIMENSION RATIO(100),R(100),EK(50),A(50)
         READ(5,1)N,M1,M2
C     N=NO. OF CARDS,M1=MAX.NO. OF TERMS, M2=ORDER OF CORRECTION
         READ(5,2)(EK(I),A(I),I=1,N)
C     EK(I)=K(O),A(I)=ALPHA
25       DO 70 I=1,N
         EL=10.
         J1=1
         A2=A(I)**2
         AM2=M2
         RR=1.+AM2*A2
         RA=1./SQRT(RR)
         R(1)=RR+A2
         RATIO(1)=SQRT(RR/R(1))
         DO 6 K=2,M1
         AK=K
         R(K)=R(K-1)+A2
6        RATIO(K)=SQRT(R(K-1)/R(K))/AK
C        MAJOR SERIES
624      EKM2=EK(I)**M2
         T=EKM2*RA
         EKL=EK(I)*EL
         EKL1=-EKL*RATIO(1)
         TERM=T*EKL1
         M=2
28       IF(ABS(TERM).LT..0001) GO TO 17
         T=T+TERM
         IF(M.GE.M1) GO TO 17
         EKL2=EKL*RATIO(M)
         TERM =-TERM*EKL2
         M=M+1
         GO TO 28
17       M3=M
C        MINOR SERIES
         EKM2=(.104*EK(I))**M2
         T1=EKM2*RA
         EKL=.104*EK(I)*EL
```

```
          EKL1=-EKL*RATIO(1)
          TERM=T1*EKL1
          M=2
128       IF(ABS(TERM).LT..0001) GO TO 117
          T1=T1+TERM
          IF(M.GE.M1) GO TO 117
          EKL2=EKL*RATIO(M)
          TERM=-TERM*EKL2
          M=M+1
          GO TO 128
117       T=(T+T1)/1.094
          WRITE(6,76)EK(I),A(I),EL,T,M3,M,M2
          GO TO(50,50,50,53,53,70),J1
50        EL=EL+5.
          J1=J1+1
          GO TO 624
53        EL=EL+10.
          J1=J1+1
          GO TO 624
70        CONTINUE
          GO TO (60,61,62,63),M2
60        M2=2
          GO TO 25
61        M2=3
          GO TO 25
62        M2=4
          GO TO 25
63        STOP
          END


$IBFTC   NDCOR2
C                   TO COMPUTE MOMENTS OF DELTA L FOR END CORRECTIONS OF ABS TUBE
          READ(5,1)N
C                   N=ORDER OF MOMENT
1         FORMAT(I2)
          THETA=3.14159
          M=50
C                   M=DIVISION OF INTEGRATION INTERVAL
          R=1.27
```

```
      D=.76
      RR=1.07
      RD=R+D
      R2=R*R
      RR2=RR*RR
      AM=M
      DO 8 J=1,50
      H=THETA/AM
      L=1
      SUME=0.
      SUMO=0.
      K=0
      DO 2 I=1,M
      AI=I-1
      X=AI*H
    6 RM=RD+SQRT(R2-RR2*(SIN(X)**2))
      EL=SQRT(RM*RM-(RD+RR*COS(X))**2)
      DEL=EL-RD
      F=DEL**N
      IF(I.EQ.1) GO TO 3
      IF(L.EQ.2) GO TO 4
      IF(K.EQ.1) SUMO=SUMO+F
      IF(K.EQ.0) SUME=SUME+F
      IF(I.EQ.M) GO TO 5
      GO TO 2
    3 FI=F
      GO TO 2
    5 X=THETA
      L=2
      GO TO 6
    4 FF=F
    2 K=1-K
      SUM=1.3333*SUMO+.66667*SUME+.33333*(FI+FF)
      SUM=2.*SUM*H/THETA
      ANGLE=THETA*180./3.14159
      WRITE(6,7) SUM,ANGLE
    7 FORMAT(1X,E14.7,4X,F6.2)
    8 THETA=THETA-3.14159/50.
      STOP
      END
```

```
$IBFTC  NDCOR3
        READ(5,1)N,Z,ZMIN,DZ
1       FORMAT(I2,3F6.3)
        M=50
        R=1.27
        D=.76
        RR=1.07
        RD=R+D
        RR2=RR*RR
        R2=R*R
        AM=M
        H=3.14159/AM
9       L=1
        SUME=0.
        SUMO=0.
        K=0
        DO 2 I=1,M
        AI=I-1
        X=AI*H
6       RM=RD+SQRT(R2-RR2*(SIN(X)**2))
        EL=SQRT(RM*RM-(RD+RR*COS(X))**2)
        DELZ=EL-Z
        F=DELZ**N
        IF(I.EQ.1) GO TO 3
        IF(L.EQ.2) GO TO 4
        IF(K.EQ.1) SUMO=SUMO+F
        IF(K.EQ.0) SUME=SUME+F
        IF(I.EQ.M) GO TO 5
        GO TO 2
3       FI=F
        GO TO 2
5       X=3.14159
        L=2
        GO TO 6.
4       FF=F
2       K=1-K
        SUMO=1.33333*SUMO+.66667*SUME+.33333*(FF+FI)
        SUM=2.*SUMO*H/3.14159
        WRITE(6,7)SUM,Z
```

```
7    FORMAT(5X,E14.7,4X,F6.2)
     Z=Z-DZ
     IF(Z.GE.ZMIN) GO TO 9
     STOP
     END
```

REFERENCES

/1/   A. Einstein, Verhandl. Deut. Phys. Ges. <u>18</u>, 318 (1916).

        A. Einstein, Physik. Z. <u>18</u>, 121 (1917).

/2/   B. M. Glennon and W. L. Wiese, N.B.S. Mono. <u>50</u>, (1962).

/3/   W. J. Karzas and R. Latter, Astrophys. J. Suppl. <u>6</u>, 167 (1961).

/4/   R. Herdon and T. P. Hughes, Astrophys. J. <u>133</u>, 249 (1961).

/5/   D. R. Bates and A. Damgaard, Phil. Trans. Roy. Soc. <u>242</u>, 101 (1949).

/6/   L. H. Aller, <u>The Abundance of the Elements</u>, Interscience, New York (1961) p. 194.

/7/   R. Ladenburg, Zeits. f. Phys. <u>48</u>, 15 (1928).

        R. Ladenburg and H. Kopfermann, Zeits. f. Phys. <u>48</u>, 26 51 (1928).

        R. Ladenburg and H. Kopfermann, Zeits. f. Phys. <u>65</u>, 167 (1930).

        R. Ladenburg and S. Levy, Zeits. f. Phys. <u>65</u>, 189 (1930).

        R. Ladenburg, Rev. Mod. Phys. <u>5</u>, 243 (1933).

/8/   S. A. Korff and G. Breit, Rev. Mod. Phys. <u>4</u>, 482 (1932).

/9/   A. Pery-Thorne and J. E. Chamberlain, Proc. Phys. Soc. <u>82</u>, 133 (1963).

/10/   R. Doherty, Ph. D. Thesis, University of Michigan (1962).

/11/   H. Friedrichs, Zeit. f. Astrophys. <u>60</u>, 176 (1964).

/12/   J. C. Irwin, Ph. D. Thesis, University of British Columbia 1965.

        J. C. Irwin and R. A. Nodwell, Can. J. Phys. To be published.

/13/ J. H. E. Griffiths, Proc. Roy. Soc. 143, 588 (1934).

/14/ W. R. Bennett, P. J. Kindlmann, and G. N. Mercer, Appl.
Optics, Suppl. 2, 34 (1962).

/15/ J. Z. Klose, Phys. Rev. 141, 181 (1966)

/16/ S. M. Hamberger, Proc. V Int. Conf. Ioniz. Phen. Gases,
Munich (1961) Vol. II p. 1919.

/17/ H. W. H. van Andel, Ph. D. Thesis, University of
British Columbia (1966).

/18/ M. Garbuny, Optical Physics, Academic, New York (1965)
p. 98.

/19/ A. C. G. Mitchell and M. W. Zemansky, Resonance
Radiative and Excited Atoms, C. U. P.,
Cambridge (1961) Ch. 3.

/20/ G. Herzberg, Atomic Spectra and Atomic Structure, Dover,
New York (1944) p. 195.

/21/ H.W.H. van Andel, Masters' Thesis, University of
British Columbia (1963).

/22/ M. I. T. Rad. Lab. Ser., 18, 384 (1948).

/23/ N. A. Schuster, Rev. Sci. Inst. 22, 254 (1951).

/24/ R. L. Christensen and I. Ames, J.O. S. A. 51, 224 (1961).

/25/ J. C. de Vos, Physica 20, 690 (1954).

/26/ R. D. Larrabee, J. O. S. A. 49, 619 (1959).

/27/ G. A. W. Rutgers and J. C. de Vos, Physica 20, 715
(1954).

/28/ E. V. Condon and G. H. Shortley, The Theory of Atomic
Spectra, C. U. P., Cambridge (1963)
p. 188.

/29/   F. Paschen,   Ann. d. Physik 60, 405 (1919).

/30/   K. Lang,   Acta Phys. Austr. 5, 376 (1951).

/31/   S, M. Hamberger,   Plasma Phys. 5, 73 (1963).

/32/   G. Ecker and O. Zöller, Phys. Fluids 7, 1996 (1964).

/33/   K. Lang,   S. B. Öster.Akad. Wiss. 161, 65 (1952).

/34/   S. E. Frish and O. P. Bochkova,   Optical Transition
                Probabilities,Isreal Program for Scientific
                Translations, Jerusalem,(1963) p. 204.

/35/   J. D. Cobine, Gaseous Conductors, Dover, New York
                (1958) p. 235.

/36/   T. Donahue and G. H. Dieke, Phys. Rev. 81, 248 (1951).

/37/   K. Krebs, Z. f. Physik 101, 604 (1936).

/38/   J. Topping, Errors of Observation and Their Treatment,
                Chapman, Hall, London (1958) p.88.

/39/   M. Gadsden, Appl. Optics 4, 1446 (1965).

/40/   S. E. Frish and V. F. Rivald, Optics and Spectroscopy
                                    15, 395 (1963).

/41/   V. F. Rivald, Optics and Spectroscopy 18, 318 (1965).

/42/   T. R. Conner and M. O. Biondi, Phys. Rev. 140, 778 (1965).

/43/   H. Nagaoka and T. Mishima, Sci. Pap. I. P. C. R. 13, 293
                    (1930), Sci. Pap. I. P. C. R. 25, 223 (1934)

/44/   W. A. Young, J. Appl. Phys. 35, 460 (1964).